PRECIPITATED MICROBIALITES

R. S. Shapiro and D. T. Wilmeth

INTRODUCTION

Microbially induced, lithified structures known as microbialites are both geologically and biologically significant, forming extensive sedimentary, geochemical, and microbiological records in modern and ancient environments. Depositional settings range from deep ocean hydrocarbon seeps, hydrothermal vents, and whale falls, to cool water carbonate banks—abundant occurrences within peritidal zones and, finally, to non-marine environments such as lakes, rivers, and springs. More than three billion years of Earth's biosphere is primarily recorded within microbialites, including the oldest macrofossils on the planet (Walter, Buick, & Dunlop, 1980; Van Kranendonk, Webb, & Kamber, 2003; Van Kranendonk, 2006). Even with diminished diversity and abundance during the Phanerozoic, periodic microbialite resurgences after mass extinctions are used as indicators for relative environmental recovery (Mata & Bottjer, 2012). Microbialites are also targeted by astrobiology studies for their ability to form in harsh environments and their capacity to preserve specific biosignatures (Corsetti & Storrie-Lombardi, 2003; Shapiro, 2004a; Ibarra & Corsetti, 2016). Yet, despite the broad scientific significance of microbialites, many authors note a lack of consistent terminology (Riding, 1999), whereas others address the challenges of differentiating microbialites from numerous abiogenic sedimentary deposits (Buick, Dunlop, & Groves, 1981; Grotzinger & Rothman, 1996; Grotzinger & Knoll, 1999; Awramik & Grey, 2005).

The aim, herein, is to provide the reader with a basic working guide for field and laboratory descriptions of microbialites and to synthesize the various terminologies present in the literature. As a guide, this contribution is meant to complement the various review articles that focus more specifically on the fossil record of microbialites (Hofmann, 1973; Awramik & Riding, 1988; Awramik, 1991; Hofmann, 2000; Rowland & Shapiro, 2002; Riding, 2011a, and references therein). For example, Flügel (2004) provided an excellent analysis of microbialite as a carbonate lithologic unit with much discussion on genesis, diagenesis, and terminology. There have also been significant contributions from non-English literature, primarily by Russian workers (e.g., Maslov, 1960; Krylov, 1963; Raaben, 1991) in addition to other international researchers, including the earliest description of stromatolites (Kalkowsky, 1908). The diversity of unique microbialite textures has produced many study-specific nomenclatures in the primary literature, and increases the difficulty of succinct review. Instead, this chapter synthesizes key features of previously published guides over multiple decades of microbialite research. Nomenclature that has gained acceptance by extensive utilization in the literature is given preference herein, with references provided for more detailed discussions beyond the scope of this review.

HISTORICAL PERSPECTIVE AND WORKING DEFINITION OF THE TERM MICROBIALITE

The word microbialite was introduced by Burne and Moore (1987) as a general term for sedimentary deposits created by the actions of microorganisms (see historical discussion in Riding, 2011a). Current researchers employ the term for microbially induced deposits in general, or when specific discrimination of stromatolitic, thrombolitic, or other textures is untenable. An alternative spelling, microbolite (Riding,

1991), while perhaps more accurate, has not gained traction in the literature. In contrast to microbialites, microbial mats (often shortened to mats) are unlithified, macroscopic microbial communities in modern environments, commonly divided into layers with distinct microbial metabolisms. Special care should be taken to use the terms microbialite and microbial mat only for lithified and unlithified communities respectively, especially in modern and Holocene locations where both structures may be present.

Microbial activity preserved in the sedimentary record includes 1) mineral precipitation within mats due to the physico-chemical properties of microbial communities, and 2) the trapping and binding of detrital grains on and within mat layers (Awramik, Margulis, & Barghoorn, 1976; Burne & Moore, 1987; Noffke & Awarmik, 2013). Microbial deposits predominantly formed by trapping, binding, and stabilization of detrital grains are prevalent in siliciclastic environments and have distinct nomenclatures described in greater detail on p. 76–81. Microbialites described herein are primarily formed via mineralization of mat textures, although detrital grains are commonly important components. The vast majority of microbialites are comprised of calcium carbonate, although many examples have been described comprised of primary opaline silica, oxides, sulfides, phosphates, and other minerals (Walter, Bauld, & Brock, 1972; Wallace, Keays, & Gostin, 1991; Martín-Algarra & Sánchez-Navas, 1995; Berelson & others, 2011). Whereas individual microbes are very rarely preserved within microbialites, specific features in macro- and microscopic textures indicate origination via microbial activity, as opposed to abiogenic sedimentation or precipitation. When microfossils are preserved, the lithified microbialite structure on a microscopic scale may be largely comprised of permineralized skeletons or mineralized molds.

Further refinement of microbialites is based on the mesostructure scale of observation (Fig. 18). Mesostructure refers to the millimeter to centimeter scale elements visible with the unaided eye or hand lens (Kennard & James, 1986). In contrast, microstructure encompasses all observations with a light or scanning electron microscope. The macrostructure refers to the larger association of mesostructural elements (Fig. 19, Fig. 20). For instance, laminae (mesostructure) may be stacked to form a cylindrical column (macrostructure). Some authors employ a larger hierarchical stage, megastructure, to describe the bed or overall stratigraphy of the microbialite-bearing units (Kennard & James, 1986). The necessity of using several scales of description of microbialites is one of the distinguishing features of their taxonomy relative to other fossils (Awramik, 1991; Shapiro & Awramik, 2006). Importantly, microbialites are organosedimentary constructions, and all scales of structure need to be studied for both biogenic and sedimentologic signals. The next sections describe five major categories of microbialites based on mesostructure.

STROMATOLITES

Substrate-attached microbialites with laminated fabrics are defined as stromatolites, deriving from the word stromatolith in Kalkowsky (1908). More than a century of successive studies has produced various definitions of the term stromatolite, both genetic and purely descriptive, as recounted in detail by Riding (2000, 2008). Many arguments center on the difficulty of directly identifying biogenicity in laminated deposits, which stems from 1) the removal of specific biosignatures by secondary alteration, and 2) the morphological similarity of laminated abiological structures to biogenic stromatolites (Grotzinger & Rothman, 1996; Grotzinger & Knoll, 1999). For simplicity, this chapter defines laminated microbialites as stromatolites, as opposed to abiogenic structures formed without the mediation of microbial communities. Recommended guides to stromatolite morphologies and textures include Logan, Rezak, and Ginsburg (1964); Walter (1976); Preiss (1976);

Buick, Dunlop, and Groves (1981); Grey (1989); Riding (1999); and Shapiro (2007), to name a select few.

On a macrostructural level, stromatolites vary from stratiform morphologies with low vertical relief, to simple columns, domes, and cones, to complex branching structures (Fig. *20*). Furthermore, individual stromatolites can change morphologies with successive generations of laminae accretion. For example, slight irregularities of stratiform stromatolites can propagate into larger domes or cones with continued growth. A standard stromatolite classification scheme that accounts for vertical changes in structure is provided in Logan, Rezak, and Ginsburg (1964). Changes in stromatolite morphology can arise from shifting depositional environments, biological communities, hydrochemistry, or all of these factors over time. As previously mentioned, many stromatolite macrostructures resemble laminated textures formed by abiogenic mineral precipitation, especially less complex stratiform or domal morphologies (Grotzinger & Knoll, 1999). Branching and conical morphologies have been hypothesized in simulations of abiogenic mineral growth (Grotzinger & Knoll, 1999; Dupraz, Pattisina, & Verrecchia, 2006), but such macrostructures have not been abiogenically replicated in physical experiments. One detailed method to study stromatolite macrostructure involves serially sectioning samples so that true three-dimensional reconstruction can be quantitatively assessed (see discussion in Hofmann, 1973). A number of publications describe serial sectioning techniques (Krylov, 1963; Preiss, 1976), and the capabilities have been significantly enhanced with modern illustration computer programs. A critical aspect is recognizing that one or several two-dimensional planes are insufficient to truly understand the complexity of stromatolite structures.

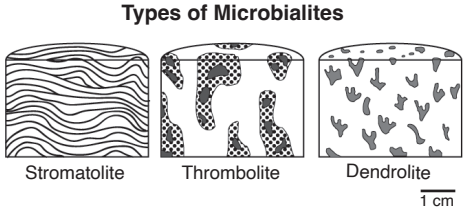

Fig. 18. Main groups of attached microbialites. The different groups are defined based on the mesostructure or constructional elements. Stromatolites are laminated, thrombolites are clotted, and dendrolites are comprised of bushes (new).

Because laminae are the defining mesoscale feature of stromatolites, special detail must be given to describing mesoscale textures. Laminae are typically comprised of light and dark couplets, with darker layers formed

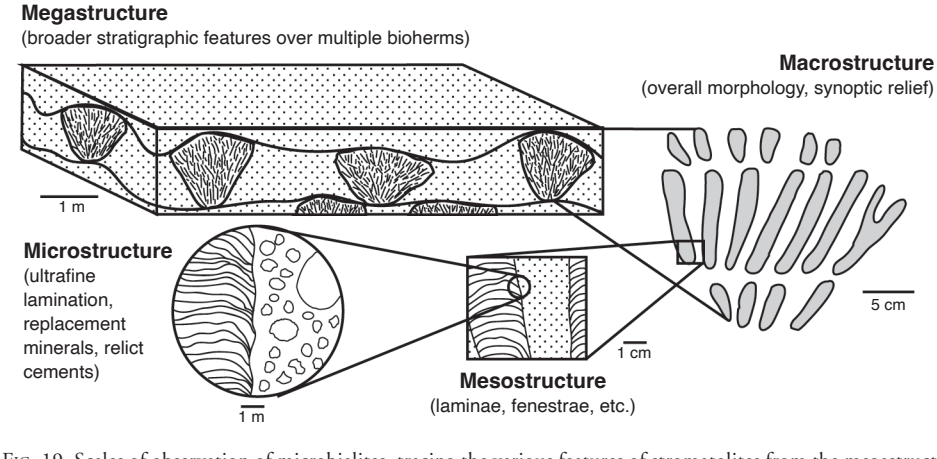

Fig. 19. Scales of observation of microbialites, tracing the various features of stromatolites from the megastructure through the microstructure (adapted from Shapiro & Awramik, 2006, fig. 2).

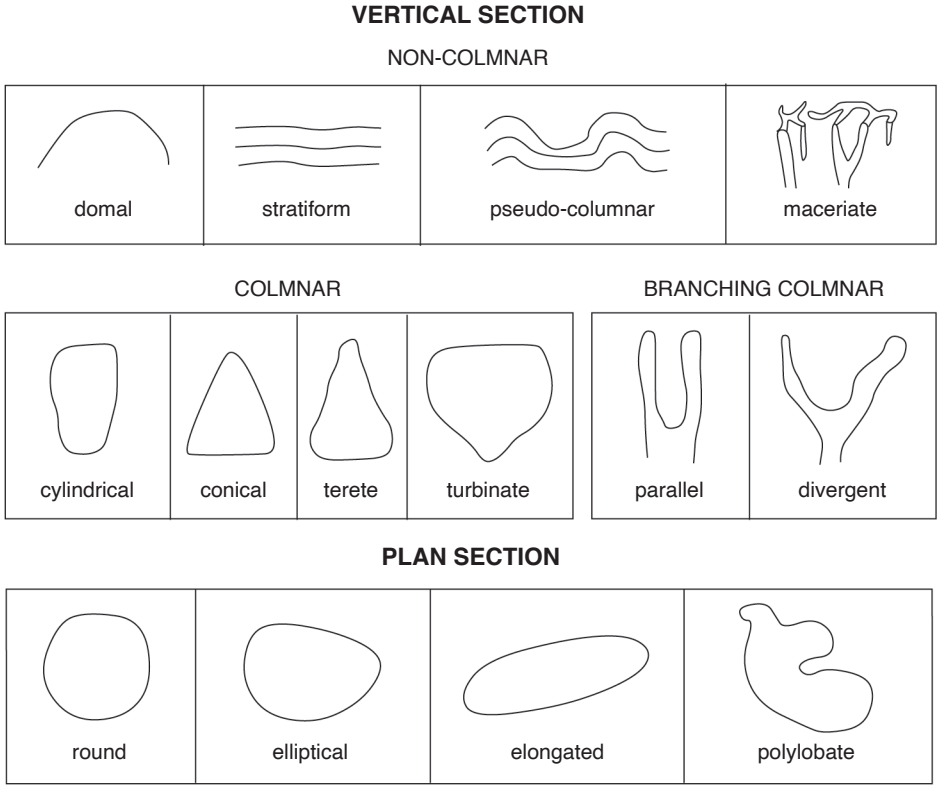

FIG. 20. Descriptive terminology as applied to the macrostructure of all microbialites (new).

by finer-grained, less porous micrite or microspar in carbonates or microcrystalline quartz in cherts (GROTZINGER & KNOLL, 1999). Darker zones can also be attributed to higher concentrations of organic material or insoluble residue such as iron oxides. Lighter laminae are generally defined by higher amounts of cemented interstitial spaces, filled with spar in carbonates or macroquartz in cherts. Microfossils in well-preserved stromatolite laminae have different orientations of filamentous cells, with laminae-parallel filaments in dark layers and laminae-normal or vertical filaments in light layers (GEBELEIN, 1969; WALTER, BAULD, & BROCK, 1972; GOLUBIC & FOCKE, 1978).

Key differences between stromatolites include laminae smoothness or waviness, thickness variation, nature of the laminae over the growth axis (apex), and nature of the laminae against the stromatolite margins (Fig. 21). For example, the height of a stromatolite at a single point in time (synoptical relief) can be established by measuring the vertical distance between the apex of a single layer and the same layer's intersection with the stromatolite margin. Another useful parameter when describing stromatolite textures is inheritance, or how well laminae inherit the shape of preceding layers. For example, a stromatolite that progresses upward from stratiform through domal to conical textures has low inheritance, as laminae over time do not resemble the shapes of lower layers. Conversely, a stromatolite that maintains consistent layer morphologies throughout the structure, whether flat, domal, or conical, has high inheritance.

In well-preserved carbonates, the laminar mesostructure can also help distinguish biogenic stromatolites from abiogenic

precipitates (Grotzinger & Knoll, 1999). Laminae formed within microbial mats are typically comprised of micrite or microspar and have irregular, wavy laminae resulting in low inheritance. In contrast, many laminated abiogenic carbonates are comprised of bladed or acicular needles, maintaining isopachous thicknesses across the stromatolite and extremely high inheritance. There are exceptions to these trends, but a meaningful assessment of biogenicity cannot be accomplished without first analyzing laminae petrography. For example, several lacustrine stromatolites exhibit both styles of lamination, alternating between irregular micritic layers and isopachous bladed fabrics, and have been correlated with changes in lake environments (Frantz & others, 2014; Fedorchuk & others, 2016).

Microstructural attributes vary widely between stromatolites (Fig. 22). The variety of textures observed is due to both depositional heterogeneity and subsequent diagenesis. Original fabrics include detrital grains (micrite, silt to fine sediment, coated grains, skeletal fragments), organic films, and various cements (isopachous rims, bladed fringes, botryoids, etc.). Among the many potential microscopic features within stromatolites, several diagnostic textures can help increase the confidence of stromatolite biogenicity (Buick, Dunlop, & Groves, 1981; Grotzinger & Knoll, 1999). Some Phanerozoic stromatolites preserve microfossils as carbonate permineralized sheaths, such as the filamentous morphotype *Girvanella* (Nicholson & Everidge, 1878), but these are relatively uncommon. Rounded fenestrae, which do not crosscut primary stromatolite textures, represent the preservation of former void spaces within microbial mats, which can be produced either by metabolic gas production or by natural irregularities in microbial mat textures (Sumner, 2000; Bosak & others, 2009, 2010; Mata & others, 2012; Wilmeth & others, 2019). Finally, the presence of detrital grains on sloped laminae that exceed the angle of repose indicate the

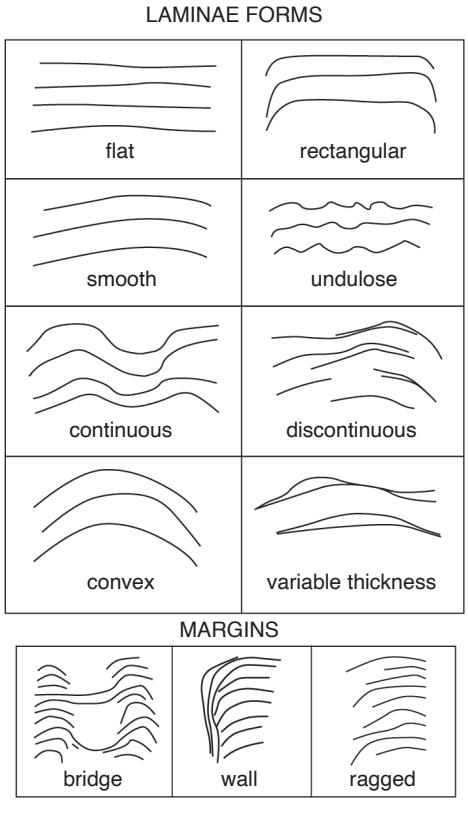

Fig. 21. Descriptive terminology as applied to the mesostructure of stromatolites (new).

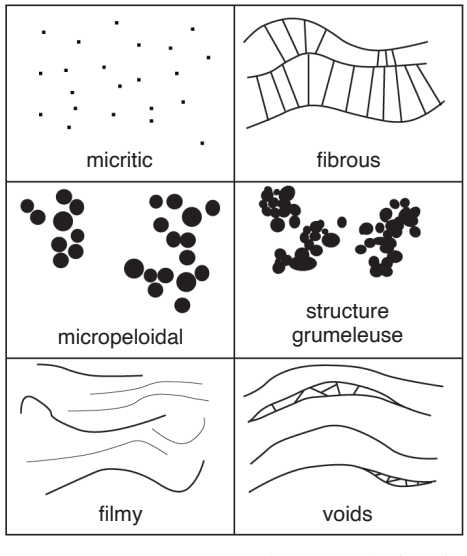

Fig. 22. Descriptive terminology as applied to the microstructure of all microbialites.

presence of adhesive microbial mats rather than pure mineral precipitates (Bailey & others, 2009; Tice, 2009; Frantz, Petryshyn, & Corsetti, 2015).

Early diagenesis in carbonates commonly leads to both micritization and aggrading neomorphic spar, obscuring original textures. Additionally, many stromatolites have destructive replacement of primary fabrics by mosaic dolomite. In some cases, placing a white card underneath a thin section increases the potential to view original textures on a microscope stage (Folk, 1987). Examples indicate that dolomitization is fabric selective, even down to individual laminae (Glumac & Walker, 1997; Riding, 2008). Dolomitization can be accentuated by staining with Alizarin Red to differentiate calcite (stained) from dolomite (unstained). Regardless of the preservation, describing stromatolite microstructure is critical when possible, noting presence or absence of microfossils, and any variation in mineralogy.

ONCOIDS

Oncoids are laminated microbialites that form unattached grains (Heim, 1916; Pia, 1927), in contrast to stromatolites attached to benthic substrates. Oncoids are typically spherical to ellipsoidal in shape, with variably smooth, pustular, or lobate surfaces (Fig. 23) resulting from patterns of primary precipitation and mechanical weathering. Most oncoids are comprised of calcium carbonate, with some siliceous examples surrounding hot springs (Jones & Renaut, 1997; Jones, Renaut, & Rosen, 1999; Konhauser & others, 2001), and several phosphatic and oxide-rich samples are known in ancient lithologies (Krajewski, 1983; Schaefer, Gutzmer, & Beukes, 2001; Gradziński & others, 2004; Sallstedt & others, 2018). For a detailed review of oncoid terminology and sedimentology, including comparisons with other coated grains, see Flügel, 2010.

Internal oncoid mesostructure consists of a nucleus surrounded by a cortex of variously concentric laminae. Nuclei vary depending on depositional environment, and include clastic grains, fossils, or reworked chemical sediments, such as surrounding carbonates or cherts. Nuclei are sometimes absent from samples, depending on diagenetic alteration, the angle of dissection, or an initial particle that was soft and/or featureless (Flügel, 2010). Cortices contain micritic or fine-grained laminae, which vary in thickness and concentricity, in contrast to grains such as ooids and pisoids, which contain radially fibrous, highly concentric laminae. Variable thicknesses of oncoid laminae typically result in low inheritance, leading to asymmetrical shapes including small domes and even cones (Logan, Rezak, & Ginsburg, 1964; Wilmeth & others, 2015). Logan, Rezak, and Ginsburg (1964) included a classification scheme for oncoid morphologies in addition to stromatolite textures. Oncoid laminae are similar in microstructure to biogenic stromatolites, including light and dark couplets, variously oriented microfossils, and rounded fenestrae (Peryt, 1981; Flügel, 2010; Wilmeth & others, 2015; Sallstedt & others, 2018). Microfossils are commonly present as filamentous permineralized sheaths, usually described as the morphotype *Girvanella* (Peryt, 1981; Riding, 1983).

The unattached nature of oncoids, unique among microbialites, provides useful insights into paleoenvironment. An oncoid-rich facies is called an oncolite, as opposed to singular oncoid grains. Oncolites can be described in a similar manner to other grain-dominated facies in terms of sorting, roundness, and grain vs. matrix support. Oncoids and oncolites provide evidence for agitated environments, requiring frequent exposure of fresh surfaces for microbial colonies to grow and eventually mineralize (Dahanayake, 1977; Ratcliffe, 1988). As oncoids grow larger, layers typically become increasingly asymmetrical due to longer periods of quiescence (Wright, 1983; Smith & Mason, 1991; Shapiro, Fricke, & Fox, 2009; Wilmeth & others, 2015). Oncoids

that become too large for continued agitation become the stable base for subseqatolite nucleation (Martín-Algarra & Vera, 1994; Burne & Moore, 1987).

THROMBOLITES

Thrombolites are clotted microbialites (Aitken, 1967). Although the term is nongenetic, the study of thrombolites has indicated that clotted fabrics are largely constructional and not merely secondarily altered stromatolitic textures. Shapiro (2000) addressed the terminological confusion of thrombolites, and further elaboration was provided by Shapiro and Awramik (2006). Because thrombolites lack laminae as a mesostructural fabric, synoptic relief is more difficult to assess. However, column margins and their relationship with surrounding sediments can still hold clues to syndepositional relief, with margins varying between smooth, invaginated, wrinkled, or lobate morphologies. If margin walls are not smooth, it is important to recognize whether surrounding sediments interfinger (low synoptic relief) or truncate against the margin (potentially higher synoptic relief).

The mesostructure of thrombolites is dominated by mesoclots separated by either cements or sediment (Kennard & James, 1986). Mesoclots are millimeter- to centimeter-scale zones of variable texture in both plan and longitudinal sections. Petrographic analysis of the mesoclots reveal them to be comprised of a variety of elements, including coccoid calcimicrobes (Kennard & James, 1986), botryoidal calcimicrobes (Latham & Riding, 1990), filamentous calcimicrobes (Moore & Byrne, 1994), algal-foraminiferal colonies (Toomey & Cys, 1979), dense micrite (Glumac & Walker, 1997), and peloids (Pratt & James, 1982). The distribution of mesoclots across two-dimensional thrombolitic surfaces imparts a clotted composition (see Fig. 24 for a compendium of the more common mesoclot forms as described in the literature).

The term mesoclot was first proposed by Kennard and James (1986) as an emendation for Aitken's (1967) clots, as the latter term was ambiguous and could be mistaken for submillimeter-size clotted microstructures. Other terms employed include fenestrae (Pratt & James, 1982) or thromboids (Kennard, 1994) (see review in Shapiro, 2000). Thromboid is unacceptable because the term is confusing when considering the present non-parallel usage of stromatoid and the multiple, conflicting definitions in the literature. The term fenestrae is not appropriate because it refers to a former void within a rock (Bates & Jackson, 1987) and not all mesoclots were open spaces. As with stromatolite laminae, the morphology and texture of the mesoclots are referred to as the fabric of a thrombolite. Microscopic features of the mesoclots should be described under microstructure. Using the terms macroclots or microclots is not advised, as this will only exacerbate confusion.

The three-dimensional morphology of a mesoclot is referred to as the mesoclot shape. There has not been a quantification scheme proposed for the study of mesoclots;

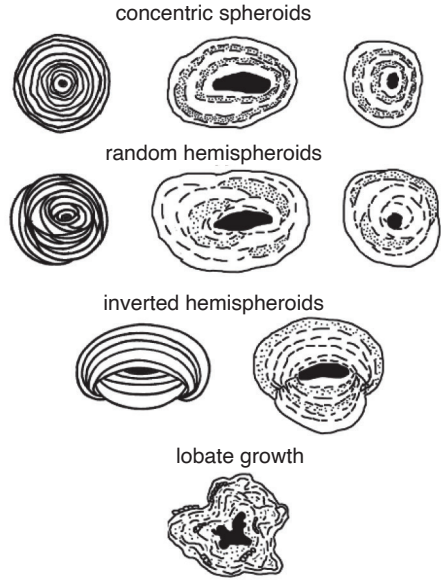

Fig. 23. Descriptive terminology as applied to the macrostructure of all oncoids (adapted from Logan, 1964, as presented in Flüge, 2010).

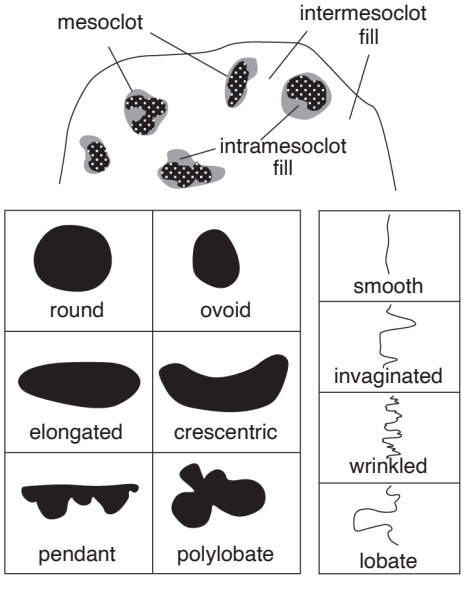

FIG. 24. Descriptive terminology as applied to the mesostructure of thrombolites (new).

the method of geometric study is left up to the discretion of the researcher, with the hopes that clear explanations are given. As with stromatolites, mesostructural aspects of thrombolites are best studied in three-dimensional preparations as their typically polymorphic shapes may present a variety of patterns on two-dimensional surfaces (SHAPIRO & AWRAMIK, 2006). Qualitative description of two-dimensional surfaces are still of great use for field and comparative study and should also be undertaken. To date, most studies have featured longitudinal sections, or mesoclot profiles (e.g., AITKEN & NARBONNE, 1989; KENNARD, 1994). However, much information can be gleaned from plan-view sections or mesoclot outlines. A good practice is to trace the mesoclots physically or digitally to demonstrate clear shapes, and then present patterns in a simple, two-tone scheme. Instead of using vague terms such as irregular or globular, measurements should be made of mesoclot height, length, and width, citing the orientation of the viewing plane relative to the growth axis of the thrombolite. Mention should be made if the mesoclot dimensions vary in different spots within one thrombolite, particularly from the base toward the top of the structure or from the margins toward the center.

The spatial relations of mesoclots can be isolated, interconnected, or coalesced (KENNARD & JAMES, 1986; SHAPIRO & AWRAMIK, 2006). The degree of coalescence can further be qualified as slightly coalesced or highly coalesced. In turn, mesoclots can be arranged in parallel to subparallel patterns within the thrombolite, presenting a horizontal, radial, or vertical mesostructure. Mention should be made of the amount of mesoclots (as percent abundance) within thrombolites.

In addition to mesoclots, the mesostructural analysis should also include descriptions of any voids, inter-mesoclot fill, calcimicrobes, and metazoans. Laminae are extremely rare, but if present should be described following the guidelines set forth for stromatolitic mesostructure. Care should be taken to note the relationship of the laminae to the mesoclots, whether gradational, alternating, or adjacent.

It is common for mesoclots in localized portions or in the entire thrombolite to be oriented in a regular pattern. Although much of the existing literature describes the orientation of thrombolite columns (macrostructure)—often misidentifying the elements as clots or thromboids (see RIDING, 2011a)—the terms here are still applicable to mesoclot orientation. Orientations of the columns should be described under macrostructure. For example, SHAPIRO and AWRAMIK (2006) presented a variety of plan-view shapes of arabesque columns (maceriae) that are macrostructural, as opposed to the mesoclots that comprise the mesostructure of maceriae.

DENDROLITES

Dendrolites are neither laminated nor clotted but are comprised of branching millimeter-scale bushes (RIDING, 1991). The bushes are inferred to be organic in origin, although the exact nature of the biota neces-

sary for the construction is not known. In many structures, bushes can be identified as (inferred genera of) calcimicrobes such as Epiphyton (Bornemann, 1886), *Renalcis* (Vologdin 1932), *Gordonophyton* (Korde, 1973), or *Angusticellularia* (Vologdin, 1962)(Rowland & Shapiro, 2002). The term dendrolite should not be utilized for structures that display branching crystalline growth, which can be easily recognized by clear crystal boundaries and more regular arrangement of the branches (Shapiro, 2004b). Thrombolites and dendrolites may represent end members of a continuum of diagenetic alteration, in which dendrolite bushes recrystallize to amorphic micrite that may then be considered a thrombolitic mesoclot (Riding, 1991).

Dendrolites occur as meter-scale domes, tabular biostromes, and centimeter-scale crusts. It may also be most accurate to refer to the microbial frameworks within archeocyath and lithistid reefs as dendrolite although the term has not been used in that regard. Dendrolites are distinctive but are present alongside and even interfingering with thrombolites and stromatolites. To date, there are few described dendrolites in the literature, although it is likely that some published accounts of thrombolites should more accurately be termed dendrolites. The original papers discussing dendrolites (Riding, 1991; Riding & Zhuravlev, 1995; Turner, James, & Narbonne, 2000; Shapiro & Rigby, 2004) did not propose a formal definition of dendrolite morphology. In a study of three-dimensional dendrolite reconstruction, Howell, Woo, and Chough (2011) proposed terminology for the dendrolite elements. Herein, a model (Fig. 25) is provided that merges the suggestions of that paper with published accounts of other occurrences, including Cambrian and Devonian samples (Riding & Zhuravlev, 1995; Turner, James, & Narbonne, 2000; Kruse & Zhuravlev, 2008). Howell, Woo, and Chough (2011) suggested several tiers of mesostructure based on growth structure of the dendroids, which

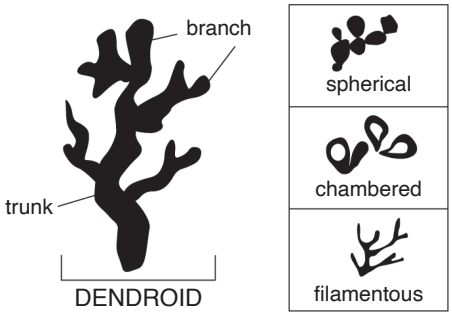

Fig. 25. Descriptive terminology as applied to the mesostructure of dendrolites (new).

may prove to be a valuable level of differentiation in future studies.

LEIOLITES

Braga, Martin, and Riding, 1995 suggested the term leiolite to encompass microbial constructions that lack diagnostic mesoscale structure. There are many pathways to create massive structure (e.g., irregular accretion of microspar, extensive boring or bioturbation, or burial dolomitization), but the term leiolite is valuable as it is non-genetic and does not presume a prior mesostructure. If, however, the microbialite can be shown to have originally been laminated, clotted, or dendrolitic, the pre-alteration terminology should be utilized. It may be possible to recognize pre-alteration original fabrics in dolomitized leiolites using the white card technique of Folk (1987). Leiolites have not received the same amount of descriptive study as other microbialites, although a further short review can be found in Riding (2000).

MODELS OF MICROBIALITE FORMATION

No single model of formation produces the variety of microbialites described above. The mineralization of a microbial mat is the final result of interplay between the physical sedimentary environment, surrounding chemical parameters (temperature, mineral saturation states), and biological processes within microbial communities themselves (Riding, 2000;

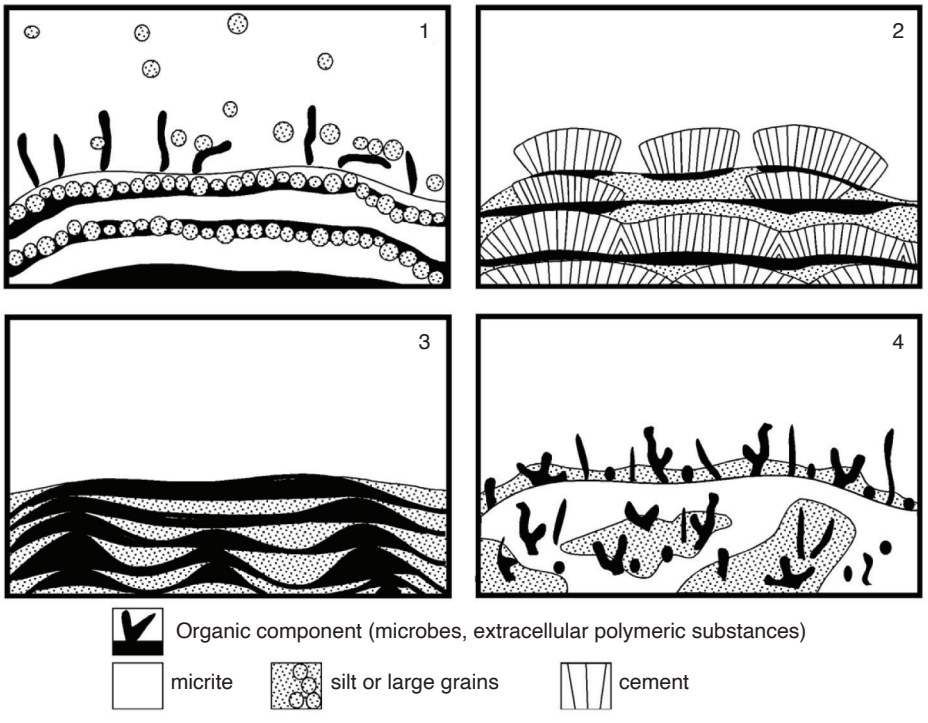

FIG. 26. Models of formation of microbialites. *1,* Trapping and binding of particles; *2,* precipitation of cement layers; *3,* entombing of sediments by mats or extracellular polymeric substances; *4,* skeletal algae or metazoans (adapted from Shapiro, 2007, fig. 3).

SHAPIRO, 2007; DUPRAZ & others, 2009). In contrast, the shells and tests of organisms described in other volumes of the *Treatise,* although influenced by surrounding chemistry, are directly formed from the cellular activity of eukaryotes (WEINER & DOVE, 2003). Microbialites can also be considered as trace fossils, recording the previous activity of localized microbial ecosystems, but only rarely preserving the organisms themselves (SHAPIRO, 2007). A further discussion on the differences between microbial and metazoan biomineralization, as well as modern processes of microbialite formation, is provided in DUPRAZ and others (2009).

Broadly speaking, there are four models that encompass microbialite formation, and any one deposit may have components of all four (Fig. 26). 1) The physical properties of microbial mats commonly result in the trapping and binding of sedimentary particles, either by filamentous cells or adhesive extracellular polymeric substances (EPS) produced by the mat (GEBELEIN, 1969; RIDING, 1991; FRANTZ, PETRYSHYN, & CORSETTI, 2015). Most Phanerozoic and many Proterozoic marine stromatolites preserve detrital material, with grains ranging from clay through sand-sized particles. Further cementation of the grains within mats may be accomplished below the accreting and stabilizing surface by heterotrophic bacteria and other biota. 2) Mineral precipitation within microbial mats is induced by elevated saturation states in surrounding waters, occurring both on cells and on organic compounds such as EPS (ARP, 2001; ARP, REIMER, & REITNER, 1999, 2004; REID & others, 2000; DUPRAZ & VISSCHER, 2005; BRAISSANT &

others, 2007). Mineral saturation states can be altered by metabolic processes of living organisms, such as photosynthesis, respiration, or chemosynthesis (biologically induced mineralization; Dupraz & others, 2009). Alternatively, chemical changes in the surrounding environment can also force mineral precipitation, with mats serving as a nucleation site (biologically influenced mineralization; Dupraz & others, 2009). Many Archean and Paleoproterozoic stromatolites are comprised of precipitated cement layers (Riding, 2008, 2011a), although the role of diagenesis in promoting aggrading neomorphic spar must also be considered. 3) A third model, typified by the Omachta Formation of Siberia, comprises stromatolites that form not from trapping sediments but from microbial mats enclosing sediments that have already been deposited. This construction preserves signatures of mechanical deposition such as crossbeds and ripples (Knoll & Semikhatov, 1998). 4) A fourth model of formation recognizes the importance of skeletal algae, foraminifera, and invertebrates in comprising a significant component of Phanerozoic microbialites (Riding, 1977). There may be secular trends to both abundance and diversity of these skeletal microbialites related to evolutionary patterns of the constructors as well as ocean chemistry (Riding, 1977, 2011a).

Important to note, the vast majority of described microbialites occur in carbonates and thus are susceptible to the myriad of diagenetic processes that affect all carbonate facies (Beukes, 1987; Burne & Moore, 1987; Planavsky & others, 2009; Pace & others, 2016). Such considerations include near-surface void cementation and dissolution in the phreatic and vadose zone, recrystallization or aggrading neomorphism in shallow burial conditions, and significant dissolution and reprecipitation under deeper burial conditions. Replacement by silica is common and can be either fabric retentive or destructive. Therefore, interpreting the model of formation of all microbialites must take into account the effects of secondary diagenesis.

MODERN STRUCTURES

Both microbial mats and subsequently mineralized microbialites are known from many different facies. Rather than attempt to provide a comprehensive list or to fit microbialites into generic facies models, this section will highlight unique attributes of several key modern environments.

Peritidal Open Marine and Reef

Some of the most well-studied modern microbialites are found in the intertidal embayment of Shark Bay, Western Australia (Logan, 1961; Hofmann, 1973; Chivas, Torgersen, & Polach, 1990; Reid & others, 2003) and unrestricted tidal channels of the Bahamas (Dravis, 1983; Dill & others, 1986; Shapiro & others, 1995; Andres & Reid, 2006; Planavsky & Ginsburg, 2009). These microbialites are predominantly stromatolites with laminae comprised of fine- to medium-sized grains and cement, although coarser textures have been diagnosed as thrombolites (Planavsky & Ginsburg, 2009; Riding, 2011a).

Other significant but overlooked modern peritidal microbialites include reef and cryptic crusts (Camoin & others, 1999), which are also well described from Paleozoic and Mesozoic reefs (e.g., Flügel & Steiger, 1981; Leinfelder & others, 1996). Whereas the textures of modern peritidal deposits are fairly uniform, macrostructure varies with respect to current and wave conditions. In particular, modern peritidal stromatolites have very high relief from the seabed (although not necessarily a high synoptic relief within individual laminae), and columns typically have a pronounced elongation of the major axis. In most cases, the elongation is parallel to tidal flow and perpendicular to wave crests. Overall stromatolite size also decreases away from the tidal zone toward the margins of deposits.

Biological studies of peritidal microbialites typically focus on extensive cyanobacterial

communities, both for the ability of cyanobacteria to bind detrital grains and for influence local carbonate saturation states (Gebelein, 1969; Reid & others, 2000). However, many other organisms also contribute to microbialite growth, including diatoms and other algae trapping grains (Awramik & Riding, 1988) and cement precipitation mediated by heterotrophic bacteria (Visscher & others, 1998; Reid & others, 2000). Modern stromatolites also host localized ecosystems of corals and sponges in addition to algae and microbial mats. Similar microbialite-metazoan reefs are well known throughout the Phanerozoic and Neoproterozoic (Riding, 1991; Rowland & Shapiro, 2002; Grotzinger, Adams, & Schröder, 2005). However, the relatively coarse grains and common presence of eukaryotes within modern peritidal microbialites limits their capabilities as faithful analogs for many ancient examples, especially in Precambrian environments.

Lacustrine

Microbialites are present in a number of lacustrine settings across various climates, typically as calcitic thrombolites and stromatolites with distinct micritic or micrite-microspar laminae (Burne & Moore, 1987; Winsborough & others, 1994; Laval & others, 2000; Gischler, Gibson, & Oschmann, 2008). Lacustrine microbialites occur across a greater range of depths than within marine peritidal zones, although most deposits form near lake surfaces (e.g., Kempe & others, 1991). Sharp depth gradients of geochemistry, temperature, and light produce distinct microbialite biofacies. For example, microbial mats within deeper lake waters typically have higher vertical relief for photosynthetic organisms to access more sunlight, forming textures such as pillars or cones (Laval & others, 2000; Andersen & others, 2011). Lake depth profiles and chemistry also change more dramatically during short-term climate fluctuations than in marine peritidal environments, especially in closed basin lakes where evaporation and precipitation dominate water budgets (see *Geological Significance of Microbialites,* p. 69). Relatively rapid depth and climate changes can produce distinct fabrics in lacustrine microbialites, particularly in stromatolites (Frantz & others, 2014; Fedorchuk & others, 2016).

Springs

Both carbonate and silica microbialites are well known from modern hot and cold springs (Weed, 1889; Jones & Renaut, 1997; Turner & Jones, 2005). Modern spring microbialites are of low areal extent compared with peritidal and lacustrine examples, although wetter climates generally lead to increased discharge rates and more extensive deposits (Bargar 1978; Guo & Riding, 1998). Most described spring microbialites are stromatolitic, with macrostructure varying as flow gradients shift from the vent to outflow apron (Walter, Bauld, & Brock, 1972; Jones, Renaut, & Rosen, 1998). Differentiating true biologically mediated microbialites from abiogenic deposits (e.g., tufa, travertine, and sinter) is a continuing challenge, because many spring deposits are thinly laminated without the presence of microbial mats (Konhauser & others, 2003; Riding, 2008). However, recent work on silica-cemented microbial textures has demonstrated exquisite preservation of microbial cells (Schultze-Lam & others, 1995; Konhauser & others, 2001; Mata & others, 2012), although it remains to be shown if this preservation would persist through early diagenesis.

Hydrocarbon Seeps

Both stromatolitic and thrombolitic textures have been described at hydrocarbon seeps, but many deposits are neither laminated nor clotted and would best be termed as leiolites (Greinert, Bohrmann, & Elvert, 2002; Shapiro, 2004a; Lloyd & others, 2010). The microstructure of seep microbialites is noteworthy for abundant non-fecal micropeloids, dissolution surfaces, yellow, bladed calcite cements, and arago-

nitic botryoids (Campbell, Farmer, & Des Marais, 2002), although carbonate fabrics themselves are not conclusive of a hydrocarbon source. Instead, microbial carbonates with substantially depleted $\delta^{13}C$ signatures are a common indicator of hydrocarbon seeps (Aharon, 2000) and reflect either thermogenic or biogenic methane as sources of carbon (Birgel & others, 2006). The co-occurrence of chemosynthetic metazoans alongside localized carbonate deposits within a siliciclastic lithofacies provides additional biological and sedimentary evidence for hydrocarbon seeps.

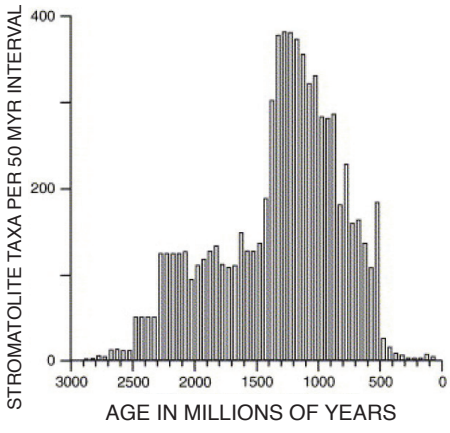

Fig. 27. Stromatolite abundance plot of Awramik and Sprinkle (1999) as presented in Riding (2006).

ANCIENT EXAMPLES

Precambrian

The great antiquity of stromatolites cannot be overstated. Dating back nearly 3.5 billion years (Ga), stromatolites have a sporadic but impressive preserved fossil record through Archean and Proterozoic deposits (Hofmann, 2000; Schopf, 2006b). Nutman and others (2016) recently report stromatolitic textures in 3.7 Ga carbonates from Isua, Greenland, but subsequent studies argue that domal and conical textures are the result of secondary alteration (Allwood & others, 2018). The oldest definitive Archean stromatolites are from the Pilbara Craton of Australia, including the 3.5 Ga Dresser Formation (Walter, Buick, & Dunlop, 1980; Van Kranendonk, 2006; Van Kranendonk, Webb, & Kamber, 2003), and the 3.2 Ga Strelley Pool Chert (Lowe, 1980; Allwood & others, 2006), as well as 2.7–2.5 Ga Fortescue and Hamersley Group deposits (Buick, 1992; Lepot & others, 2008; Hickman, 2012).

The Kaapvaal Craton of South Africa also contains a variety of Archean stromatolites and other microbial textures, including the Buck Reef Chert, Pongola and Ventersdorp Supergroups, and the Campbellrand-Malmani Dolomite (Buck, 1980; Beukes, 1987; Beukes & Lowe, 1989; Sumner, 1997, 2000; Tice & Lowe, 2006; Homann, 2019; Wilmeth & others, 2019). Other Archean stromatolite locations include the Superior and Slave Cratons (Canada), the Dharwar and Singhbhum Cratons (India), the Yilgarn Craton (Australia), and the Zimbabwe Craton (Hofmann, 2000; Schopf, 2006b).

The Precambrian microbialite record is rich and diverse enough to suggest secular variation in stromatolitic attributes (Grotzinger & Knoll, 1999). In general, stromatolites are less common in the Archean (although this is likely a function of lack of preserved suitable facies within greenstone belts) and increase in both diversity and abundance through the Paleoproterozoic, reaching a maximum in the Mesoproterozoic (Awramik & Sprinkle, 1999) (Fig. 27). The Proterozoic increase in microbialite abundance and diversity has been linked to the development of large continents with stable continental shelves where extensive shallow-marine carbonates can form (Eriksson & others, 2006, 2007). Although stromatolites and thrombolites continued to dominate shallow water carbonates during the Neoproterozoic, overall microbialite diversity decreased during this era (Grotzinger, 1990; Awramik & Sprinkle, 1999). Lacustrine and spring microbialites have also been described as early as the Archean, although smaller primary spatial extents limit the number of known locations (Buck,

1980; Buick, 1992; Djokic & others, 2017; Wilmeth & others, 2019). Many researchers have developed biostratigraphic schemes for correlating Precambrian deposits (e.g., Cloud & Semikhatov, 1969; Knoll & Semikhatov, 1998; Semikhatov & Raaben, 2000) although not without controversy.

There are several features of Precambrian stromatolites that segregate them from younger, Phanerozoic counterparts. Precambrian stromatolites are fine grained, with most Archean and Paleoproterozoic forms dominated by crystalline microfabrics (Riding, 2008). Some have argued that Precambrian stromatolites are more likely to host abiotic crystal precipitate layers than their Phanerozoic counterparts (Grotzinger & Knoll, 1999). Precambrian deposits contain extremely large stromatolites, measured in tens of meters in height and diameter, including size ranges that are not known from the Phanerozoic (Beukes, 1987; Fralick & Riding, 2015). In contrast, ministromatolites one to several millimeters across are most common in the Neoarchean and Paleoproterozoic (Hofmann & Jackson, 1987; Medvedev & others, 2005). Upper Paleoproterozoic and Mesoproterozoic marine stromatolites display many diverse macrostructures rarely observed in Phanerozoic deposits, including simple and complexly branching forms (Cloud & Semikhatov, 1969; Awramik & Sprinkle, 1999). In terms of size, fabric, and morphology, uniformitarian principles do not allow for clear correlation from modern marine stromatolites to the vast Precambrian record.

Phanerozoic Marine and Lacustrine

Phanerozoic marine microbialites are noteworthy for their relatively simplistic morphologies compared with Proterozoic forms. Even when comprising kilometer-scale bioherms and biostrome deposits, most Phanerozoic microbialites are dominated by simple centimeter- to meter-scale, unbranched columns comprised of irregular but roughly parallel laminae. Detrital grains become increasingly important fabric components over time, typically as fine- to medium-grained sediments.

Another noteworthy development in Phanerozoic (and Neoproterozoic) microbialites is the addition of algae, foraminifera, poriferans, and other metazoans to the construction. The role of metazoans ranges from passive benthic filter feeders that use the rigid developing microbialite as a base to active constructors (Dupraz & Strasser, 1999; Kershaw, Zhang, & Lan, 1999; Ricardi-Branco & others, 2018). Thrombolites first appear in the Neoproterozoic (although there are reports from the Paleoproterozoic) and are common during the middle Cambrian through Lower Ordovician (Kennard & James, 1986; Kah & Grotzinger, 1992; Rowland & Shapiro, 2002). Thrombolites also increase in abundance during the Devonian, Mesozoic, and locally during the Neogene (Kennard & James, 1986; Shapiro, 2000).

The fossil record of dendrolites is still poorly established, but deposits are abundant in the Cambrian with potential resurgences in the Devonian and Jurassic (Shapiro & Awramik, 2000). It is likely that previously published reports of thrombolites will be revised as dendrolites with further study, because the two forms were not distinguished in the past. Oncoids, which had been present since the Archean, also had an increase in abundance during the Cambrian, as well as the appearance of filamentous *Girvanella* microfossils (Shapiro, 2004b).

It is important to note that Phanerozoic lacustrine and fluvial stromatolites can be quite diverse with respect to macrostructure, with many forms developing columns and pseudocolumns on upper surfaces. In microstructure, lacustrine stromatolites are typified by more regular, repeating couplets of laminae, separated by sharp boundaries. Primary cement fabrics such as botryoids and isopachous bladed calcite are also more common in lacustrine stromatolites than their marine counterparts (Casanova, 1994), and a challenge of lacustrine stromatolite description and terminology is

differentiating organically mediated accretion from presumably abiogenic tufa (Riding 2008; Petryshyn & Corsetti, 2011).

GEOLOGICAL SIGNIFICANCE OF MICROBIALITES

Hofmann (1973) detailed 15 different geological topics where microbialites can be utilized, ranging in scale from geopetal indicators to evidence for the oldest life on Earth. Subsequent studies have further expanded the significance of microbial deposits, particularly in the fields of geochemistry, geobiology, and astrobiology. Rather than cover each topic in detail, this section lists several applications for researchers to consider when studying microbialites. A unifying principle behind many of these applications is that as benthic trace fossils, microbialites can faithfully record *in situ* biological, sedimentary, and geochemical conditions during formation.

MICROBIALITES AS FACIES INDICATORS

For many geologists, a significant value of microbialites is their use as facies indicators. For example, microbialite facies definitions have recently become important after the announcement of vast carbonate reservoirs in the deep pre-salt deposits of offshore Brazil, which may be microbialite or tufa in origin (Awramik & Buchheim, 2012; Muniz & Bosence, 2015). Yet, like most carbonate deposits, there are few generalities that apply to the vast rock record, and uniformitarian principles do not always apply to ancient microbialites. In particular, the utility of stromatolites has been hampered due to what has been termed the Shark Bay Effect. Although Black (1933) described modern stromatolites from the intertidal flats of Abaco Island, Bahamas, the forms were small and the widespread applicability was not realized. The discovery of meter-scale buildups in Shark Bay, Western Australia (Logan, 1961) revolutionized the field and provided a key analog of a restricted marine, hypersaline, intertidal setting. Subsequently, nearly all fossil stromatolite buildups were interpreted—or reinterpreted—as hypersaline and intertidal, even when the deposit lacked additional criteria for recognition such as mudcracks, herring-bone crossbeds, or evaporate molds. Therefore, the discovery of morphologically similar stromatolites in subtidal, normal marine tidal channels of Eleuthera (Dravis, 1983) and the Exuma (Dill & others, 1986) Islands, Bahamas, opened the door to much broader interpretation of microbialite depositional environments.

Although the diversity of microbial forms produces many unique sedimentary facies, there are several trends in the facies applicability of microbialites that are corroborated across multiple studies. A few general observations are listed below, with the volume edited by Riding and Awramik (2000) providing an excellent resource for more detailed comparisons of different facies models. In most deposits, microbialites form on flooding surfaces, with stromatolites occurring in shallower water than thrombolites do. Stratiform deposits are typically indicative of intertidal conditions, as is the case with crinkly microbial mats. In plan view, if a significant major axis develops, it is likely that the axis parallels the dominant current. Branching appears to be related to an increase in sedimentation relative to growth rates. Other models will no doubt be added as additional studies are published.

BIOSTRATIGRAPHY OF MICROBIALITES

The biostratigraphic utility of microbialites remains a debated topic. Because microbialites are produced by microbial ecosystems rather than by individual organisms, biostratigraphic studies are often highly scrutinized (Grotzinger & Knoll, 1999; Bosak, Knoll, & Petroff, 2013). However, even though microbial structures are not subject to the same evolutionary patterns that govern eukaryotic index fossils, Proterozoic deposits typically contain temporally constrained patterns of unique stromatolite

morphologies. Early observations led Soviet scientists to employ a biostratigraphic zonation for the Siberian Platform (see reviews in Cloud & Semikhatov, 1969). Similar patterns have subsequently been described across various Proterozoic basins, most notably in Australia (Grey & Thorne, 1985; Hill, Cotter, & Grey, 2000). Most stratigraphic studies are restricted to intra-basinal deposits, although some have attempted to expand correlations between cratons (Medvedev & others, 2005; Grey, Hill, & Calver, 2011). A few case studies have also employed microbialites for correlation in early Phanerozoic deposits (Shapiro & Awramik, 2000, 2006). The governing forces behind widespread changes in Proterozoic stromatolite morphologies still remain enigmatic, potentially representing large-scale shifts in climate, biology, or geochemical cycles (Semikhatov & Raaben, 2000).

MICROBIALITES AS SIGNALS OF ENVIRONMENTAL CHANGE

Microbialite abundance and diversity broadly decrease across the Phanerozoic, and relatively sudden increases in microbialite deposits appear to be linked to shifts in climate, metazoan ecology, or both. For example, the end-Devonian and end-Permian mass extinctions are associated with increased microbialite abundance, as reviewed in Mata and Bottjer (2012). Many studies note the expansion of microbialites across ramp, platform, and shelf environments after the end-Permian mass extinction, the most devastating in Earth history (Schubert & Bottjer, 1992; Baud, Cirilli, & Marcoux, 1997; Baud, Richoz, & Pruss, 2007; Pruss & others, 2006; Kershaw & others, 2007; Mata & Bottjer, 2011). Even though the end-Devonian event was less severe regarding metazoan diversity, microbialites flourished during the aftermath (Playford, 1980; Wood, 2000; Webb, 2002; Whalen & others, 2002). Various hypotheses exist as to why microbialite abundances are less pronounced during other mass extinctions, including ecospace competition from bioturbating and reef-building organisms, as well as carbonate availability (Mata & Bottjer, 2012).

In addition to providing sedimentary evidence for ecological shifts, microbialites have the potential to record geochemical signatures of climate and environmental change. Stromatolites can contain especially detailed records of local geochemistry over time, with each layer representing a distinct period of microbial growth and mineral precipitation. Strong climate signals are observed from stromatolites within closed lake systems, where concentrations and isotopes of stable elements are controlled by variations in evaporation and precipitation (Talbot, 1990). Studies of lacustrine stromatolites have focused on several Cenozoic climate changes relevant to modern interest, including the Early Eocene Climatic Optimum and Plio-Pleistocene trends (Abell & others, 1982; Frantz & others, 2014; Petryshyn & others, 2016), with occasional studies investigating Mesozoic environments (de Wet & Hubert, 1989; Woo & others, 2004). Geochemical analyses of microbialites from any age or environment need to first analyze diagenetic and/or metamorphic alteration of minerals before collecting data, especially in easily altered carbonate minerals.

CONCLUSION

More than three billion years of interactions between microbial mats and their surrounding environments has produced a staggering diversity of microbialites. Many macroscale morphologies and mesoscale textures are specific to certain times and facies, and a detailed analysis of every form of microbial deposit would require a separate treatise for adequate description. The reader is invited to further investigate specific topics presented by consulting the reviews and primary literature cited herein.

MICROBIALLY INDUCED SEDIMENTARY STRUCTURES (MISS)

Nora Noffke, Hugo Beraldi-Campesi, Flavia Callefo, Noelia Carmona, Diana G. Cuadrado, Keyron Hickman-Lewis, Martin Homann, Ria Mitchell, Nathan Sheldon, Francis Westall, and Shuhai Xiao

INTRODUCTION

To date, microbialites include five groups: stromatolites, thrombolites, leiolites, and dendrolites. All these microbialites occur in carbonate or silica lithologies. However, research during the past 25 years has defined an additional group of microbialites that occurs predominantly in clastic deposits. These structures are called microbially induced sedimentary structures, commonly simply abbreviated to MISS. The morphologies of MISS do not resemble those of precipitated microbialites due to the much different formation and different location of these structural groups. The genesis of the main types of MISS has been elucidated in studies in modern environments. The results were key for the search of such structures in the fossil record. Systematic exploration from youngest to oldest stratigraphic successions has given rise to a data set that allows identification of MISS in respective paleoenvironments. MISS are biosignatures helpful to understanding aspects of prokaryote evolution and the search for life on other planets.

BIOFILMS AND MICROBIAL MATS

Modern sedimentology recognizes that benthic microbiota are (and have always been) part of every sediment and that microbial activities may substantively contribute to sediment formation and lithification (Fig. 28).

In close-up view, sedimentary deposits are widely colonized by a great variety of benthic microorganisms. Most of these microbes organize into aggregates called biofilms, which are attached to a surface. Biofilms are probably the most common organization of life, developing everywhere in nature provided that water molecules and a surface are present (Stoodley & others, 2002; Neu, 1994; Gerbersdorf & others, 2008; Stal, van Gemerden, & Krumbein, 1985; Ramsing, Ferris, & Ward, 2000; Franks & Stolz, 2009; Gerbersdorf & Wieprecht, 2015; Espinoza-Ortiz & Gerlach, 2021). Biofilms include both microbial cells and their extracellular polymeric substances (EPS); (e.g., Decho, 1990, 1994). EPS are cohesive mucilages comprised of complex polysaccharide biomolecules that provide a suitable microenvironment for the microorganisms, buffering against rapid environmental changes, such as desiccation, sudden salinity changes, and other environmental stressors (Decho, 1994; Flemming, Neu, & Wozniak, 2007; Westall & Rince 1994; Westall & others, 2000). These mucilages serve to anchor cells on their substrate or enable the motion of cells within the structure of the biofilm. Biofilms are therefore assemblages of cells working interdependently with each other with the ultimate aim of effective resource exploration. In a biofilm community, cells are arranged in certain positions relative to one other, allowing collaborative nutrient harvesting and consumption (Decho, 1994). Biofilm research, especially in the medical sciences, reveals a complex pattern of communication between cells. Such communication takes place between different groups of prokaryotes and even some eukaryotes. Quorum sensing between members of the biofilm ensures targeted action of the community (Waters & Bassler, 2005; Decho, Norman, & Visscher, 2010; Decho, & Gutierrez, 2017).

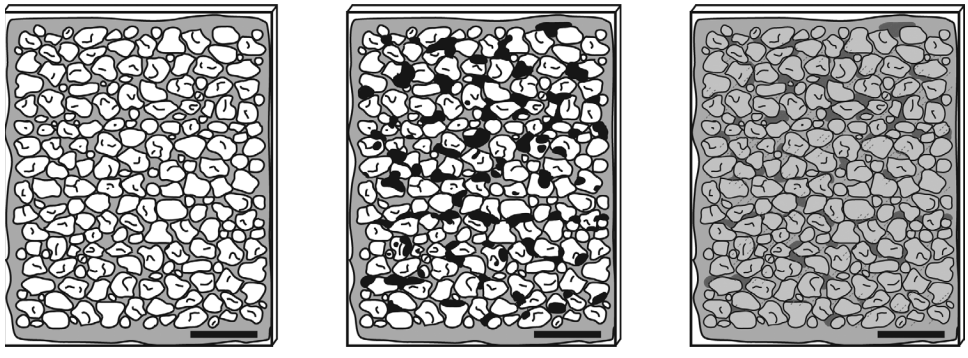

FIG. 28. Biofilms in classic and modern sedimentology. Modern sedimentology understands sediment not as a mere assemblage of mineral grains. Rather, biofilms colonize particles of sediment as long as water molecules are present. *In situ* lithification of the biofilm adds to cementation during diagenesis.

In marine settings, biofilms may merely envelope a sedimentary grain (Fig. 29.1); however, at suitable natural sites, they may develop into large, macroscopically visible layers. Such large-scale organic layers are termed microbial mats (Fig. 29.2–29.3).

In sedimentology, classical and well-studied examples of microbial mats include so-called algal mats in tidal settings, predominantly those constructed by cyanobacteria (BLACK, 1933; HARDIE & GARRETT, 1977; HORODYSKI, BLOESER, & VONDER HAAR, 1977; KRUMBEIN, 1983; GERDES, KRUMBEIN, & REINECK, 1985; COHEN & ROSENBERG, 1989; GERDES & KRUMBEIN, 1987; REINECK & others, 1990; GINSBURG, 1991; VAN GEMERDEN, 1993; STAL & CAUMETTE, 1994; TAHER & others, 1994; REID & others, 1995; STOLZ, 2000; PEARL, PINKNEY, & STEPPE, 2000; GERDES, KRUMBEIN, & NOFFKE, 2000; VASCONCELOS & others, 2006; TAHER, 2014). However, there are many types of microbial mats in a great array of environments including the deep-water marine (e.g. GALLARDO, 1977; HEIJS, SINNINGHE DAMSTE, & FORNEY, 2005; GALLARDO & ESPINOZA, 2007). Despite their impressive sizes—sometimes many square kilometers—microbial mats are still nothing more than biofilms.

A look at the vertical organization of a microbial mat reveals that it is comprised of a stack of horizontal layers, each of which is dominated by a microbial community different to that of the layer above or below (Fig. 30). This arrangement into layered communities has been investigated with the example of the multicolored sand flat (microbial mats in tidal flats) in great detail (STAL, VAN GEMERDEN, & KRUMBEIN,1985; VISSCHER & STOLZ, 2005). The metabolic activities of the community of each layer interlock with the metabolic activities of the communities in the layers directly above and below. This interlocking arrangement results in a complex interactive system best described as a cooperative of microbial groups. It functions as what could be called a "disassembly line" that harvests energy from the environment and transforms it through many steps first into organic matter and then into mineral substances (STAL, VAN GEMERDEN, & KRUMBEIN,1985; DES MARAIS & CANFIELD, 1994; VISSCHER & STOLZ, 2005; DUPRAZ & others, 2009; BLUMENBERG, THIEL, & REITNER, 2015) (Fig. 30).

In modern tidal flats, the top layer of microbial mats comprises photoautotrophic cyanobacteria that, as primary producers, harvest sunlight and store this energy as biomass. The layer immediately beneath the cyanobacteria includes chemoorganotrophic microbes that gain energy by disintegrating

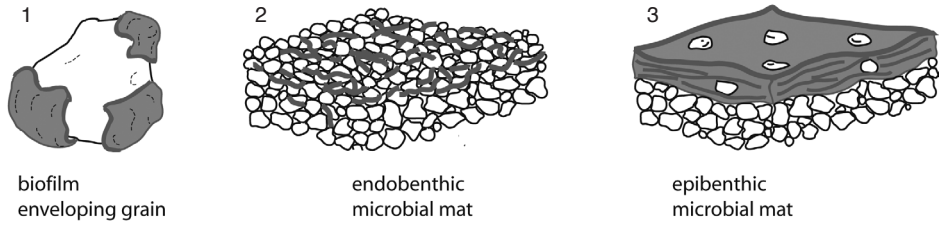

FIG. 29. The three endmembers of microbenthos type in an aquatic setting. A biofilm (*1*) is a microscopic coating around individual mineral grains. A microbial mat (*2–3*) is a macroscopic biofilm covering wide areas of sedimentary surfaces, sometimes square kilometers. Microbial mats can be separated into endobenthic mats, which occur within the uppermost layers of sediment (*2*), and epibenthic mats (*3*), which grow on top of the sediment surface. Sizes of grains, ~0.2 mm.

the complex biomolecules of the primary producers into inorganic compounds. Further beneath, in the third layer, these inorganic compounds are further disassembled by chemolithotrophic microbes. At the base of this stack of layers, small molecules such as methane and ions are released, for example by methanogenic bacteria or archaea (KINSMAN-COSTELLO & others, 2017). The finally released cations and anions at the base of the disassembly line immediately react with chemical compounds suspended in the surrounding water and sediment (SCHULTZE-LAM & others, 1996). The results of these reactions can be nucleation points for mineral precipitates. Because the first mineral precipitates still include water molecules, they are commonly amorphous. In carbonate regimens, early crystalline dolomite or calcite may form, typically directly nucleating in the EPS (VAN LITH & others, 2002; SÁNCHEZ-ROMÁN & others, 2008; DUPRAZ & others, 2009). Later, during diagenesis, larger-scale crystallinity develops. Such processes lead to the replacement of organic matter by inorganic mineral

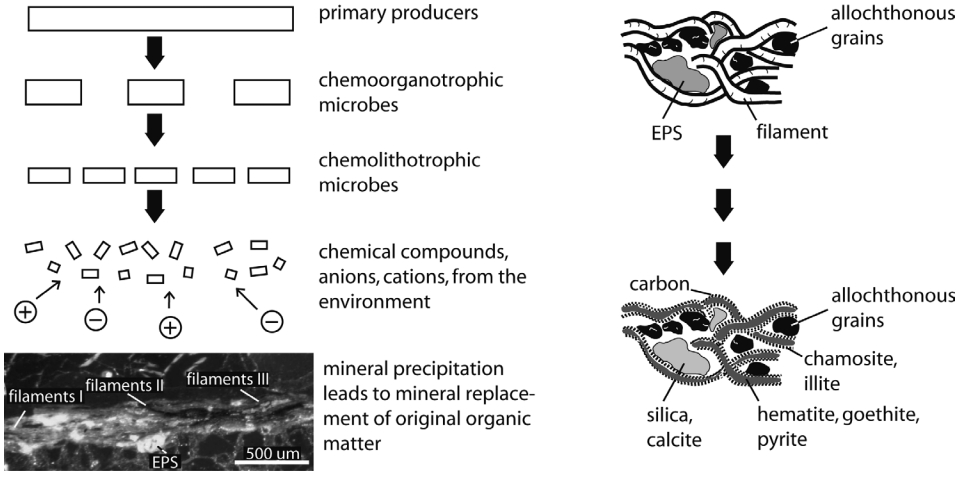

FIG. 30. The microbial energy disassembly line of a microbial mat (*left*) and the resulting formation of minerals (*right*). Left: The primary producers in the top of the mat harvest solar energy via photosynthesis and transform it into organic matter. This organic matter serves as the energy source for various heterotrophic microbial groups in deeper parts of the mat. *In situ* precipitation of minerals is a consequence of this metabolic disassembly line. Right: Dependent on the chemical composition of water in sediment, typical minerals crystallize, replacing the original organic matter. In many fossil microbially induced sedimentary st, the cell walls of filaments still include some of the original carbon, and chamosite and illite may form. Pyrite, goethite, and hematite may have replaced the ancient trichomes, whereas silica and calcite may have replaced fossil extracellular polymeric substances (EPS).

substances and ultimately to the preservation of microbial mats (Ferris, Beveridge, & Fyfe, 1986; Ferris, Fyfe, & Beveridge, 1987, 1988; Schultze-Lam & others, 1996; Konhauser & Riding, 2012). Impressions of mat textures, as known from carbonate microbialites, have to our knowledge not been observed in siliciclastic material. In summary, the cooperative action of this microbial disassembly line transforms and transfers the original amount of solar energy, via several steps, first into organic matter and then into chemical compounds (Schultze-Lam & others, 1996). The microbes work as a cooperative until almost all of the original energy is used up.

The difference between MISS and carbonate/silica microbialites, such as stromatolites, is that in the latter rapid and ubiquitous *in situ* lithification of EPS takes place (Dupraz & others, 2009). The EPS constitute organic matrix, providing a template for nucleation of carbonate minerals (Dupraz & others, 2009). In MISS, such EPS lithification plays only a minor role in structure formation (Noffke & Awramik, 2013). Here, *in situ* replacement of filaments happens very quickly (Schieber & others, 2007; Noffke, 2010; Gomes & others, 2020).

FORMATION OF MISS AND MAIN MORPHOTYPES

In general, three main types sedimentary systems are distinguished: 1) clastic, 2) clastic-evaporitic, and 3) carbonatic (Warren, 1999). Clastic deposits are comprised of mineral grains, bioclasts, and lithoclasts. Such deposits are governed by physical sedimentary dynamics (erosion and deposition). Dynamic events are interrupted by a time period of quiescence called latency. Clastic-evaporitic settings are likewise characterized by such physical sedimentary dynamics but, in addition, also by evaporite mineral crystallization. Carbonate sediments are subject to both physical dynamics and evaporite mineral formation but are dominated by carbonate precipitation. The term sediment, however, cannot be understood as substrate merely comprised of particles that by diagenetic processes turn into a cement-stabilized sedimentary rock. The hydraulic activities are reflected by the wealth of sedimentary structures that are well familiar to sedimentologists (Pettijohn & Potter, 1964). In order to survive, macro- and microbenthos must be able to actively respond to sedimentary dynamics.

Clearly, given the small scales relevant to the microbial world, any instability of the substrate affects microbenthos significantly. In a high-energy setting, strong waves and currents may erode and rip off microbial mats from their substrate, forming meter-scale roll-ups (Cuadrado & others, 2015; Maisano, Cuadrado, & Gómez, 2019). In arid, terrestrial settings, roll-ups form through desiccation of a mat. In a low-energy environment, fine particles may continuously fall out of suspension and bury the microbenthos, potentially altering the physico-chemical properties of the sediment or blocking essential sunlight from reaching the bottom. In the face of such challenges, microbes ensure the survival of the biofilm community by active upward motion and escape from burial (Bebout & García-Pichel, 1995; Paterson & Black, 2000; Shepard & others, 2005; Shepard & Sumner, 2010; Cuadrado, Carmona, & Bournod, 2011; Risgaard-Petersen & others, 2015). That means that microbes respond differently to erosion than to deposition, which results in lessened erosion rates and increased depositional rates. In fact, the microbial activities generate moderate dynamic sedimentary conditions more suitable for microbial colonization of deposits (Noffke, Knoll, & Grotzinger, 2002; Noffke, 2010). The microbenthos, thus, establishes what we've termed a "window of optimal dynamic conditions" for biofilms and microbial mats to form and thrive (Fig. 31).

Physical sedimentary dynamics include erosion, deposition, and latencies. Deformation plays a role once the sediment is deposited. Erosion differs from deposition in its physical sediment dynamics. Microbial activi-

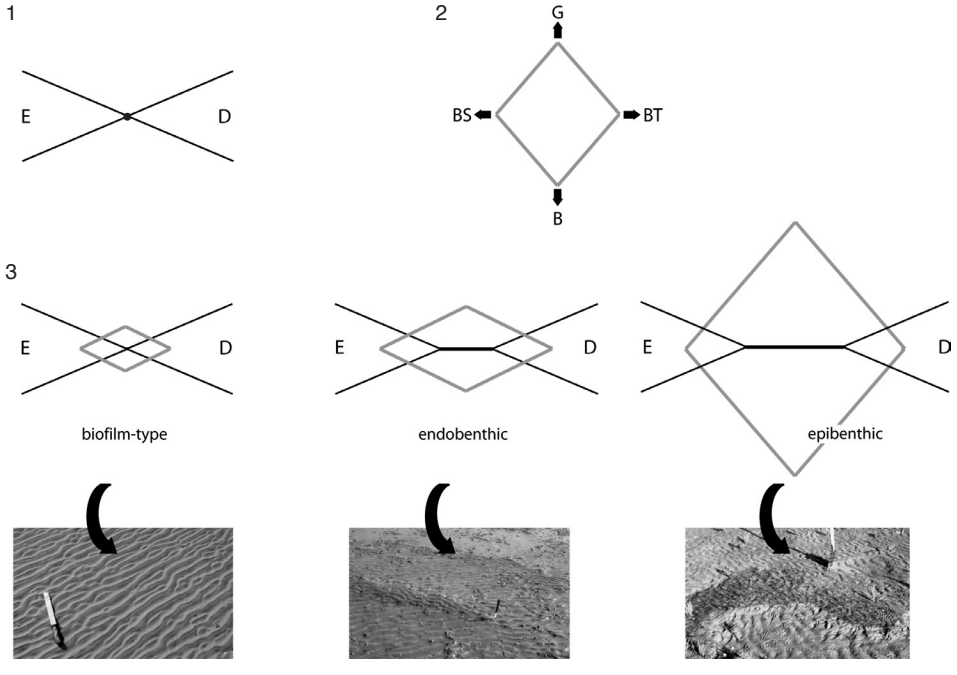

FIG. 31. Overview of the microbial modification of physical sedimentary dynamics. Microbial mats and biofilms influence physical sediment dynamics in such a fashion that the microbenthos constructs its own dynamically suitable habitat, the optimal dynamic window for mat development (see NOFFKE, KNOLL, & GROTZINGER, 2002). *1,* Physical sediment dynamics without microbial influence: E, erosion; D, deposition; *dot* at the crossing point, latency (time of no erosion or deposition). *2,* Physical sediment dynamics affected by microbial influence. The rhombus (*gray*) represents microbial activities: G, growth; BT, baffling and trapping; BS, biostabilization; B, binding. Microbial activities create the window of optimal dynamic conditions biostabilization (BS) acts against erosion, while baffling and trapping (BT) increases the rate of deposition, especially of grains of the silt- to fine-sand fraction. Growth (G) and binding (B) rise the sedimentary surface. *3,* The presence of small biofilms would not affect ripple morphologies (photo, *left*). However, where endobenthic microbial mats establish, biostabilization counteracting erosion (E) and baffling and trapping fostering deposition (D) sets in, and in consequence, the latency (black horizontal line separating E and D and representing time periods of dynamic quietness) increases. Endobenthic microbial mats modify physical sediment dynamics moderately and therefore their erosional remnants and pockets (photo, *middle*) appear as somewhat projecting surface morphologies. Epibenthic microbial mats affect erosion and deposition significantly and in consequence their erosional remnants and pockets are larger structures (photo, *right*). Color version available in *Treatise Online* 162 (paleo.ku.edu/treatiseonline).

ties differ from each other as well. Microbial growth is not the same as biostabilization, and both are distinct from baffling and trapping. Furthermore, binding also differs from the three other activities. Biostabilization is the response to erosion; baffling and trapping is the response to deposition; and growth (cell replication and EPS-production) or binding (organizing a mat fabrics by movement, not growth) is a response to latencies.

The microbiotic-physical interactions produce sedimentary structures (MISS) that, due to the different nature of their formational processes, differ morphologically from the physical sedimentary structures (*sensu* PETTIJOHN & POTTER, 1964) generated by purely physical dynamics.

GROWTH

Sediment affected neither by erosion nor by deposition provides a most suitable substrate for a biofilm or microbial mat to grow. This moment (or time period) of quiescence is called latency. Growth is herein understood as the increase of biomass, both through cell replication and the production

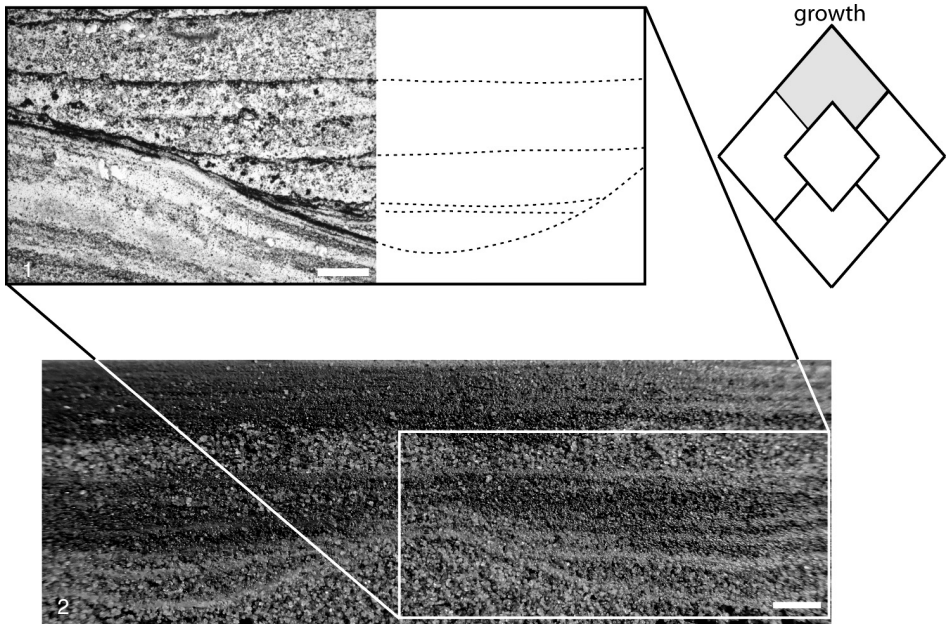

Fig. 32. Examples of microbially induced sedimentary structures formed by growth. A ripple valley is filled-in with layers of sediment (light) alternating with (dark) microbial mat laminae. *1,* Thin section of sample from 3.48 Ga Dresser Formation, Pilbara, Western Australia, scale bar, 0.1 cm. *2,* A scenario similar to (*1*) is visible in this vertical section through a modern sediment sample, Paso Seco coastal area, Argentina, scale bar, 0.5 cm. Color version available in *Treatise Online* 162 (paleo.ku.edu/treatiseonline).

of EPS and the establishment of a fully functioning biofilm community best suited for its specific environmental locale. With continuous growth of a biofilm or microbial mat, its vertical thickness increases. A microbial mat covering a bumpy sedimentary surface will—if the growth remains undisturbed—eventually smoothen this uneven surface relief. Thus, surface becomes level, or planar (Fig. 32). In this context, laminated leveling structures may form (Noffke & others, 2001; Noffke, 2010; Liu & Zhang, 2017).

In microscopic close-up of a growing microbial mat, the biomass surrounding a mineral grain increases in thickness over time. The developing biomass forces grains upward and away from each other until the original grain-grain contact is lost (Fig. 33.2). Such individual grains in the mat matrix may be observed, especially in thin sections of epibenthic microbial mats. Typically, the grains rotate to a position with their long-axes parallel to the sedimentary surface, termed oriented grain (see Noffke & others, 1997) (Fig. 33.3).

BIOSTABILIZATION

Biostabilization includes three types of processes. It may be a response to 1) erosion by horizontally directed water currents, but also to 2) intra-sedimentary gas pressure, or to 3) mechanical stress leading to ductile deformation. Species diversity, EPS structure and adhesiveness, salinity, light conditions, and other factors play a role in the effectiveness of biostabilization (Yallop & others, 1994; Paterson, 1997; Amos & others, 2004; Consalevy & others, 2004; Friend & others, 2008; Taher & Abdel-Motelib, 2014; Gerbersdorf & Wieprecht, 2015; Dick, Grim, & Klatt, 2018).

Biostabilization type 1 is the response of benthic microbiota to erosive forces by a horizontally directed water current passing the mat surface (Fig. 33). The smooth, EPS-rich surface of epibenthic microbial mats

induces a predominantly laminar flow across its surface (BS A in Fig. 33.1). Such laminar flow generally has a far less eroding effect than turbulent flow because of absence of the vertical component of motion (Stoodley & others, 2005; Noffke, 2010; Tice & others, 2011; Hagadorn & McDowell, 2012). Endobenthic microbial mats develop within the upper millimeters of a sedimentary surface such that, in microscopic close-up, individual mineral grains project upward from the surface (BS B in Fig. 33.2). The surface is rough. Thus, passing water currents have a turbulent character with a higher erosive effect. In local areas, where hydrodynamic reworking constantly exceeds mat stability, only limited biofilms can develop. They cover water-suspended grains, sometimes holding a few grains together. Constant water motion keeps such biofilm-grain-aggregates in suspension for a longer time than sterile mineral grains (BS C in Fig. 33.3). The reason for this prolonged suspension is that biofilm-grain aggregates have comparatively larger diameters and lower specific densities than individual sterile grains. It appears that one advantage of this microbially induced suspension mechanism is to prohibit the lethal burial of microbes by light-blocking sediment (Noffke, 2010). This type of biostabilization may also give rise to microsequences (Noffke & others, 1997). Microsequences are vertical successions of graded sediments layers covered by a microbial mat on the top of each bed. As soon as quiet conditions establish, the mat can develop. Each layer is preserved due to the biostabilization effect of the mat, which exceeds the erosion.

Biostabilization type 2 is the sealing of sediment by EPS that prohibit gas exchange between deposits and water or the atmosphere. Consequently, gases (O_2, CO_2, CH_4, H_2S, and others), which accumulate in the pore space of clastic deposits beneath microbial mats cannot escape. Consequently, gas pressure in the sediment may cause millimeter-scale pores visible in vertical section through mat-sealed sediment. Such

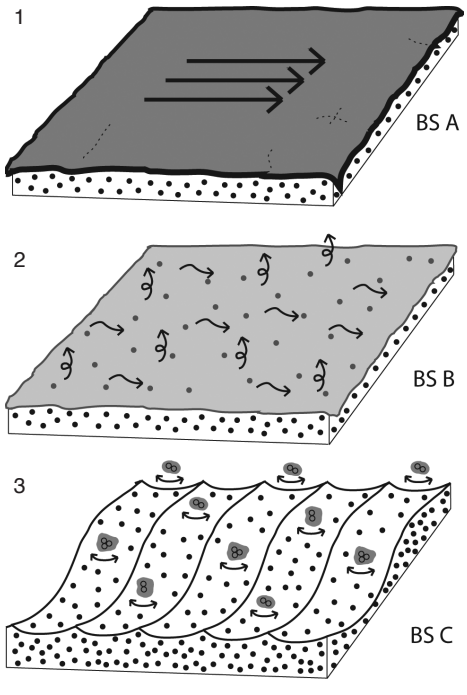

Fig. 33. Biostabilization type 1 by microbial mats and biofilms. Biostabilization BS A (*1*) is observed in epibenthic microbial mats sealing the sedimentary surface; biostabilization BS B (*2*) is observed in endobenthic microbial mats that form organic networks within the upper layers of the sedimentary deposits; biostabilization BS C (3) is observed in microbial-sediment aggregates.

sedimentary textures are termed sponge pore sand (Tebbutt, Conley, & Boyd, 1965; Noffke & others, 1996; Kinsman-Costello & others, 2017) (Fig. 34).

Gas domes are local centimeter-scale upheavals associated with biostabilization type 2, which locally form as a result of gas accumulations immediately beneath a microbial mat (Noffke & others, 1996; Wilmeth & others, 2014) (Fig. 35). Commonly, sponge pore fabrics and gas domes occur together.

Biostabilization type 3 involves the reaction of mat-stabilized sediment in ductile fashion. This biostabilization is typical in areas of vertically oriented water motion, e.g. where oscillating groundwater affects the sedimentary surface. A desiccating, microbial-mat-bound sand layer contracts,

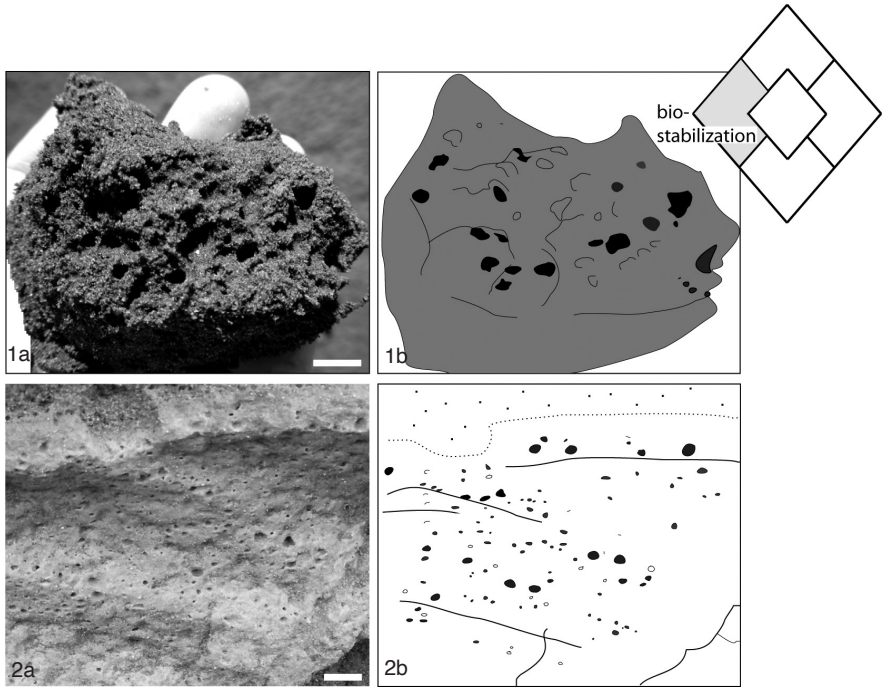

FIG. 34. Examples of microbially induced sedimentary structures caused by biostabilization. *1,* Sponge pore structure in modern sand flats, Paso Seco, Argentina (*a*), with accompanying drawing (*b*), scale bar, 1 cm. *2,* Sponge pore structure in the Rio Negro Formation (Miocene–Pliocene), Argentina (*a*), with accompanying drawing (*b*), scale bar, 1 cm. Color version available in *Treatise Online* 162 (paleo.ku.edu/treatiseonline).

curls up, and loses contact with the sediment beneath (GERDES, KLENKE, & NOFFKE, 2000). Unconsolidated, loose sand in the absence of biology would react to desiccation simply by dispersing into individual grains. However, if a microbial mat holds grains in place, the sediment does not disperse. Rather, the mat-bound sediment layer has deformation properties similar to clay (ductile deformation). Deformation of mats may also result from mechanical dislocation of a microbial mat through transport and lateral shear (PFLÜGER & GRESSE, 1996; SIMONSON & CARNEY, 1999; TICE & LOWE, 2004). MISS such as roll-ups or over-flips are good examples of this (Fig. 36).

In semi-arid climate zones, where significant seasonal changes affect sediments such that the degree of moisture switches periodically between dry and moist, MISS such as polygonal oscillation cracks form. The periodic shrinking and expanding of microbial mat polygons causes their edges to increasingly budge (NOFFKE, GERDES, & KLENKE, 2003). Additionally, the effects of gas pressure are thought to play a role in this process, since seasonally occurring gas domes are frequently associated with polygonal oscillation cracks.

BAFFLING AND TRAPPING

Microorganisms respond to deposition by baffling and trapping (BLACK, 1933), which are two different processes (Fig. 37). Baffling is the response of the microbenthos to sedimentation (NOFFKE, 1997; GERDES, KRUMBEIN, & NOFFKE, 2000; SCHIEBER, 2004). In laboratory experiments, filaments of cyanobacteria are shown to orientate vertically and move upward in accordance with sedimentation rate (GERDES, KRUMBEIN, & REINECK, 1991). Such vertical movement of cyanobacteria (and other photoautotrophic microorganisms) is called phototaxis;

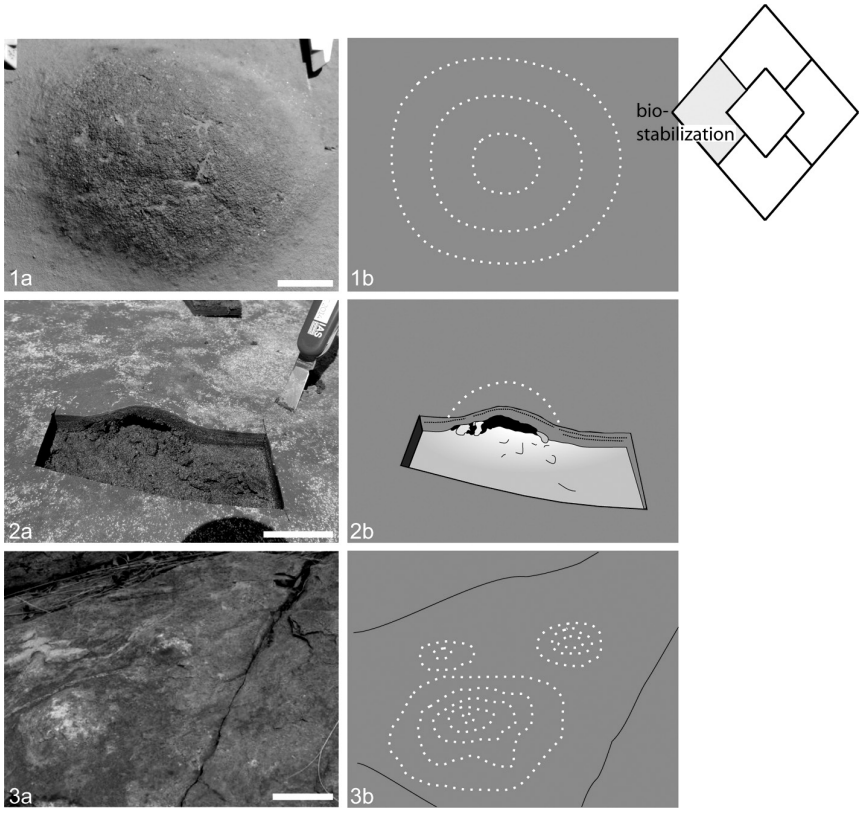

FIG. 35. Examples of microbially induced sedimentary structures caused by biostabilization (*a*), with accompanying drawings (*b*). *1,* gas dome in top view, Paso Seco, Argentina; scale bar, 2 cm. *2,* The cross-section view through a gas dome reveals a hollow cavern beneath the dome, scale bar, 5 cm. *3,* Gas domes *in situ* preserved in the 2.8 Ga Pongola Supergroup, South Africa; scale bar, 5 cm. Color version available in *Treatise Online* 162 (paleo.ku.edu/treatiseonline).

it allows the organisms to position themselves in optimal light conditions. Baffling caused the fall-out of grains of small sizes which, under the same hydraulic conditions but without microbial presence, would remain in suspension. Essentially, microbial baffling increases the rate of deposition of finer-grained material relative to that under ambient hydraulic conditions. This baffling-induced fall-out of suspended particles may clear the water column from fine particles that would otherwise cloud the water, hindering the penetration of light and thus impairing photosynthetic processes (NOFFKE, 2010).

Trapping commonly refers to the adhesive effect of sticky extracellular polymeric substances (EPS) from microbial mats on ambient particles (GEHLING & DROSER, 2009). Mineral particles (commonly of silt size) and other lithic fragments are baffled and trapped, and therefore adher to mat surfaces. Baffling and trapping may be a function of the length of filament protrusion above the mat or sediment surface, grain size and availability, grain weight, frequency and constancy of current transport, as well as the angle of incline of the mat (FRANTZ, PETRYSHYN, & CORSETTI, 2015 for stromatolites; SUAREZ-GONZALEZ & others, 2019). The stickiness or adhesiveness of EPS, which appears to differ between microbial groups, may also play a role in grain trapping (KAWAGUCHI & DECHO, 2000; TICE & others, 2011). Adhesiveness may also be controlled by electrolyte concentration or salinity in the ambient environment (SPEARS & others, 2008). Sometimes, heavy

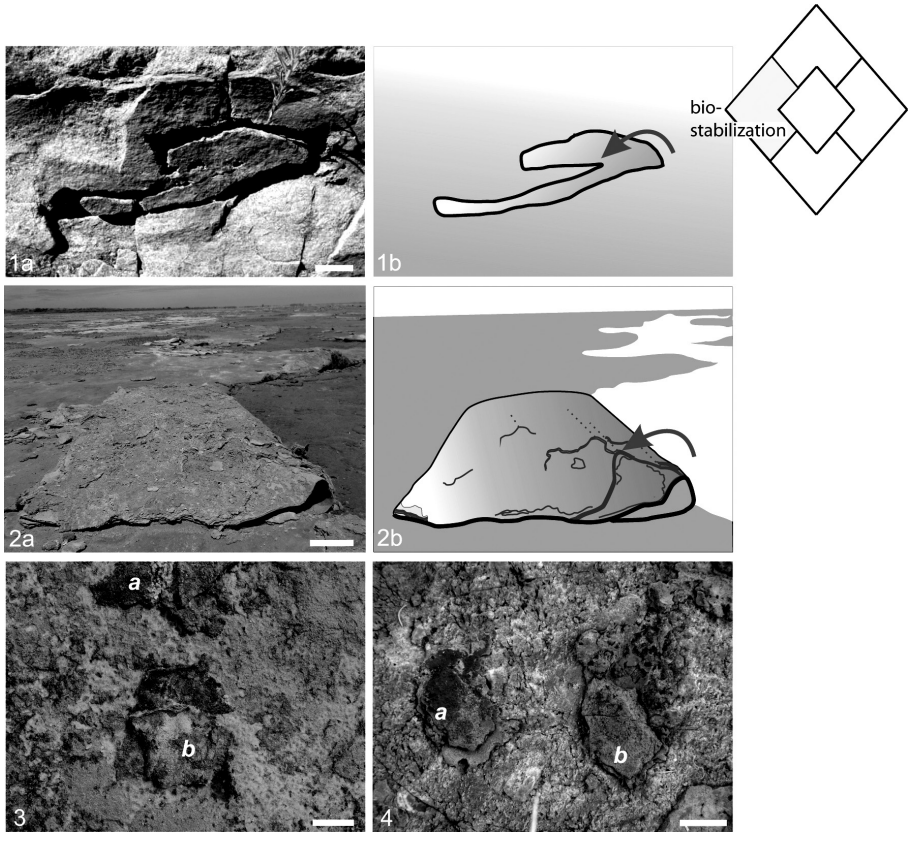

FIG. 36. Examples of microbially induced sedimentary structures caused by biostabilization. *1a,* Large-scale roll-up preserved in the 2.8 Ga Pongola Supergroup, South Africa, scale bar, 5 cm. *1b,* drawing, yellow arrow shows direction of roll-up. *2a,* Modern example of an overflip (roll-up, still connected to the parent mat), Paso Seco, Argentina, scale bar, 5 cm. *2b,* Color-coded drawing showing direction of roll up. *3,* Modern microbial mat chips on the tidal flats of Portsmouth Island, North Carolina, USA. Note that chip (*a*) is turned top-down, whereas chip (*b*) is turned top-up, scale bar, 2.5 cm; *4,* Top-down (*a*) and top-down (*b*) oriented mat chips preserved in the 3.48 Ga Dresser Formation, Pilbara, Western Australia, scale bar, 2.5 cm. Color version available in *Treatise Online* 162 (paleo.ku.edu/treatiseonline).

mineral grains and redox-sensitive metals can be found preferentially enriched in mat layers (GERDES, KRUMBEIN, & NOFFKE, 2000; TAHER & ABDEL-MOTELIB, 2015; TICE, QUEZERGUE, & POPE, 2017; RICO, SHELDON, & KINSMAN-COSTELLO, 2020).

If a biofilm is to function effectively in harvesting energy, each microorganism must place itself into the most suitable position with respect to the other members of the community (STOLZ, 2000; FRANKS & STOLZ, 2009). The coordinated arrangement of filaments into a biofilm or mat fabrics is not possible if the substrate is constantly being reworked. Therefore, as soon as water motion settles down, microbes start to form a biofilm or mat network by actively moving through the sediment.

BINDING

The arrangement of a consortium of microbes into a biofilm or microbial mat is referred to as binding. Examples of active movement by cyanobacteria have been shown in lab experiments (BEBOUT & GARCÍA-PICHEL, 1995; SHEPARD & SUMNER, 2010; BIDDANDA

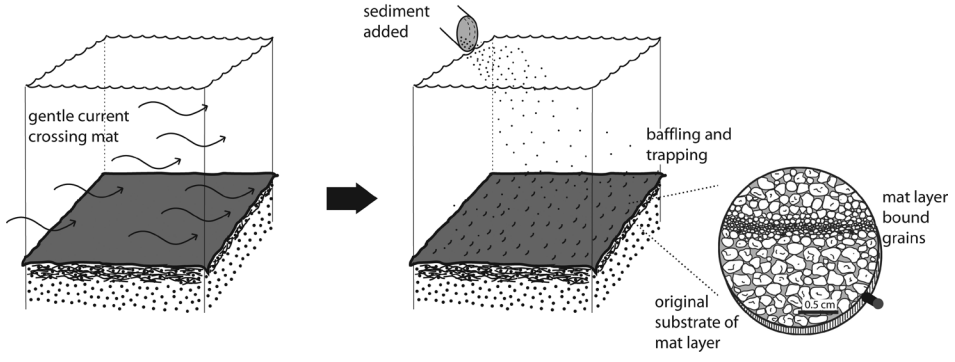

FIG. 37. Baffling and trapping. Left: gentle currents cross an epibenthic microbial mat. Right: When finer-grained sediment is introduced to the system, filaments orientate perpendicularly and promote deposition of the finer grains. The finer-grained sediment forms distinct layers in the deposits (see close-up view on the far right).

& others, 2015) and observed in nature (WALTER, 1976, DECH, NORMAN, & VISSCHER, 2010). Ancient products of binding are described in FLANNERY and WALTER (2011). In contrast to biomass increase (which is largely dependent on nutrient supply, the dynamics of nutrient diffusion through the biofilm, and light availability), binding is controlled only by sedimentary parameters (SHEPARD & SUMMER, 2010). No biomass accumulation is involved. Binding causes structures, such as reticulate patterns comprised of centimeter- to millimeter-scale ridges and tufts, which may cover large areas of microbial mats (GERDES, KRUMBEIN, & NOFFKE, 2000; SHEPARD & SUMNER, 2010) (Fig. 38).

Field observations of modern mats show that such patterns may withstand high energy events (CUADRADO & PAN, 2018). Sinoidal structures are features caused by biofilms covering ripple mark troughs as seen in cross sections through buried sediment (CUADRADO, 2020) (Fig. 39). Fossil examples of such features are also known from the Dresser Formation, Pilbara, Western Australia (NOFFKE & others, 2013).

Field studies monitoring the formation of MISS in modern tidal flats have shown that some MISS form due to an overlap between all of the above-mentioned microbial activities. Good examples of MISS with complex formational histories are multidirectional ripple marks (NOFFKE, 1998; HAGADORN, PFLÜGER, & BOTTJER, 1999) and erosional remnants and pockets (REINECK, 1979; NOFFKE, 1999; NOFFKE & KRUMBEIN, 1999; SCHIEBER, 2007a; NOFFKE, HAGADORN, & BARTLETT, 2019) (Fig. 40).

Highly abundant in the depositional record are wrinkle structures (HAGADORN & BOTTJER, 1997; NOFFKE, 2010; CHU & others, 2015; HOMANN, 2019) (Fig. 41), and several studies have investigated their formation. Wrinkle structures induced by microbes are crinkled surfaces commonly found on the upper bedding planes of fine-grained sandstone beds. They are composed of crests and grooves with irregular directions, with crests generally ranging between 0.1 to 2 mm in height, and a crest-to-crest distance of 0.1 mm to 2 cm. Patterns of crests and valleys vary from specimen to specimen (Fig. 41).

Elephant-skin textures—textured organic surfaces (TOS)—are very common (Fig. 41.4) and well preserved in Ediacaran sandstones (GEHLING, 1999; GEHLING & DROSER, 2009; BOTTJER & HAGADORN, 2007). Fossil impressions have been described as wrinkled surfaces by FEDONKIN (1992). Elephant skin textures are commonly associated with fossils of the Ediacara biota and may have influenced their preservation, according to the iconic death-mask-model (GEHLING, 1999; GEHLING & DROSER, 2009). In both the modern environment and the lab, such

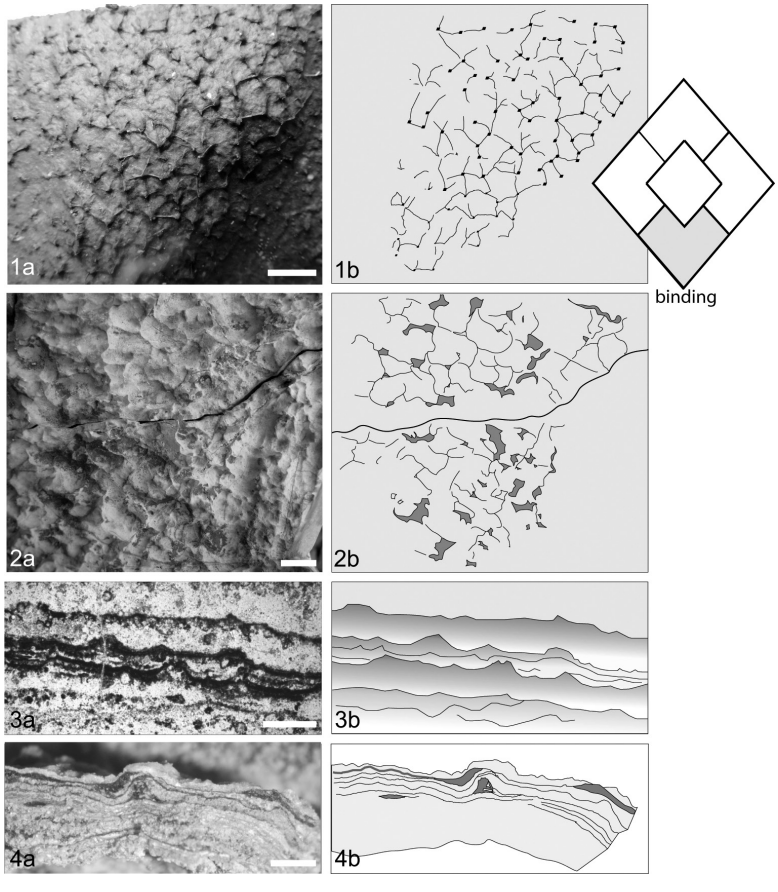

FIG. 38. Examples of microbially induced sedimentary structures caused by binding (*a*), with accompanying drawings (*b*). *1,* Reticulate pattern covering the surface of a modern microbial mat, Paso Seco, Argentina, scale bar, 1 cm. *2,* Reticulate pattern on the surface of a fossil microbial mat from the 3.48 Ga Dresser Formation, Pilbara, Western Australia, scale bar, 1 cm. *3,* Tufts preserved in the 3.48 Ga Dresser Formation, Pilbara, Western Australia, scale bar, 0.1 mm. *4,* Tufts overgrown by microbial mat laminae, Paso Seco, Argentina, scale bar, 1 mm. Color version available in *Treatise Online* 162 (paleo.ku.edu/treatiseonline).

reticulate structures and tufts on sedimentary surfaces result from migrating trichomes (SHEPARD & SUMNER, 2010, CUADRADO & PAN, 2018). The gliding motility and tangling behavior of filaments leads to the formation of tufts resembling centimeter-scale needles on the mat surfaces (GERDES, 2007; STRADER & others, 2009; SIM & others, 2012).

Shearing off a microbial mat from its surface by passing bottom currents (THOMAS & others, 2013) may cause irregularly crinkled surfaces. A microbial mat layer may be arranged into irregular tissue-like folds (Fig. 42.2) and the rapid preservation of such microbial mat fabrics produces crinkled mat surfaces, which sometimes have tears in the originally tissue-like material (fossil examples in NOFFKE, 2000, NOFFKE & others, 2008).

In lab experiments, wrinkle structures (Fig. 42.3) have been shown to form at the sediment-water interface by microbial-mineral aggregates moving back and forth with wave motion creating a *Kinneyia*-like pattern (MARIOTTI & others, 2014). Due to the original fossil *Kinneyi* WALCOTT, 1914 probably being abiotic, the name *Rugalichnus matthewii* was suggested for such *Kinneyiya*-like wrinkle structures, although the trace fossil character of MISS is debatable (STIMSON & others, 2017).

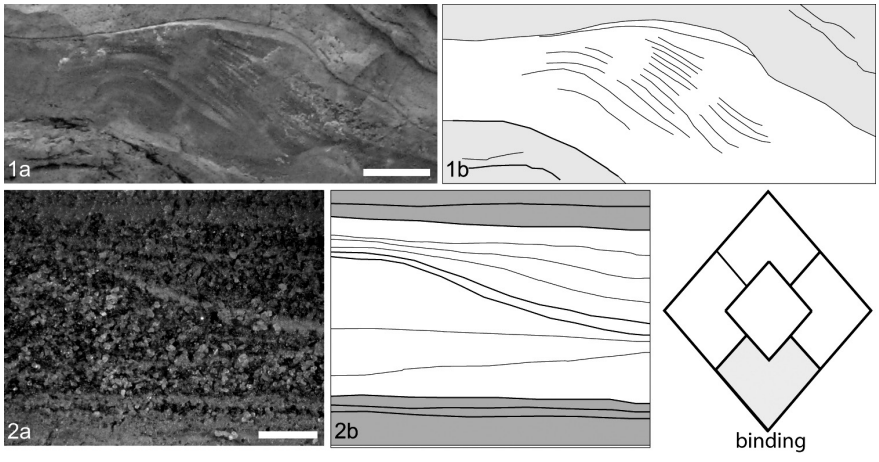

FIG. 39. Example of microbially induced sedimentary structures caused by binding (*a*), with accompanying drawings (*b*). *1,* Biofilms (*black*) overgrow ripple valleys, 3.48 Ga Dresser Formation, Pilbara, Western Australia. Such structures are called sinoidal structures, scale bar, 2 cm. *2,* Similar example for a sinoidal structure in a modern sediment, with mat layers appearing light in color, Paso Seco, Argentina, scale bar, 1 cm. Color version available in *Treatise Online* 162 (paleo.ku.edu/treatiseonline).

Finally, if a microbial mat is suddenly buried by a substantial amount of sediment, the squeezing out of mat-bound water can cause lateral grooves to form in the mat (PFLÜGER, 1999) (Fig. 42.4). Two main types of such wrinkle structures exist: transparent, in which any proceeding (physical) sedimentary structure, such as ripple marks, remain still visible underneath the wrinkles, and non-transparent, in which proceeding surface morphologies are covered completely by wrinkles and are therefore invisible. These two main types reflect endobenthic (transparent) and epibenthic (non-transparent) microbial mats (NOFFKE, 2000). *In situ* preservation of microbial mats occurs in several steps (NOFFKE, KNOLL, & GROTZINGER, 2002). It requires a pause in sedimentation, during which the mat develops and fine-grained material falls out, draping the mat surface and becoming incorporated into the mat fabrics. Subsequently deposited sediment must not be able to erode the mat during placement for *in situ* preservation to occur (NOFFKE, KNOLL, & GROTZINGER, 2002).

It is important to understand that there are different ways to arrive at wrinkled patterns in clastic sediment and that such structures are not always biologically induced patterns (HAGADORN & BOTTJER, 1997; HAGADORN, PFLÜGER, & BOTTJER, 1999; NOFFKE, 2010; see details in DAVIES & others, 2016). Nonbiological mechanisms of formation include, for example, the imprinting of a surface by foam (foam marks), by rapid water motion in very shallow water depths (millimeter ripple marks), or through the deformation of semi-consolidated material by slumping or by ball and pillows formation on the lower bedding plane. Abiotic wrinkle structures may also be caused by tectonic crinkling or biased diagenetic processes (HAGADORN & BOTTJER, 1999).

One last important aspect to consider, if sediment (at least on Earth) always includes biofilms, the question may arise as to whether purely physical sedimentary structures truly exist. Would the presence of biofilms in all deposits not mean that physical sedimentary structures in a natural environment are actually always microbiotic-physical structures? In answering this question, even where biofilms may smother surfaces, they commonly are of too little mechanistic impact to affect a structural representation. However, microbially induced sedimentary structures (MISS) exist, and so the question may be asked, where is the boundary between physical sedimentary

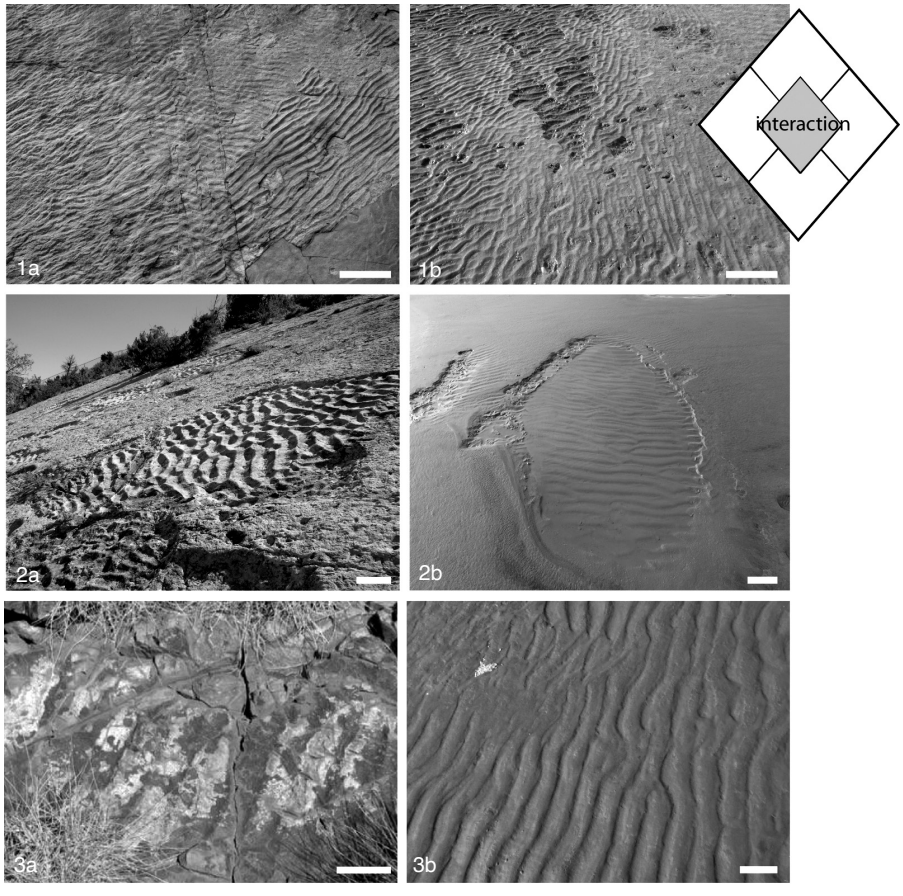

FIG. 40. Examples of microbially induced sedimentary structures produced by the interaction of all microbial activities. *1,* Multidirectional ripple marks in the 2.8 Ga Pongola Supergroup, South Africa (*a*) and in the modern sandflat of Bahia Blanca Estuary, Argentina (*b*), scale bars, 30 cm. *2,* Erosional pocket showing ripple marks in the Cretaceous Dakota Sandstone, USA (*a*), and in a tidal flat, Paso Seco, Argentina (*b*), scale bars, 10 cm. *3,* Rippled surface covered by minute fossil biofilm in the 3.48 Ga Dresser Formation (*a*) and in the modern Paso Seco, Argentina (*b*), scale bars, 10 cm. Color version available in *Treatise Online* 162 (paleo.ku.edu/treatiseonline).

structures and MISS? This question was approached by examining a tidal flat (NOFFKE & KRUMBEIN, 1999). The study developed a modification index (MOD-I) that describes the degree of microbial influence on tidal surface morphologies (erosional remnants and pockets). A MOD-I of 0 would describe sedimentary surface morphologies that show no influence by microbenthos, a MOD-I of 1 describes maximal influence. The boundary between microbially induced or not would be any value >0, with fluctuations of structure-modification in response to seasons being typical. While this study worked well for a local tidal flat with a simple biofilm catena, any conclusion for general sedimentology or even the sedimentology of other planets is unwarranted.

PRESERVATION OF MISS

In thin sections through fossil microbially induced sedimentary structures (MISS), the different components of an ancient microbial mat texture may be visible. Mat textures are fossilized by different minerals depending on the ancient water chemistry providing anions and ions that nucleate into first precipitates.

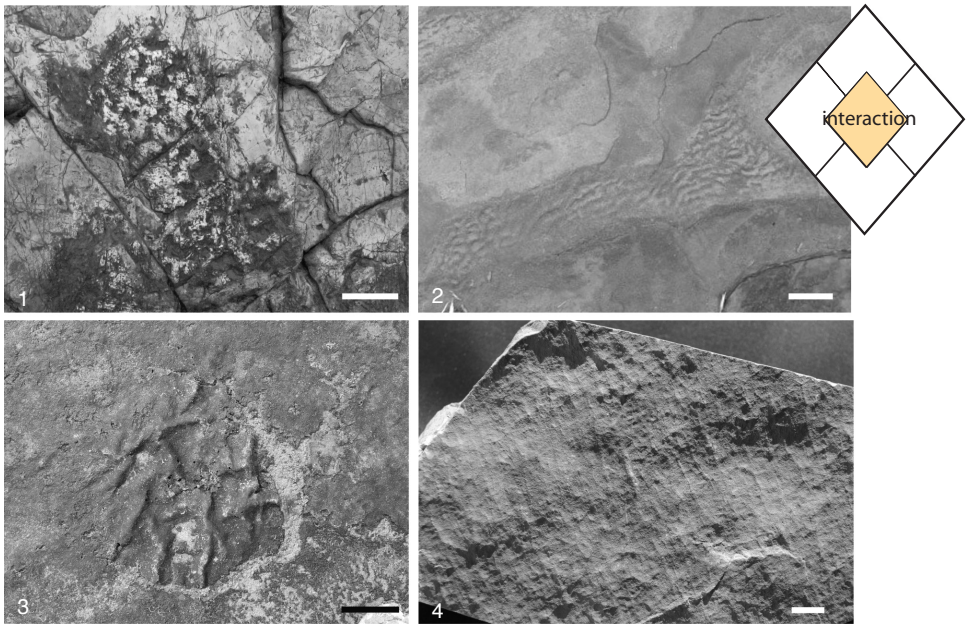

Fig. 41. Biogenic wrinkle structures. *1,* One of the oldest wrinkle structure known in the fossil record is preserved in the 3.48 Ga Dresser Formation, Pilbara, Western Australiam scale bar, 5 cm. *2, Kinneyia*-like wrinkle structure, 2.8 Ga Pongola Supergroup, South Africa, scale bar, 10 cm. *3,* A round piece of microbial mat became detached from its sandy substrate and crinkled. The cause may have been a current crossing the microbial mat in fall, when mats in this area start to compose; Portsmouth Island, North Carolina, USA, scale bar, 10 cm. *4,* Elephant skin texture, Tonian, circa 750 Ma, Qingshuijiangh Formation, South China, scale bar, 1 cm. Color version available in *Treatise Online* 162 (paleo.ku.edu/treatiseonline).

1) Illite or chamosite, pyrite or goethite, and limonite may line the original trichomes of the microbes (Schieber, 1986, 1989, 1999; Pflüger & Gresse, 1996; Hagadorn & Bottjer, 1997, 1999; Logan & others, 1999; Noffke, 2000; Noffke, Hazen, & Nhleko, 2003; Westall & others, 2006; Noffke, Beukes, & others, 2006; Noffke, Eriksson, & others, 2006; Noffke & others, 2013; Heubeck & others, 2016). The formation of clay coats in sandy estuarine and tidal environments can occur as a result of clay-EPS complexes developing along hydroxylated biofilm-clay interfaces or between biofilm proteins and the neutral siloxane surface in quartz sands (Duteil & others, 2020; Worden & others, 2020). Such precipitative clay mineral coatings can develop on microbial biomass surfaces within days as a result of metal ion binding (e.g. Fe, Al), which reduces the nucleation energy of aluminosilicates (Ferris, Fyfe, & Beveridge, 1987; Laflamme & others, 2011; Newman & others, 2016, 2017).

2) Cell walls may still include fragments of the original carbonaceous materials. The organic carbon remains provide opportunity for organic carbon isotope measurements and Raman and infra-red spectroscopic characterization. Anoxic conditions promote the *in situ* preservation of organic carbonaceous matter, as evidenced by the fossilization processes of Burgess Shale macrofossils (Briggs, 2003, Gaines, Briggs, & Zhao, 2008). However, cellular organic matter may also be protected against oxygenation by EPS, which reduces gas exchange between sediment and atmosphere or water significantly.

3) EPS is frequently recorded as silica (Westall & others, 2001, 2011; Noffke & others, 2013). In modern hot springs and also in peritidal sedimentary rocks formed in the silica-rich Archean oceans, rapidly precipitating silica produces an

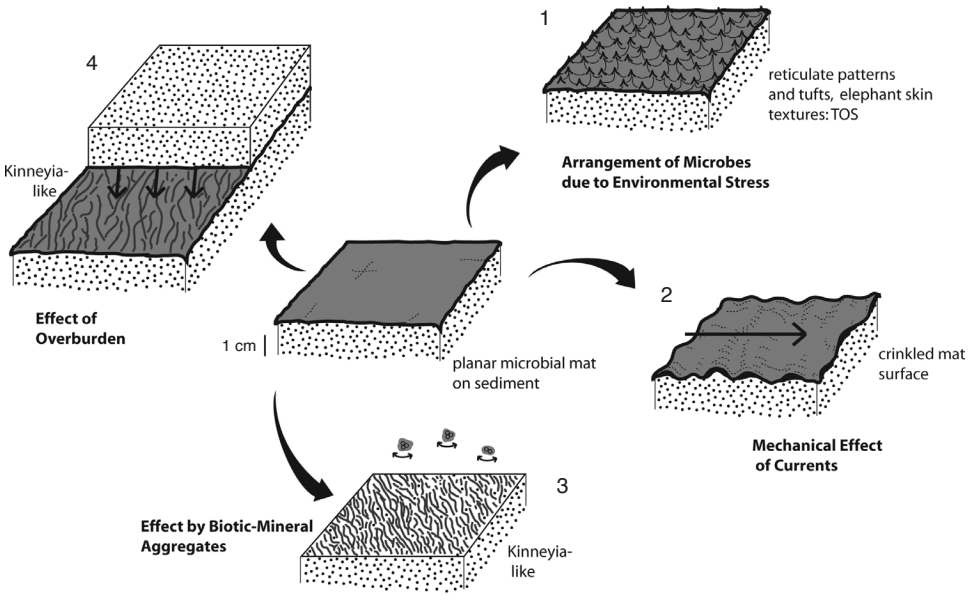

FIG. 42. Various causes and types of microbially induced wrinkle structures. A planar microbial mat is shown in the center of this figure. Variations are shown from *1* to *4. 1,* filamentous microbes form tufts and reticulate patterns in response to environmental stresses causing textured organic surfaces (TOS); *2,* a coherent epibenthic mat is affected by a strong current dislocating the mat and folding it into irregular crinkles resembling folds in a tablecloth, tearing may also occur; *3,* mineral-biofilm-aggregates moved by waves give rise to *Kinneyia*-like structures. *4, Kinneyia*-like structures are caused by jetting water squeezed out of the underlying microbial mat layer when buried by new deposits.

almost impermeable preservational time capsule, resilient even to low-grade metamorphism (TREWIN, 1996; KAH & KNOLL, 1996; MANNING-BERG & others, 2019; HICKMAN-LEWIS, WESTALL, & CAVALAZZI, 2019; HICKMAN-LEWIS & others, 2019; HICKMAN-LEWIS, CAVALAZZI, & others, 2020). The embedding of silica in mat textures has been demonstrated in modern hot spring microbial mats and in lab experiments (TAHER & ABDEL-MOTELIB, 2015; JOHANNESSEN, MCLOUGHLIN, & VULLUM, 2018). Silicification may be microbially mediated within EPS even when silica concentrations within aqueous media are below supersaturation (KAH & KNOLL, 1996; MANNING-BERG & KAH, 2017; MOORE & others, 2020). Calcite formation in EPS has also been studied in great detail in lab experiments and natural settings by DUPRAZ & others (2009) and DECHO (2010).

In most if not all cases of exceptional preservation of microbial mat textures, lithification must have occurred very quickly. In thin sections, fossil MISS may reveal upright tufts (filament bundles) preserved *in situ* (KAH & KNOLL, 1996; NOFFKE, 2000; CAO, YUAN, & XIAO, 2001; HOMANN & others, 2018; HICKMAN-LEWIS, & others, 2018; HICKMAN-LEWIS, WESTALL, & CAVALAZZI, 2019; HICKMAN-LEWIS & others, 2019).

Textures preserved in MISS are essential for determining biogenicity. The example of wrinkle structures is quite frequently debated with respect to their biogenicity. In order to distinguish microbially induced wrinkle structures from abiotic wrinkle structures, thin sections should be examined to reveal the presence or absence of fossil microscopic textures. If a wrinkle structure-bearing specimen is too valuable to be destroyed by thin section analysis, X-ray micro Computed Tomography (X-ray CT) can be used to nondestructively resolve 3D morphologies using density contrasts between the different

materials constituting the internal build-up of such structures (Fig. 43). The primary density contrast comes from the presence of laminated organic matter on top of and inside the rock bed. A number of views of a sample with tufts (Fig. 43) is quite revealing (Sheldon, 2012). Surface mapping (Fig. 43.2) indicates consistent tuft-peak height, which is verified by the 2D- and 3D-segmentation of internal organic-rich laminations (Fig. 43.3). Thus, it can be shown that the example consists of more than just a single microbial mat on the bedding plane surface but rather a series of microbial mats. Each microbial mat may exhibit tufts or evidence of deformation by loading pressure.

CLASSIFICATION OF MISS AND MIST

Conforming to the nomenclature of stromatolites, thrombolites, dendrolites, and leiolites, the overall group of microbially induced sedimentary structures (MISS) constitute the fifth group of microbialites (Riding, 2011b; Noffke & Awramik, 2013; Grey & Awramik, 2020). The main characteristics of MISS that differ from other microbialites are: 1) structure-forming biofilms or microbial mats occur on top or within clastic deposits; 2) only minor to negligible mineral precipitation may occur and is predominantly caused by the biological degradation of organic matter of deceased primary producers and EPS; and 3) as a consequence, the structures are predominantly planar and have, in contrast to most of the other microbialites, low morphological relief.

MISS are divided into five classes, each of which includes individual structures (Fig. 44). These classes are named according to the dominant microbial activity that governs the formation of the structures within the respective class: class 1, structures caused by growth; class 2, structures caused by biostabilization; class 3, structures caused by baffling and trapping; class 4, structures caused by binding (formerly, Noffke & others, 2001, ascribed this class to imprinting); and class 5, structures caused by the interference of all above-mentioned microbial activities (Fig. 44), in center dashed-line diamond). Each structure within each class is named according to its morphological appearance. This enables the surveying geologist to identify a structure even without any knowledge or prejudgment of its genesis. To date, 18 main MISS structures have been distinguished and no

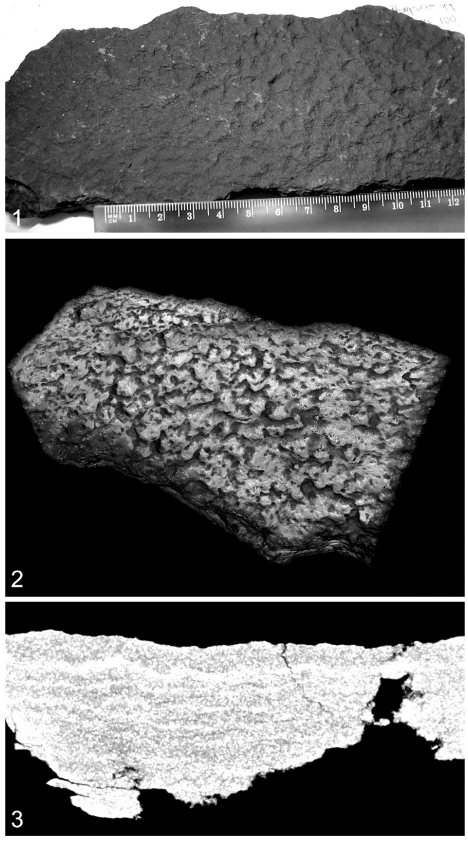

Fig. 43. X-ray CT scans of a microbially induced sedimentary structure sample. *1, Kinneyia*-like wrinkle structure on sandstone slab. *2,* X-ray CT scan of top surface exhibiting *Kinneyia* structure; the corresponding thickness map shows the morphology of the surface peaks. *3,* 2D side-on views of the *Kinneyia* slab, where black microbial-like laminations are visible beneath the surface. Each lamination has been individually segmented to highlight the wavy morphology, which correlated with the peaked surface texture. All images collected with the Advanced Imaging of Materials (AIM) Facility at Swansea University, UK, and rendered using ORS Dragonfly software. Color version available in *Treatise Online* 162 (paleo.ku.edu/treatiseonline).

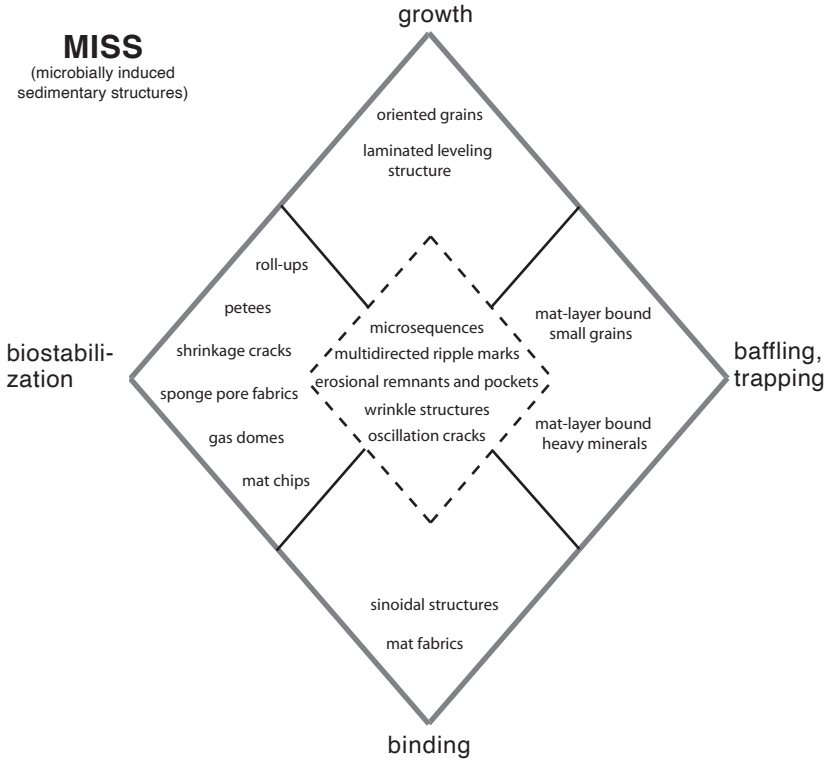

FIG. 44. Classification of MISS and their MIST (on facing page). The classification of both macroscopic and microscopic features each includes five genetic groups related to their means of formation. Descriptive names of individual structures and textures are listed to aid in identification in the field or laboratory.

transitions seem to exist between them (NOFFKE & others, 1996, 2001; NOFFKE, 2010).

MISS include, in thin-section view, a wealth of microscopic microbially induced sedimentary textures (MIST) that witness the former presence of the MISS-producing biofilms or microbial mats (Fig. 44). Textures are divided into five classes according to their genesis: class 1, textures caused by microbial-physical interaction; class 2, textures caused by entombment of carbon; class 3, textures caused by mineralization of organic matter; class 4, textures caused by microbial-chemical interaction; and class 5, textures that rise from the combination of all the four processes. Following the classification of MISS, each MIST within each class is named according to its morphological appearance and pattern of chemical signals. Eleven MIST textures are suggested herein (Fig. 44), but future discussions and contributions will certainly add to this catalog.

SCHIEBER (2004) suggested different groups of mat structures, each categorized according to a leading process: 1) mat growth (comprising binding, baffling and trapping); 2) metabolism (encompassing mineral precipitation); 3) physical destruction (encompassing dehydration, erosion and transport); and 4) mat decay (gas development) and diagenesis (organic matter destruction and mineral precipitation). However, processes that the specific groups cannot be clearly distinguished from each other. For example, (2) metabolism encompassing mineralization overlaps with diagenesis and mineral formation, listed under (4).

Following the broad definition proposed by BURNE and MOORE (1987, p. 241–242)

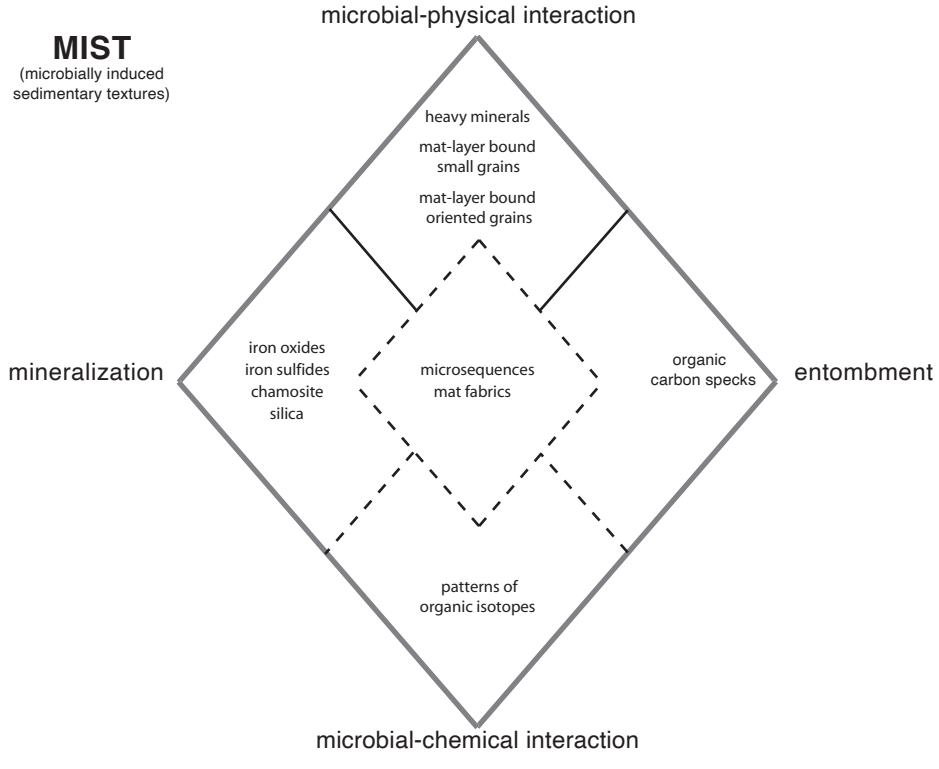

FIG. 44. (continued from previous page). Classification of MISS (facing page) and their MIST. Descriptive names of individual structures and textures are listed to aid in identification in the field or laboratory.

that microbialites are "organosedimentary deposits that have accreted as a result of a benthic microbial community trapping and binding detrital sediment and/or forming the locus of mineral precipitation," RIDING (2011b) and GREY and AWRAMIK (2020) classified MISS in the broad category of microbialites. Overall, MISS constitute the fifth category of microbialites—bedding modified by microbial mats and biofilms—in PETTIJOHN and POTTER's (1964) classification of primary sedimentary structures (NOFFKE & others, 2001).

MISS IN THE COURSE OF EARTH HISTORY

Microbially induced sedimentary structures (MISS) and microbially induced sedimentary textures (MIST) are known in clastic rocks of all Earth ages. Specimen occur in one of the oldest non-metamorphosed sedimentary rock successions, the 3.48 Ga old Dresser Formation in Western Australia (BUICK & DUNLOP, 1990; NOFFKE & others, 2013). Marine stratigraphic successions with Archean MISS once formed by photoautotrophic mats include the 2.9 Ga old Pongola Supergroup and the Witwatersrand Supergroup (BEUKES & LOWE, 1989; NOFFKE, BEUKES, & others, 2006; NOFFKE, ERIKSSON & others, 2006; NOFFKE & others, 2008; TICE, 2009). Fossil microbial mats and biofilms are also widespread in carbonaceous cherts and sandstones of the Paleoarchean Barberton Greenstone Belt in South Africa (see HICKMAN-LEWIS & others, 2018 and HOMANN, 2019 for a review). There, they occur in the 3.472 Ga Middle Marker horizon (HICKMAN-LEWIS & others, 2018); the 3.45 Ga Hooggenoeg Formation cherts (WALSH, 1992; HICKMAN-LEWIS, CAVALAZZI, & others, 2020); the 3.416 Ga Buck Reef

Chert (Walsh & Lowe, 1999; Tice & Lowe, 2004, 2006; Tice, 2009; Tice & others, 2011; Greco & others, 2018); the 3.334 Ga Footbridge Chert (Hickman-Lewis, Cavalazzi, & others, 2020); the 3.33 Ga Josefsdal Chert (Westall & others, 2001, 2006, 2011, 2015); the 3.26 Ga Mendon Formation (Byerly, Lower, & Walsh, 1986; Trower & Lowe, 2016); and sandstones of the 3.22 Ga Moodies Group (Noffke, Eriksson, & others, 2006; Heubeck, 2009, Homann & others, 2015, 2016, 2018). In these deposits, wavy-crinkly laminations have been interpreted as fossil microbial mats based on their laminated structure, sediment trapping and cohesive behavior, carbonaceous and carbon isotopic composition, and the occurrence of eroded and in places rolled-up mat fragments. Wrinkle structures occur but are quite rare. Most fossil mats occur either in carbonaceous banded cherts or interbedded with volcaniclastic sand- and siltstones and quartz-rich sandstones.

The nearly *in situ* preservation of the delicate carbonaceous mat laminae in the Barberton Greenstone Belt show textures such as mat-laminae-bound small grains and oriented grains. Phototactic behavior may be recorded by an increase of mat thickness toward crests in undulating laminae (Tice & Lowe, 2004; Noffke, Gerdes, & Klenke 2003; Homann & others, 2015; Hickman-Lewis & others, 2016, 2018).

Trace and rare earth element data from mat-bearing horizons in cherts up to 3.47 Ga also show strong influences from continental weathering in the form of light rare earth element enrichment, chondritic to sub-chondritic Y/Ho ratios and negligible La and Y anomalies, and it is therefore evident that microbial life inhabited semi-restricted epicontinental basins by this time ~1.09 Ga Mesoproterozoic Copper Harbor Conglomerate (Elmore, 1983; Fedorchuk, 2014). Sheldon (2012) reported 1.1 Ga terrestrial MISS from low-energy fluvial floodplain paleoenvironments preserved in siliciclastic deposits from North America.

Late Neoproterozoic seafloors were widely overgrown by significant microbial mats (Schieber, 1986; Awramik, 1991; Hagadorn & Bottjer, 1997; Hagadorn, Pflüger, & Bottjer, 1999; Bottjer, Hagador, & Dornbos, 2000). Neoproterozoic textured organic surfaces (TOS) record relationships between the Ediacara biota, the earliest macroscopic, multicellular organisms, and contemporaneous microbial mats (Gehling & Droser, 2009; Callow & Brasier, 2009; Laflamme & others, 2011; Darroch & others, 2012; Tarhan, Droser, & Gehling, 2015; Dunn, Liu, & Donogue, 2018). The extraordinary preservation of this soft-bodied biota suggests the extensive presence of microbial mats during this period of time (e.g., Hagadorn & Bottjer, 1999; Gehling, 1999; Seilacher, 1999; Liu & others, 2011; Tarhan, Droser, & Gehling, 2015; Menon & others, 2016; Liu & Dunn, 2020). Terrestrial MISS arising from microbes interacting with aeolian processes are known from the Neoproterozoic Venkatpur Sandstone (Basilici & others, 2020).

Phanerozoic occurrences are known from the Cambrian (Buatois & Mángano, 2003; Seilacher, Buatois, & Mangano, 2005; Mata & Bottjer, 2012; Buatois & others, 2014; Liu & Zhang, 2017; Bayet-Goll & Daraei, 2020); the Ordovician (Gerdes, Klenke, & Noffke, 2000; Noffke, 2000; Buatois & others, 2009; Hints & others, 2014; the Silurian (Hillier & Morrissey, 2010; Calner & Eriksson, 2012); the Devonian (Draganits & Noffke, 2004; Gaillard & Racheboeuf, 2006); the Carboniferous (Mángano & others, 2002; Buatois & others, 2013; Callefo & others, 2019); the Permian (Webb & Spence, 2008); the Triassic (Pruss, Fraiser, & Bottjer, 2004; Pruss, Corsetti, & Bottjer, 2005; Pruss & others, 2006; Mata & Bottjer, 2009; Feng & others, 2019; Wignall & others, 2020); the Jurassic (Porada, Ghergut, & Bouougri, 2008; Peterffy, Calner, & Vajda 2016); the Cretaceous (Gerdes, Krumbein, & Noffke, 2000; Schieber 2007a; Fernández & Pazos, 2014; Noffke, Hagadorn, & Bartlett, 2019); the Neogene (Carmona & others, 2012); and the Quaternary (Kilias & others, 2020).

BANDED IRON FORMATIONS

Adriana Heimann

INTRODUCTION

Banded iron formations (BIFs) are widespread marine chemical sedimentary rocks typical of the Precambrian with no perfect analogs in chemical composition and volume having formed since then. These enigmatic rocks, characterized by banding defined by the alternation of iron-rich minerals and chert, not only are the testimony of a very different young Earth but also the main source of iron worldwide. Extensive BIFs are used as important indicators of the redox state of the ancient oceans, and their characteristics and variations also reflect the evolution of the biosphere-atmosphere-solid Earth system from the Archean to the present. The literature on BIFs is immense and continues to grow. This chapter provides a summary and review of the current knowledge about BIFs, focusing on the hypotheses of BIF formation, both organic and inorganic, recognizing that such an overview will be far from complete. For a conceptual framework for the deposition of BIFs through time, see Bekker and others (2010) and references therein. For an alternative interpretation of the significance of BIFs in the rock record, see Ohmoto and others (2006). The main characteristics of BIFs, including their classification, temporal and geographic distribution, mineralogy, precursor phases, and geochemistry are presented here, followed by the main hypotheses of BIF genesis, including the sources of iron and silica, the genesis of the banding, inorganic hypotheses for their formation, and the ideas and evidence for the likely role of various bacterial processes in their formation. Geochemical (carbon isotopes, iron isotopes, molecular biomarkers), physical (microfossils), experimental, theoretical (cell calculations), and natural (biofilms) lines of evidence that provide insights into the various hypotheses of BIF formation are reviewed. Finally, possible Phanerozoic and modern environmental analogs to Archean–Proterozoic BIFs and their settings are described.

Although BIFs have been the focus of a huge number of studies, their genesis is still a matter of considerable debate. In particular, the origin of the oxidized iron present in BIFs has been debated for decades. Oxidation and precipitation of iron led to the deposition of some BIFs but exactly how this process operated is yet to be fully deciphered. The origin of the negative carbon isotope composition of carbonate carbon in BIFs, whether biotic or abiotic, has also been debated. Because of their age, BIFs are metamorphosed to various degrees and some are highly deformed. However, some BIFs only experienced a very low degree of metamorphism and a low degree of deformation and are beautifully preserved. Banding occurs at diverse scales, from microbanding (micrometric to millimetric laminations), to mesobanding (centimeter-scale), to macrobanding (meter-scale). How this banding originated has also been debated for decades and is still a matter of controversy. The mineralogy of BIFs is defined by various combinations of the main iron phases (magnetite, hematite, siderite, ankerite, and Fe-silicates) and chert.

Large BIFs range in age from the Eoarchean (~3.8 Ga) Isua BIF from Greenland, to the late Paleoproterozoic (~1.8 Ga) Biwabik and Gunflint BIFs from North America (Canada and USA). The abundance of BIFs in the rock record peaked during the late Archean (2.7–2.5 Ga) and early Proterozoic (2.5–1.8 Ga). After a hiatus of at least 1.1 billion years, BIFs briefly appeared again during the Neoproterozoic (~0.8–0.6 Ga), for example as the ~0.6 Ga BIFs of Urucum, Brazil, and the ~0.75 Ga Rapitan BIFs, Canada. BIFs are most commonly classified based on tectonic setting and age. Algoma-type BIFs are

mostly Archean BIFs that formed in active tectonic settings, whereas Superior-type BIFs formed in stable platforms mostly during the Archean–Paleoproterozic. Neoproterozoic BIFs are referred to as Rapitan BIFs and are spatially and temporally associated with Snowball Earth glacial deposits. Snowball Earth refers to a time when Earth's surface is thought to have been entirely or nearly entirely frozen (KIRSCHVINK, 1992). In this chapter, the term BIF is used to refer to all iron formations unless a particular type of BIF is noted. Geographically, BIFs are distributed throughout the planet, but some of the largest and most studied ones include the low metamorphic grade Kuruman BIF from the Transvaal Supergroup in South Africa, the Brockman BIF from the Hamersley Range in Western Australia, and the Biwabik-Gunflint BIF from the Animikie Basin of North America.

The most traditional view holds that BIFs were formed by inorganic chemical and physical processes by which $Fe(II)_{aq}$ emanating from hydrothermal vents would, for example, combine with inorganic bicarbonate dissolved in ocean water and precipitate directly as siderite ($FeCO_3$). Alternatively, after upwelling, $Fe(II)_{aq}$ would become oxidized by small amounts of dissolved O_2 in the upper water column and form hematite (Fe_2O_3) or magnetite (Fe_3O_4) after recrystallization of Fe(III)-hydrated precipitates, such as ferrihydrite. However, based on an increasing body of evidence, other hypotheses have been proposed to explain the formation of BIFs mediated by biological processes. Oxidation of $Fe(II)_{aq}$ and reduction of Fe(III) mediated by various kinds of bacteria, including chemolithoautotrophic iron-oxidizing bacteria, photoferrotrophic bacteria, and dissimilatory iron-reducing bacteria, have been invoked to explain the formation of magnetite, hematite, and siderite.

The disappearance of BIFs from the rock record at ~1.8 Ga, except from the resurgence in the glacial Neoproterozoic successions, is highly debated and has been attributed to various processes. These include the complete oxidation of the atmosphere and oceans after the Great Oxidation Event (GOE) and the increase in seawater sulfate concentration with subsequent expansion of bacterial dissimilatory sulfate reduction and the formation of a sulfidic deep ocean.

Some Phanerozoic ironstones, Phanerozoic iron formations related to massive sulfide deposits (MSDs), and modern siliceous ferric oxide precipitates from marine hydrothermal vents and the Red Sea, are the closest younger equivalents to BIFs. Modern environments that serve as possible analogs to those in which BIF deposition took place in the Precambrian—and where similar processes occur today—include deep ferruginous lakes, such as Lake Matano, Indonesia; iron-rich phototrophic microbial mats, such as those in Yellowstone National Park, USA; and the Iron Mountain acid mine drainage site in California, USA. However, it is important to note that considering size, mineralogy, and environmental conditions together, no real modern analogs of BIFs and their depositional environments occur today on Earth.

See the Glossary, p. xxvi, for terms and common abbreviations used in this chapter.

TYPES OF BANDED IRON FORMATIONS

Various classification schemes have been used to refer to different varieties of banded iron formations (BIFs), variably considering features such as age, tectonic setting, mineralogy, and texture (JAMES, 1954; GROSS, 1965, 1980; KIMBERLEY, 1978; SIMONSON, 1985). The most currently used classification considers mainly age and tectonic setting to divide BIFs into two main classes: 1) Algoma-type BIFs, found in volcano-sedimentary sequences of greenstone belts and typical of Eoarchean age; and 2) Superior-type BIFs, formed in stable platform sedimentary successions and characteristic of late Archean to late Paleoproterozoic age (e.g., GROSS, 1965; BEUKES & GUTZMER, 2008). There are also occurrences of BIFs in the Neoproterozoic

related to Snowball Earth (Kirschvink, 1992) glaciogenic sedimentary rocks, which are commonly referred to as Rapitan BIFs (Gross, 1965; Klein, 2005; Macdonald & others, 2010). In addition, BIFs and exhalites occur spatially associated with massive sulfide deposits (MSDs) (e.g., Spry, Peter, & Slack, 2000; Corriveau & Spry, 2014). Exhalites, however, are chemically different than BIFs because they commonly contain a higher metal content (Pb and Zn, for example) compared to normal, non-MSD-related BIFs, and are not included here. Other iron-rich deposits include the Devonian Lahn-Dill-type iron ores in Germany, which occur as lenses and layers of massive iron associated with bimodal and pyroclastic volcanism and carbonate rocks (e.g., Flick, Nesbor, & Behnisch, 1990). The most likely origin of these iron ores is mobilization and redeposition of iron related to secondary diagenetic alteration of pyroclastic rocks (Flick, Nesbor, & Behnisch, 1990). Because some of these iron ores are different than Archean–Proterozoic BIFs, they are not included here. Many Phanerozoic ironstones are different than BIFs in mineralogy and texture but some can be considered similar; therefore, a brief description of these ironstones is included in *Phanerozoic Ironstones* (p. 122–124). Algoma, Superior, and Rapitan BIFs, as well as those associated with massive sulfide deposits (MSDs), are described in separate sections. However, all other mention of BIFs with no specific reference to a particular type imply Archean–Paleoproterozic BIFs and mostly Superior type, and not those related to MSDs.

Texturally, iron formations have been divided into banded iron formations (BIFs) and granular iron formations (GIFs) (see Klein, 2005 and references therein). BIFs are typical of Archean to early Paleoproterozoic successions and formed prior to the rise of atmospheric oxygen during the great oxidation event, ~2.4 Ga (Holland, 1984), whereas GIFs are clastic sedimentary rocks that became abundant after the GOE and are typical of the late Paleoproterozoic (e.g., Klein, 2005). Based on the lack of structures indicative of wave or storm action, Archean BIFs are generally considered to have been deposited in relatively deep water. In contrast, the granular textures typical of late Paleoproterozoic (1.8 Ga) GIFs indicate that they were deposited in shallow water under the influence of waves, likely close to or above storm and fair-weather wave base (e.g., Klein & Beukes, 1992). Granular iron formations can be slaty and cherty and can also be associated with stromatolites (e.g., Pufahl & Fralick, 2004). Both Algoma- and Superior-type BIFs were deposited in open marine environments during high sea level (Simonson & Hassler, 1996; Krapež, Barley, & Pickard, 2003; Fralick & Pufahl, 2006). However, some Superior-type BIFs contain banded and granular textures, the latter of which represent remobilization, transport, and redeposition of BIFs (Beukes & Gutzmer, 2008). GIFs are mainly restricted to Paleoproterozoic continental basins, such as those surrounding the Superior Craton of North America. Examples of BIFs include the giant Brockman Iron Formation of Western Australia (e.g., Klein, 2005), whereas the type examples of GIFs are those from the Lake Superior Region, USA; Labrador Trough, Canada; and Nabberu Basin of Western Australia (James, 1954; Goodwin, 1956; Simonson, 2003; Klein, 2005).

ALGOMA-TYPE BIFs

Algoma-type banded iron formations (BIFs) occur within Eoarchean to early Paleoproterozoic volcano-sedimentary sequences in greenstone belts, range in age from 3.8 Ga to ~2.6 Ga, and are characterized by currently being relatively small occurrences (lateral extent <10 km, thickness <100 m) (Goodwin, 1973; James, 1983; Isley & Abbott, 1999; Huston & Logan, 2004). These BIFs are typically associated with volcanic rocks and greywackes and formed in tectonically active areas in volcanic arcs and spreading centers (Gross, 1995). Because of this association, scientists have hypothesized

that Algoma-type BIFs formed by exhalative hydrothermal processes during pulses of magmatic and hydrothermal activity coeval with the deposition of the volcano-sedimentary successions of greenstone belts (Barley & others, 1998). Many Algoma-type BIFs are typically intensely deformed and folded, in contrast to Lake Superior BIFs that are commonly undeformed. Mineralogically, Algoma-type BIFs are characterized by iron that occurs in ferric and ferrous states in silicates, siderite, magnetite, and hematite.

The ~3.8 Ga Isua BIF, from the Isua Supracrustal Sequence in West Greenland, is an Algoma-type BIF and possibly the oldest BIF in the world. It is found in association with greenstones with low-K tholeiitic characteristics and turbidites, and experienced medium grade (amphibolite facies) metamorphism (Dymek & Klein, 1988; Komiya & others, 1999; Dauphas & others, 2004; Kato, Yamaguchi, & Ohmoto, 2006). Other Algoma-type BIFs include those in the Nulliak supracrustal sequence in Labrador, Canada, dated at ~3.95 Ga (Shimojo & others, 2013) associated with mafic rocks and metamorphosed to amphibolite facies (e.g., Aoki & others, 2013), and those in the 3.13–2.92 Ga Sargur greenstone belt in India, associated with mafic-ultramafic rocks, quartzites, pelites, and calc-silicate rocks and metamorphosed to upper amphibolite-granulite facies (e.g., Kato, Kano, & Kunugiza, 2002; Kato, Yamaguchi, & Ohmoto, 2006).

SUPERIOR-TYPE BIFs

Superior-type banded iron formations (BIFs) mostly formed in the late Archean to late Paleoproterozoic (3.0 to ~1.8 Ga) on stable, passive-margin continental shelf and slope. They are characterized by great areas and lateral extent (up to hundreds of meters thick, >100,000 km^2), are associated with marine siliciclastic (shale and quartzarenite) and carbonate rocks, and lack direct relationships with volcanic rocks (Trendall & Blockley, 1970; Gross, 1983, 1995; Klein, 2005; Kato, Yamaguchi, & Ohmoto, 2006; Beukes & Gutzmer, 2008; Bekker & others, 2010). They are also thought to have formed during periods of global high sea level and during pulses of enhanced magmatic (mantle plumes) and hydrothermal activity (e.g., Bekker & others, 2010). Mineralogically, Superior-type BIFs are characterized by iron in the ferrous state hosted in silicates, siderite, and magnetite, as well as iron in mixed-state minerals (most commonly magnetite) (e.g., Klein & Ladeira, 2004). Late Paleoproterozoic Superior-type BIFs, which have been studied extensively, commonly exhibit granular textures (e.g., Beukes & Gutzmer, 2008), are generally undeformed, and have been metamorphosed to only very low grades (see Klein, 2005; Beukes & Gutzmer, 2008 and references therein).

Examples of Superior-type BIFs include the giant ~2.5 Ga Brockman Iron Formation (Fig. 45.1, see p. 98); the extensive ~2.6 Ga Marra Mamba Iron Formation, and the smaller Weeli Wolli and Boolgeda BIFs of the Hamersley Range, Western Australia; the ~2.5–2.4 Ga Kuruman-Griquatown-Penge Iron Formations of the Kaapvaal craton, South Africa; the ~2.5 Ga BIFs from the São Francisco craton in Minas Gerais, Brazil; the ~2.4 Ga Kursk BIFs from the Kursk magnetic anomaly, Russia; the ~1.88 Ga Biwabik and Gunflint Iron Formations from the Animikie-Marquette basin, North America; and the ~1.88 Ga BIFs from the Yilgarn craton (Nabberu basin), Australia (see Klein, 2005; Beukes & Gutzmer, 2008; Bekker & others, 2010, and references therein).

RAPITAN BIFs

Neoproterozoic (~0.8–0.6 Ga) Rapitan banded iron formations (BIFs) are found in marginal marine settings, some in broad extensional graben settings, and some are located in mobile belts, such as the Pan African and Brazilian-African belts (Gross, 1995; Trompette, Alvarenga, & de Walde, 1998; Ilyn, 2009). They are typically temporally and spatially associated to Sturtian (~716.5 Ma) and Marinoan (~635 Ma) glacial deposits of global Snowball Earth events (e.g., Kirschvink, 1992; Hoffman

& others, 1998). However, studies based on mapping, stratigraphy, and geochemistry of Neoproterozoic BIFs from Namibia and South Africa suggest that all Neoproterozoic iron formations may be of 716.5 Ma Sturtian age (Macdonald & others, 2010). If this is the case, Rapitan BIFs formed as a result of the secular evolution of the redox state of the ocean, which is considered to have been anoxic at the time of iron concentration (Klein & Ladeira, 2004; Macdonald & others, 2010). Because the oceans were covered by ice, hydrothermal iron was able to accumulate in the water and precipitate as ferric oxyhydroxides when mixed with more oxic waters, either derived from subglacial meltwater plumes (Hoffman & others, 1998) or surface waters at the onset of ice melting (Klein & Beukes, 1993).

Rapitan BIFs are commonly associated with diamictite, are typically succeeded by cap carbonates (usually dolomite and rarely limestone), and may contain dropstones (e.g., Bekker & others, 2010; Macdonald & others, 2010). Texturally, these BIFs are commonly laminated, nodular, and oolitic. Mineralogically, Rapitan BIFs consist almost entirely of iron in the ferric state in hematite, in contrast to Archean and Paleoproterozoic BIFs (Klein & Ladeira, 2004). In addition, these iron deposits sometimes host economic manganese concentrations (Klein & Beukes, 1992; Klein & Ladeira, 2004; Halverson & others, 2011). Examples of Neoproterozoic BIFs, some of them large, include the Rapitan BIFs of the Northwestern Territories, Canada; the Urucúm region of Brazil; the Arroyo del Soldado Group, Lavalleja, in Uruguay; the Damara orogen in Namibia; and the Serranía de Mutum in Bolivia (Gross, 1983; Bühn, Stanistreet, & Okrusch, 1992; Klein & Ladeira, 2004; Klein, 2005; Pecoits & others, 2008).

BIFs RELATED TO MASSIVE SULFIDE DEPOSITS

Banded iron formations (BIFs) are commonly associated with metamorphosed base metal (Pb, Zn, Cu) massive sulfide deposits (MSDs) in sedimentary sequences and in felsic volcanic belts (Spry, Peter, & Slack, 2000; Slack, Grenne, & Bekker, 2009; Corriveau & Spry, 2014). These BIFs generally form below, above, in, or along strike from stratiform, exhalative, or volcanogenic ore deposits (e.g., Spry, Peter, & Slack, 2000). Less commonly, they form lateral to the ore deposits and extend for kilometers. Typically, the BIFs form layers less than two meters thick, although they can also reach tens of meters in thickness. They are also normally laminated with varying mineralogy from layer to layer. Geochemical data and diagrams, including those of Al/Al+Fe+Mn vs. Fe/Ti and ternary Al-Fe-Mn, indicate that the BIFs have variable amounts of hydrothermal and detrital components, but usually the detrital content is less than 30 wt% (Corriveau & Spry, 2014). BIFs related to MSDs tend to have a higher detrital component than non-MSD related BIFs but are very similar in most other aspects. Most BIFs associated with sulfide mineralization are chemical sedimentary rocks similar to Algoma-type iron formations and likely formed by venting of hydrothermal fluids into submarine basins (Stanton, 1972, 1976; Spry, Peter, & Slack, 2000).

BIFs occur in spatial association with some of the largest base metal sulfide deposits of the world. The most extensive BIFs associated with massive sulfide deposits (MSDs) are found in volcano-sedimentary sequences of continental rift systems, such as those near the giant Paleoproterozoic (~1.69 Ga) Broken Hill deposit, Australia (Fig. 48.3–48.4) and the Ordovician Bathurst deposit, New Brunswick, Canada (Spry, Peter, & Slack, 2000). BIFs appear close to the Broken Hill and Pinnacles deposits in the southern Curnamona Province of Australia, but also extend laterally and intermittently for about 100 km throughout the province (Stanton, 1972; Plimer, 1988; Parr, 1992; Parr & Plimer, 1993; Spry, Peter, & Slack, 2000; Heimann & others, 2009, 2013). Many of these BIFs do not have a clear temporal relationship with the sulfide ores (Spry, Peter, & Slack, 2000). In the Bathurst mining camp, BIFs and sulfide ore

extend for 12 km (Peter & Goodfellow, 1996). Other important occurrences of BIFs associated with large MSDs appear in the Mesoproterozoic Gamsberg and Aggeneys deposits in South Africa and the Bergslagen deposit in Sweden (e.g., Plimer, 1988; Spry, Peter, & Slack, 2000).

Typical lithologies associated with BIFs related to metamorphosed MSDs include metamorphosed clastic sedimentary rocks and felsic volcanic rocks, as well as minor mafic igneous rocks that do not occur within the ore (Spry, Peter, & Slack, 2000). The mineralogy of the BIFs may include carbonates, oxides, silicates, and/or sulfides. Sulfide-bearing iron formation is present at the Gamsberg deposit (South Africa), the carbonate iron formation at the Bathurst deposit (Canada), the oxide-silicate iron formation at the Broken Hill deposit (Australia), and the Bergslagen deposit (Sweden) (Plimer, 1988; Peter & Goodfellow, 1996; Spry, Peter, & Slack, 2000).

SPATIAL AND TEMPORAL DISTRIBUTION OF BIFs

Archean–Paleoproterozoic banded iron formations (BIFs) range in age from ~3.8 Ga to ~1.88 Ga. Recent studies suggest that all Neoproterozoic BIFs may be ~716.5 Ma, although previous studies considered their ages to be ~0.8–0.6 Ga. The oldest BIFs are those (~3.8 Ga) from the Isua Supracrustal Belt of Western Greenland (Appel, 1987; Dymek & Klein, 1988). Other Archean BIFs include the ~3.6–3.2 Ga BIFs from the Sebakwian Group in Zimbabwe and the ~2.8–2.6 Ga BIFs of the Dharwar Supergroup in India (Manikyamba, Balaram, & Naqvi, 1993; Arora & others, 1995; Khan & others, 1996; Kato, Kano, & Kunugiza, 2002). There is some evidence that indicates that the largest peak in Algoma-type BIF deposition is related to a major mantle plume event at 2.75–2.70 Ga (Huston & Logan, 2004). A second peak in BIF deposition occurred at 2.5–2.45 Ga with the deposition of the large Superior-type BIFs of the Ghaap/Chuniespoort Group of the Kaapvaal Craton, South Africa, and the Hamersley Group, Australia (Houston & Logan, 2004; Beukes & Gutzmer, 2008). Another peak in BIF deposition occurred in the late Paleoproterozoic at ~1.88 Ga in the Lake Superior region of the USA and Canada. Studies of BIFs in the Frere Formation of Western Australia, previously thought to be 1.84 Ga, concluded that they are actually ~1.88 Ga, indicating that the deposition of BIFs in the Lake Superior region of North America and those in Western Australia are coeval and likely reflect global ocean chemistry (Rasmussen & others, 2012). These BIFs are coeval with important 1.88 Ga mafic-ultramafic magmatism, a large igneous province (LIP) interpreted to be related to a mantle plume event, juvenile continental and oceanic crust formation, mantle depletion, and volcanogenic MSD formation (Heaman & others, 1986; Condie, 1998; Isley & Abbott, 1999; Condie, 2002; Franklin & others, 2005; Kemp & others, 2006; Parman, 2007; Pearson, Parman, & Nowell, 2007; Hamilton & others, 2009; Heaman, Peck, Toope, 2009; Bekker & others, 2010; Meert & others, 2011). This suggests that BIFs formed as a result of major mantle activity and crustal growth (Rasmussen & others, 2012). After this event, large BIFs disappear from the rock record for more than one billion years (Klein & Beukes, 1993), returning in the Neoproterozoic associated with global glaciations of Snowball Earth distributed on nine separate paleocontinents (Macdonald & others, 2010). After these, BIFs typical of the Precambrian are not present in the rock record.

The present day geographic distribution of BIFs reaches every continent (e.g., Klein, 2005). Algoma-type BIFs are relatively small and commonly less than 10 km in lateral extent (Beukes & Gutzmer, 2008; Bekker & others, 2010). Examples of Algoma-type BIFs occur in India, Singhbhum Group (3.5 Ga) (Mukhopadhyay & others, 2008), and South Africa, Fig Tree Group, Barberton Greenstone Belt (~3.3 Ga) (Hofmann, 2005), among other places.

The largest BIFs (10^5 km^2) are Superior-type BIFs, such as the Brockman Iron Formation of the Hamersley Range of Western Australia (~2.6–2.45 Ga) (Trendall & Blockley, 1970; Trendall, 2002; Trendall & others, 2004); the Quadrilátero Ferrífero of the Itabira Group, Minas Gerais, Brazil (~2.6-2.4 Ga) (Klein, 2005); and the Kuruman, Griquatown, and Penge Iron Formations of the Transvaal Supergroup of South Africa (~2.5–2.3 Ga) (Klein & Beukes, 1989) (Fig. 45.1). Paleogeographic reconstructions and detailed geochronological studies suggest that the Asbestos Hills-Penge Iron Formations, Kaapvaal Craton, South Africa (~2.5–2.45 Ga) and the Brockman Iron Formation, Pilbara Craton, Western Australia, were deposited synchronously in the super continent Vaalbara (Cheney, 1996; Zegers & others, 1998; Beukes & Gutzmer, 2008). However, some scientists have suggested, that the similarities, including the stratigraphy, reflect synchronized events on a global scale (Trendall, 1968; Button, 1976; Nelson, Trendall, & Altermann, 1999). Of the late Paleoproterozoic BIFs, the large Gunflint Iron Formation in the Animikie basin of North America (~1.88 Ga) contains the first undisputed microfossils that offer evidence of life on the early Earth (e.g., Barghoorn & Tyler, 1965; Awramik & Barghoorn, 1977). See *Clues from Microfossils,* p. 116–118, for elaboration. The youngest of the Paleoproterozoic BIFs include the ~1.7 Ga Baraboo BIF from the Freedom Formation, Wisconsin, USA (e.g., Weidman, 1904), which has not been studied in detail.

Examples of Neoproterozoic BIFs occur between 0.8 and 0.6 Ga in the Rapitan Group, Yukon and the Northwest Territory, Canada (~0.716 Ga); Jacadigo Group in the Urucúm District, Brazil and Bolivia (~0.6 Ga); the Damara Supergroup, Chuos Formation, Namibia (~0.75–0.65 Ga); and Arroyo del Soldado Group, eastern Uruguay (~0.6 Ga) (Breitkopf, 1988; Klein & Beukes, 1993; Klein & Ladeira, 2004; Klein, 2005; Pecoits & others, 2008). An integrated mapping, stratigraphic, geo-chemical, and geochronological study of Neoproterozoic BIFs and associated rocks in Namibia and South Africa proposed that all Neoproterozoic iron formations may be of Sturtian age (~716.5 Ma) (Macdonald & others, 2010), instead of some being Marinoan in age (635 Ma) as previously thought (e.g., Frimmel, 2008). An association between Neoproterozoic BIFs and mantle plume events has also been proposed to explain their time-related genesis (e.g., Bekker & others, 2010). See *Hypotheses of BIF Formation,* p. 103–119, for elaboration on this topic.

MINERALOGY AND GEOCHEMISTRY OF BIFs

MINERALOGY AND PRECURSOR PHASES

The main minerals present in banded iron formations (BIFs) include (Table 2): siderite, magnetite, hematite, chert, stilpnomelane, minnesotaite and accessory ankerite, ferroan dolomite, riebeckite, mica (ferri-annite), and chlorite (Klein, 2005). Pyrite may be present as a rare accessory mineral. Some of these minerals, such as siderite and minnesotaite, required low oxygen conditions, whereas others, such as hematite or its precursor Fe oxyhydroxides, clearly required at least some oxygen present in the environment of formation. Some magnetite, siderite, ferrosilicates (minnesotaite), ankerite, and pyrite likely formed during diagenesis and metamorphism (e.g., Ayres, 1972; Perry, Tan, & Morey, 1973). Ankerite, for example, overgrew early, very thin siderite laminations in the carbonate-rich Kuruman Iron Formation, likely evidencing a late diagenetic origin for ankerite and an early diagenetic origin for siderite (Fig. 45.3–45.4; Fig. 46.1–46.2) (Beukes & Klein, 1990; Beukes & others, 1990; Heimann & others, 2010).

The original mineralogy of BIFs has been debated for decades. The original or early diagenetic mineralogy of BIFs likely included the minerals siderite, amorphous or crystalline ferric hydroxides (ferrihydrite,

1

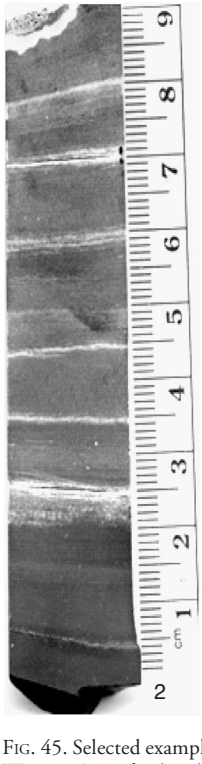

FIG. 45. Selected examples of banded iron formation with different mineralogy from the Brockman Iron Formation, Western Australia (*1–2*) and the Kuruman Iron Formation, South Africa (*3–4*). *1,* View of the Dales Gorge of the giant Brockman Iron Formation (new; image courtesy of Clark M. Johnson). *2,* Core slab sample of banded and laminated oxide and carbonate BIF; magnetite (gray), siderite + stilpnomelane (brown), pure siderite (light tan),

(*continued on facing page*)

TABLE 2. Mineralogy and chemistry of major mineral constituents in Banded Iron Formations.

Mineral Group	Mineral Species	Chemical Composition
Carbonates	Siderite	$FeCO_3$
	Ankerite	$Ca(Fe^{2+},Mg)(CO_3)_2$
	Ferroan dolomite	$(CaMg,Fe^{2+})(CO_3)_2$
Oxides	Magnetite	Fe_3O_4 (or $FeO.Fe_2O_3$)
	Hematite	Fe_2O_3
Silicates	Quartz	SiO_2 (chert or amorphous silica)
	Stilpnomelane	$K(Fe^{2+},Mg,Fe^{3+})_8(Si,Al)_{12}(O,OH)_{27}.n(H_2O)$
	Greenalite	$(Fe^{2+},Fe^{3+})_{2-3}Si_2O_5(OH)_4$
	Minnesotaite	$Fe^{2+}{}_3Si_4O_{10}(OH)_2$
	Riebeckite	$Na_2(Fe^{2+},Mg)_3Fe^{3+}{}_2Si_8O_{22}(OH)_2$
	Ferriannite	$KFe^{2+}{}_3((Fe^{3+},Al)Si_3O_{10})(OH)_2$
	Chlorite	$(Mg,Fe^{2+})_3(Si,Al)_4O_{10}(OH)_2(Mg,Fe^{3+})_3(OH)_6$
	Nontronite	$Na_{0.3}Fe_2(Si,Al)_4O_{10}(OH)_2.nH_2O$
Hydroxides	Ferrihydrite	$Fe^{3+}{}_2O_3.0.5(H_2O)$
	Ferric hydroxide	$Fe^{3+}(OH)_3$
	Goethite	$Fe^{3+}O(OH)$
Sulfides	Pyrite	FeS_2

ferric hydroxide, and goethite), greenalite, nontronite, and amorphous silica (Table 2) (e.g., KLEIN, 2005; BEUKES & GUTZMER, 2008). It has also been suggested that most siderite and pyrite in BIFs precipitated within the water column of anoxic basins, but some also formed during early diagenesis (OHMOTO & others, 2006). Silica was also present in the structure of original clays. Thermodynamic calculations and experiments indicate that ferric hydroxides (ferrihydrite or goethite) can be transformed to hematite by dehydration and recrystallization reactions during early diagenesis (BERNER, 1969; SCHWERTMANN & CORNELL, 1991). Nanoscale hematite inclusions found within siderite in the Kuruman BIF have been interpreted as reflecting the origin of siderite in a reaction involving coupled oxidation of organic matter and reduction of Fe(III) hosted in primary hematite or an original Fe(III) hydroxide by bacterial dissimilatory iron reduction (DIR) (HEIMANN & others, 2010). Similar

FIG 45. (*continued from facing page*)

Dales Gorge Member, Brockman Iron Formation, Western Australia, sample DDH#44-19. *3,* Core sample of banded and finely laminated carbonate BIF with siderite-chert laminations (dark black), pure siderite laminations (light brown), and large, diagenetic ankerite (white), Kuruman Iron Formation, Transvaal, South Africa, sample WB98-815 (*2–3,* core samples, Geology Museum, University of Wisconsin-Madison; new, photos, Adriana Heimann). *4a–b,* Iron-carbonate microlaminations, organic matter remains, and mineralogy typical of the Kuruman Iron Formation; *a,* photomicrograph showing siderite mud microlaminae (*Sid,* dark gray-brown), organic matter remains (*OM,* black), and diagenetic ankerite (*Ank,* white, coarser grained), plane polarized ×10, sample WB98-800A; *b*, back-scattered scanning electron microscope image of same sample showing siderite (almost white), coarser diagenetic ankerite (gray), and organic matter (black) remains (new). Color version available in *Treatise Online* 147 (paleo.ku.edu/treatiseonline).

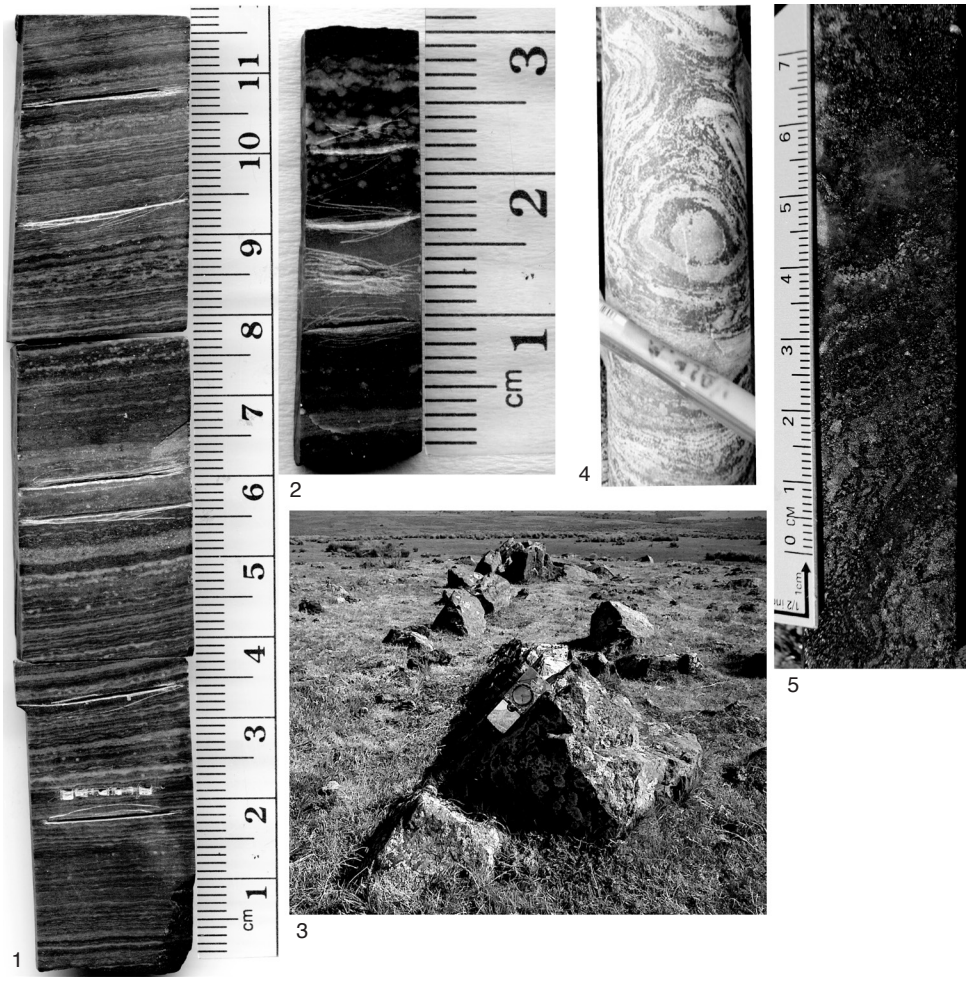

5

FIG. 46. Selected examples of banded iron formations with different mineralogy from various locations worldwide. *1,* Core slab sample showing banded and finely laminated carbonate BIF of the Kuruman Iron Formation, South Africa, pure siderite laminations (light brown/tan), lamination rich in hematite (reddish), sample DI1-213.8 (Geology Museum, University of Wisconsin-Madison). *2,* Core slab sample of banded carbonate BIF of the Kuruman Iron Formation, siderite (dark), large, late, diagenetic ankerite (white areas), sample AD5-161-9A, Geology Museum, University of Wisconsin-Madison (*1–2,* new; photos, Adriana Heimann). *3,* Field photo of the Valentines Iron Formation, Nico Pérez Terrane, Uruguay, compass for scale (new; photo courtesy of Richard Lateulade). *4,* Core sample of deformed and metamorphosed quartz-magnetite iron formation from the Valentines Iron Formation, quartz (white), magnetite (dark, brown). *5,* Core slab sample of deformed banded quartz-magnetite-pyroxene iron formation, magnetite (reddish brown), quartz (dark), pyroxene (greenish), quartz (coarse, whitish spots), Valentines Iron Formation (new; photo, Heather Lancaster). Color version available in *Treatise Online* 147.

hematite microspheroids, dusty hematite, or microcrystalline hematite have been reported from other BIFs, including the Bruno's BIF of the Mount Sylvia Formation, Hamersley Basin (Western Australia), and interpreted to be the result of recrystallization of original ferrihydrite (e.g., BEUKES & GUTZMER, 2008).

BIFs were originally classified based on their dominant mineralogy as carbonate, oxide, silicate, and sulfide facies BIFs (JAMES, 1954). Sulfide facies BIFs were originally defined as pyritic and organic carbon-rich black shales with high iron contents (>15 wt%) (JAMES, 1954), although most authors

do not consider these as BIFs but as shales (e.g., Bekker & others, 2010). These shales commonly occur stratigraphically above, below, or interbedded with oxide or carbonate. More recently, Beukes and Gutzmer (2008) classified BIF facies into oxide-, hematite-, and siderite-facies BIFs. Some BIFs contain more than one dominant type of mineral. Oxide facies BIFs are comprised predominantly of magnetite, hematite, and chert. The large Superior-type ~2.5 Ga Brockman Iron Formation (Fig. 45.1–45.2) is a good example of an oxide facies BIF but also contains carbonate (siderite)-rich bands and silicates (stilpnomelane) (Ewers & Morris, 1981; Pecoits & others, 2009, and herein). The giant ~2.5 Ga Kuruman Iron Formation is an excellent example of a carbonate-rich BIF primarily composed of siderite, ankerite, and minor ferroan dolomite with local laminations of iron oxides (Fig. 45.3–45.4; Fig. 46.1–46.2) (Klein & Beukes, 1989; Beukes & others, 1990; Heimann & others, 2010). It represents the best-preserved, carbonate-rich BIF, as it has only been affected by very low metamorphism and almost no deformation. It is characterized by millimeter-scale laminations of very fine-grained (up to 5 μm) siderite with interstitial organic matter intercalated with very fine-grained chert (Fig. 45.4a–b). Ankerite appears as an accessory, late diagenetic, medium-grained mineral in the fine-grained, siderite-rich laminations (Fig. 45.4a; Fig. 46.1–46.2). Other BIFs also contain oxide and carbonate minerals. Algoma- and Superior-type BIFs are similar mineralogically, whereas Neoproterozoic BIFs have very simple mineralogies, containing mainly iron oxides and silica (Klein & Beukes, 1992; Klein & Ladeira, 2004).

Most Archean BIFs have experienced metamorphism and deformation and only some have very low or low metamorphic grade mineral assemblages (Fig. 47). Many of the large and most-studied late Archean–early Proterozoic BIFs, such as the Kuruman and Brockman BIFs, have undergone only very low-grade metamorphism and even preserve diagenetic mineral assemblages (Fig. 45.4a) (Klein, 2005). In most cases metamorphism was isochemical, except for dehydration and decarbonation reactions. The BIFs of the Hamersley Basin in Australia have been metamorphosed to sub-greenschist to greenschist facies conditions at estimated burial temperatures of 200–300°C and burial pressures of ~1.2 kbar (Klein & Gole, 1981; Kaufman, Hayes, & Klein, 1990). The burial temperatures of the BIFs from the Kaapvaal Basin in South Africa have been estimated to be one of the lowest, at 100–150°C (Miyano & Klein, 1983).

The mineralogy of silicate-rich BIFs depends on the metamorphic grade. At low metamorphic grades of the biotite zone, the minerals can include greenalite, stilpnomelane, minnesotaite, chamosite, ripidolite, riebeckite, and minor ferriannite. At medium and high pressures and temperatures, amphiboles (cummingtonite, grunerite, actinolite, hornblende), pyroxenes, fayalite, and minor garnet form (Fig. 46.3–46.5; 48.3–48.4) (Klein, 2005).

GEOCHEMISTRY

Most researchers agree that original iron-rich minerals in banded iron formations (BIFs), except some Fe silicates, formed by oxidation and direct precipitation of iron dissolved in seawater as Fe(III) oxyhydroxides in large water bodies (Trendall & Blockley, 1970; Ayres, 1972; Ewers & Morris, 1981; Trendall, 2002). If this is the case, the geochemistry of BIFs can help scientists understand the chemistry of the water from which they precipitated. In particular, rare earth elements (REEs) in BIFs could serve as redox proxies (e.g., Bau & Möller, 1993; Planavksy & others, 2010). However, there are still some unknowns regarding the fractionation of elements and isotopes during precipitation and the effects of diagenesis and metamorphism. In addition, some scientists have argued and continue to postulate that the precursor sediments of BIFs were not direct chemical precipitates but microgranular muds or

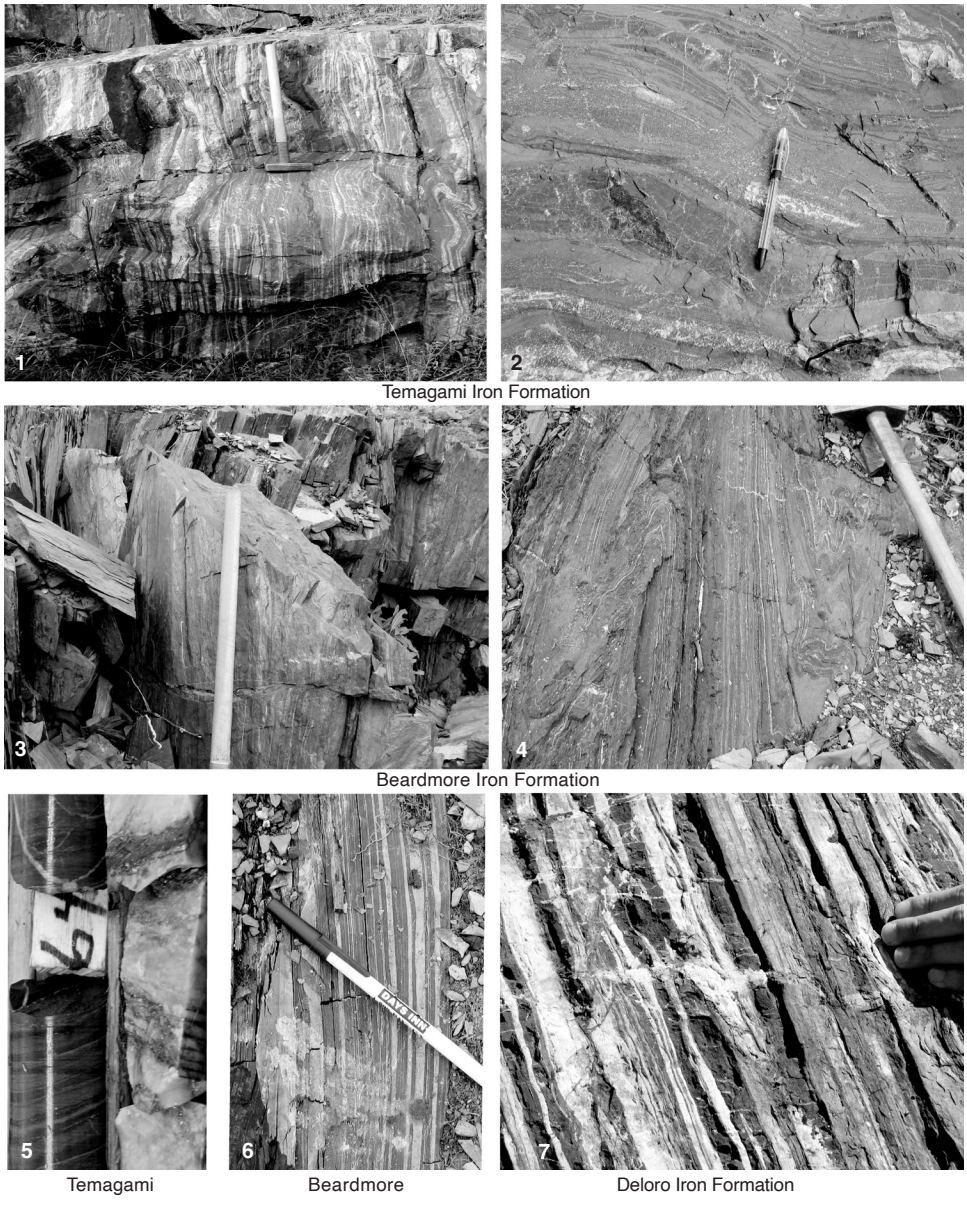

Fig. 47. Photos showing mesoscopic layering and deformation features of various deformed banded iron formations from the southwestern Superior Province, Ontario, Canada (new; all photos, Adriana Heimann). *1,* Outcrop of Neoarchean, Algoma-type, Temagami Iron Formation (2.7 Ga) showing vertical to subvertical layering and minor folding, layers of gray/black hematite (gray), red jasper (chert and hematite), and chert (white); also present, carbonates and iron silicates, Sherman Mine, Cobalt area. *2,* Close-up of outcrop showing deformation features in the Temagami Iron Formation, layers are red jasper (chert with hematite) and black-gray hematite. *3,* Neoarchean BIF (2.7 Ga), Beardmore area, BIF is red and metallic gray and characterized by vertical to subvertical layering of hematite-magnetite (gray) and jasper (red). *4,* Close-up of horizontal face of outcrop of Beardmore iron formation showing thin, deformed, folded layers of specular hematite and magnetite (gray) and chert + hematite (red). *5,* Drill core of laminated Neoarchean (2.7 Ga) Temagami Iron Formation associated with mafic-intermediate volcanic rocks, laminations composed of red hematite, gray magnetite, also a quartz vein with pyrite, Sherman Mine, sample core ORS_1-87, 64 feet. *6,* Outcrop image from the Beardmore area showing vertical laminations of oxide-rich (magnetite-hematite)

(*continued on facing page*)

Fe-rich, Al-poor silicate microgranules that were resedimented by dilute density currents. The granules were originally comprised of greenalite, chamosite, or nontronite and are now present as stilpnomelane (Table 2, see p. 99) (Krapež, Barley, & Pickard 2003; Rasmussen & others, 2013).

The iron content of BIFs typically ranges from 15 to 35 wt% Fe, and their silica content varies from 34 to 56 wt% SiO_2 (James, 1954; Klein, 2005). The concentrations of CaO, MgO, MnO, Al_2O_3, Na_2O, K_2O, and P_2O_5 are typically low. The Ca, Mg, and Mn contents reflect the presence of carbonate (siderite, ankerite, minor calcite), whereas Al, Na, and K are hosted mainly by silicates (riebeckite, greenalite, stilpnomelane; Klein, 2005). The CaO and MgO values range from 1.8 to 9.0 wt%, whereas those for Na_2O and K_2O are very low (<1.5 wt%). The very low-metamorphic-grade, siderite-rich BIF from the Kuruman Iron Formation has organic carbon contents ranging from 0.05 to 0.2 wt% (see Fig. 45.4) (Klein & Beukes, 1989). Magnetite-rich BIFs from the same sequence have even lower organic carbon contents (Klein, 2005), which has been the focus of debate regarding the role of biologic processes in mediating the deposition of BIF minerals.

It is commonly accepted that, under conditions of low fluid/rock ratios, bulk-rock REE contents are not affected by post-depositional processes, such as diagenesis and metamorphism (e.g., Taylor & McLennan, 1986; McLennan & Taylor, 1991; Bau, 1991). The REE contents and the presence of Ce and Eu anomalies in normalized REE patterns of BIFs have been used to understand their origin and the chemical composition and redox state of the Precambrian oceans. Cerium anomalies are defined as $Ce/Ce^* = Ce_N/(\{La_N+Pr_N\}/2)$ (where N refers to the normalization value of shale composites or the Chondrite concentration, and Ce* to the predicted normalized concentration calculated from the equation) and true negative Ce anomalies have Ce/Ce* <1 and Pr/Pr* ($Pr_N/[\{Ce_N+Nd_N\}/2]$) >1 (Bau & Dulski, 1996; Planavsky & others, 2010). Another way of defining the Ce anomaly is using Pr and Nd to avoid utilizing possibly anomalous concentrations of La. Thus, it is defined as $Ce^*_N = Pr^*_N(Pr_N/Nd_N)^2$ (Lawrence & Kamber, 2006). In modern oxygenated seawater, true negative Ce anomalies develop when Ce^{3+} is oxidized and removed as Ce^{4+} by Fe-Mn oxides or hydroxides, organic matter, and clays. Consequently, modern oxic seawater is depleted in Ce and has very large negative Ce anomalies. Suboxic and anoxic waters (0.05–5 μmol O_2 and no dissolved sulfide) lack significant negative Ce anomalies, and some have positive Ce anomalies. These anomalies are the result of reductive dissolution of settling Mn-Fe-rich particles that return Ce back to seawater which is then captured by precipitating Fe-Mn oxides (German & Elderfield, 1990; De Carlo & Green, 2002). Cerium has therefore been used to determine paleooceanic redox conditions. Europium anomalies ($Eu/Eu^*= Eu_N/[\{Sm_N+Gd_N\}/2]$) develop due to an abundance of Eu^{2+} in high-temperature (>250 °C), reduced, hydrothermal fluids and reflect the relative contribution of hydrothermal and riverine influx to the oceans (Klinkhammer, Elderfield, & Hudson, 1983; Sverjensky, 1984; Elderfield, 1988). For further discussion of the significance of REE compositions of BIFs as indicators of paleooceanic redox conditions, see p. 107–108.

HYPOTHESES OF BIF FORMATION

The processes responsible for the generation and precipitation of the vast amounts of iron present in banded iron formations

Fig 47. (*continued from facing page*)
Neoarchean iron formation (dark) with interbedded metapelitic rocks (lighter gray). *7,* Close-up outcrop view of Neoarchean Deloro Iron Formation (2,723 Ma) from the Abitibi Greenstone belt, Canada, exhibiting banded magnetite-hematite (gray/black), siderite (brown), and chert (not visible), with crosscutting veins. Color version available in *Treatise Online* 147 (paleo.ku.edu/treatiseonline).

(BIFs) have been the subject of extensive study during the last ~60 years (e.g., Gross, 1988; Brown, Gross, & Sawicki, 1995). A summary of some of the main ideas about BIF formation is presented here, followed by a more detailed view of the recent thinking about the source of iron and silicon, the origin of the banding in BIFs, the paleoredox ocean structure, and inorganic and biological hypotheses of BIF formation. Table 3 provides a summary of the current thinking of the processes (organic and inorganic) involved in the formation of some well-studied Precambrian BIFs.

The most accepted view of BIF genesis holds that they formed in Archean and Paleoproterozoic oceans that were characterized by extremely low sulfate and sulfide concentrations and oxygen-free deep waters that contained high amounts of dissolved ferrous Fe [$(Fe(II)_{aq}$] (Canfield, Habicht, & Thamdrup, 2000; Canfield, 2005). Most researchers agree that a large reservoir of marine dissolved Fe(II) (~20 ppm; Ewers, 1980; Veizer, 1983) in the Archean and Paleoproterozoic oceans existed due to a high hydrothermal iron flux and a reduced atmosphere, or one that had a low oxidation potential (Holland, 1973; 1984; 2006; Bekker & others, 2004; Kump & Seyfried, 2005). The low sulfate and sulfide contents were necessary to maintain the large amounts of dissolved iron (Habicht & others, 2002). In such an environment, the accumulation of large volumes of iron took place by oxidation of hydrothermally derived Fe(II) and precipitation (Jacobsen & Pimentel-Klose, 1988; Klein & Beukes, 1992; Holland & Petersen, 1995; Isley, 1995). Cloud (1965) was the first to consider the role of bacterial processes for the generation of Fe(III) in BIFs and invoked oxidation of riverine Fe(II) by O_2 produced by oxygenic photosynthesis (cyanobacteria). A contrasting view of BIF genesis, based on the similarity of ancient BIFs and modern chert-hematite deposits associated with volcanogenic massive sulfide deposits (MSDs), considers that BIFs are the result of local discharge of submarine hydrothermal fluids under a fully oxygenated atmosphere and oceans (except in local basins) since ~3.8 Ga (Ohmoto, 1997, 2004; Ohmoto & others, 2006; Kato & others, 2006).

Considerable effort in the study of the origin of BIFs has centered particularly on the mechanisms of oxidation of Fe(II) to Fe(III), the latter estimated to account for 40% of the total Fe in BIFs (Ohmoto & others, 2006; Konhauser & others, 2007; Beukes & Gutzmer, 2008). Most models of BIF formation invoke two stages of Fe cycling. First, hydrothermal Fe(II) is oxidized in the photic zone of the oceans resulting in the crystallization and deposition of Fe(III) oxides or oxyhydroxides on the seafloor. Then, $Fe(II)_{aq}$ reacts with deposited Fe(III) oxides in the sediment or during diagenesis to produce mixed valence minerals or with carbonate or dissolved silica to produce siderite or Fe(II) silicates (Klein, 2005; Beukes & Gutzmer, 2008; Johnson, Beard, & Roden, 2008). Possible mechanisms of Fe oxidation include abiologic and biologically mediated Fe(II) oxidation by oxygen (Cloud, 1965; Konhauser & others, 2002), UV Fe(II) photo-oxidation (Cairns-Smith, 1978; Braterman, Cairns-Smith, & Sloper, 1983), and anoxygenic phototrophic Fe(II) oxidation (or photoferrotrophy) (Widdel & others, 1993; Kappler & others, 2005). It is more than likely that no single mechanism was responsible for the oxidation, precipitation, and generation of the vast amounts of iron present in Precambrian BIFs (Trouwborst & others, 2007). The generation of the Fe(II) present in BIF minerals (magnetite, siderite, Fe silicates) has also been debated and ascribed to either direct inorganic precipitation of Fe(II) (e.g., Beukes & others, 1990) or bacterial DIR (Walker, 1984; Johnson & others, 2003; Johnson & others, 2008; Johnson, Beard, & Roden, 2008).

One of the most striking discoveries is the temporal relationship between the episodic deposition of giant BIFs and major mantle plume events evidenced by the emplace-

TABLE 3. Summary of the current thinking of the processes (organic and inorganic) involved in the formation of some well-studied Precambrian banded iron formations (*ank*, akerite; *cal*, calcite; *goe*, goethite; *hem*, hematite; *mgt*, magnetite; *qtz*, quartz; *sid*, siderite; *stp*, stilpnomelane).

BIF	Mineralogy	Metamorphism	Age	Type	Processes	References
Isua and Akilia, Greenland	Fe silicates, mgt, qtz	Amphibolite-granulite facies	~3.8 Ga	Algoma	Inorganic or organic mediated by anaerobic photosynthetic oxidation	Dauphas & others, 2004; Whitehouse & Fedo, 2007; Czaja & others, 2013
Carajás BIF, Brazil	Hem, ±mgt, goe, qtz, kerogen	Lower greenschist facies	~2.75 Ga	Superior	Inorganic, organic oxidation (from biomats)	Klein & Ladeira, 2002; Fabre & others, 2011; Ribeiro da Luz & Crowley, 2012
Marra Mamba BIF, Australia	Mgt, hem, qtz	Lower greenschist facies	~2.6 Ga	Superior	Organic	Brocks & others, 1999; Summons & others, 1999
Kuruman BIF, South Africa	Sid, ank, mgt, hem, qtz, kerogen	Lower greenschist facies	~2.5 Ga	Superior	Bacterial DIR (siderite); inorganic precipitation from Fe(II) waters	Johnson & others. 2003; Beukes & Gutzmer, 2008; Heimann & others, 2010; Johnson & others, 2013
Dales Gorge Member, Brockman BIF, Australia	Sid, mgt, hem, stp, qtz	Lower greenschist facies	~2.5 Ga	Superior	Bacterial DIR (siderite); chemolithotrophic or photoferrotrophic Fe(II) oxidation (Fe oxides); inorganic (Fe-rich silicates)	Konhauser & others, 2002; Johnson & others, 2003; Pecoits & others, 2009; Cradock & Dauphas, 2011; Li & others, 2013; Rasmussen & others, 2013
Hotazel BIF, South Africa	Mgt, hem, Fe silicates, qtz, ank, cal	Lower greenschist facies	~2.3 Ga	Superior	Inorganic? oxidation	Tsikos & others, 2010
Gunflint BIF, North America	Hem, qtz, carbonates	Lower greenschist facies	~1.88 Ga	Superior	Bacterial oxidation	Planavsky & others, 2009
Rapitan BIF, Canada	Hem, qtz	Lower greenschist facies	~716.5 Ma	Rapitan	Inorganic? oxidation	Halverson & others, 2011

ment of LIPs (KLEIN & BEUKES, 1992; ISLEY, 1995; ISLEY & ABBOTT, 1999). Similarly, a close temporal association of BIFs with volcanogenic MSDs was identified decades ago (e.g., VEIZER, 1976; JAMES, 1983; ISLEY & ABBOTT, 1999; HUSTON & LOGAN, 2004; HUSTON & others, 2010). In a study of BIFs, the association between BIFs of all ages and volcanogenic MSDs was attributed to the interplay among mantle plume events that led to the formation of LIPs, enhanced rates of midocean ridge spreading, high hydrothermal fluxes in the oceans, and changing surface redox states (BEKKER & others, 2010).

The disappearance of large BIFs from the rock record at ~1.8 Ga ago has been attributed to the increase in seawater sulfate concentration as a result of oxic chemical weathering of the continents due to rising atmospheric oxygen contents, the subsequent expansion of bacterial dissimilatory sulfate reduction (DSR), and the formation

of a sulfidic ocean in the Proterozoic, which would have favored iron sulfide precipitation over iron oxidation (Canfield, 1998; Habicht & others, 2002; Poulton, Fralick, & Canfield, 2004). Alternatively, their disappearance has simply been attributed to the complete oxidation of the atmosphere (e.g., Holland, 1984, 2006), but this is also a topic of debate. The hypothesis of a sulfidic ocean transition at ~1.84 Ga implies one of the most significant changes in ocean chemistry throughout Earth's history and is largely based on sulfur isotope compositions and iron speciation data from sedimentary rocks in the Paleoproterozoic Animikie Basin of North America (e.g., Poulton, Fralick, & Canfield, 2004). This transition to a global sulfidic ocean, however, was challenged on the basis of new sulfur isotope data in the context of recent tectonic and sedimentologic models from a correlative section in northern Michigan, USA. These data and models suggest that the Animikie Basin studied to support the hypothesis actually records a basin with restricted water circulation and not open circulation with the global ocean (Pufahl, Hiatt, & Kyser, 2010). However, there is also debate as to whether this basin was a restricted basin or open ocean (Fralick, Poulton, & Canfield, 2011; Pufahl, Hiatt, & Kyser, 2011).

SOURCES OF IRON AND SILICA AND THE ORIGIN OF THE BANDING

The source of iron and silicon in banded iron formations (BIFs) is considered to have been oceanic hydrothermal vents mixed with seawater plus a continentally derived freshwater input (Simonson, 1985; Gross, 1993; Hamade & others, 2003; Delvigne & others, 2012). Most studies have focused on the origin of the iron. Earlier ideas proposed a continental-weathering source for iron and that BIFs formed in continental environments by precipitation of iron and silicon due to evaporation of water (Garrels, 1987). In this model, the banding in BIFs represents cyclic episodes similar to those that produce varves (Garrels, 1987). Later studies agree on a hydrothermal iron source (e.g., Jacobsen & Pimentel-Klose, 1988; Bau & Möller, 1993). More recent studies based on the chemical composition of mesobands of the Dales Gorge Member of the Brockman Iron Formation of Western Australia proposed that metal/Si ratios could help distinguish a continental versus a hydrothermal source for the silica (Hamade & others, 2003). Iron-rich mesobands have Ge/Si ratios that reflect a hydrothermal source for the silicon. In contrast, chert-rich mesobands and mesobands with varved laminations have ratios that fall within the continental end-member range of compositions, which suggests a continental source and weathering of a landmass as the predominant source for the silica.

Precambrian ocean waters were silicon-saturated (~120 ppm Si) due to the absence of silica-secreting microorganisms (e.g., diatoms, radiolarians) at that time, which allowed the precipitation of large quantities of amorphous silica (Siever, 1992). The role of microorganisms in generating the silicon component of BIFs has not received much attention because silicon cannot be metabolized by prokaryotes (archaea and bacteria), the only organisms available during the formation of early BIFs (e.g., Koehler, Konhauser, & Kappler, 2010). However, a biological role for silica precipitation has also been proposed because bacteria are known to promote silicification through their metabolic activity (Birnbaum & Wireman, 1985). Some scientists have suggested that all the chert in BIFs is of early diagenetic origin and not a primary precipitate or diagenetic replacement of earlier silica precipitated from seawater (Krapež, Barkey, & Pickard, 2003; Pickard, Barkley, & Krapež, 2004). In this model, chert was more likely a pore-filling cement and a replacement of sediments.

A later model proposed that silica could have been adsorbed onto the surface of hydrous ferric oxides, which precipitated on the bottom of the ocean along with organic matter (Fischer & Knoll, 2009). Then, once in the sediment pile, reduction of

Fe(III) by bacterial respiration released most of the iron as $Fe(II)_{aq}$ and liberated silica to the sediment pores, which ultimately precipitated as a diagenetic mineral (Fischer & Knoll, 2009). Similarly, based on coupled Ge/Si ratios, REE+Y, and silicon isotope studies, a hypothesis for a two-stage precipitation of silica was proposed by Delvigne and others (2012). They envisioned a first stage of silicon adsorption onto Fe oxyhydroxides followed by early diagenetic release of silica to pore fluids from the Fe oxyhydroxides and consequent silica precipitation upon silica saturation at the sediment-water interface. These ideas have important consequences for the interpretation of oxygen and silicon isotope compositions in chert as indicative of a high seawater temperature in the Archean and Proterozoic (Knauth & Lowe, 2003; Robert & Chaussidon, 2006).

During BIF formation, precipitation of iron probably took place episodically, which caused the development of alternating Fe- and Si-rich bands. The origin of these alternating bands, including their presumed lateral continuity for hundreds of kilometers, has also been the matter of extensive research for more than 50 years (Trendall, 1968; Garrels, 1987; Posth & others, 2008). Based on recent detailed studies including modeling, bacteria incubations, and petrographic studies, the main hypotheses currently being considered to explain the banding include: 1) seasonal stratification or yearly climatic cycles, which would allow for periodic upwelling or pulses of hydrothermal Fe(II)-rich waters interrupted by seasonal evaporation and precipitation of silica (Holland, 1973; Garrels, 1987; Jacobsen & Pimentel-Klose, 1988; Siever, 1992; Morris, 1993); 2) temperature fluctuations, which would allow the maximum biogenic Fe(III) precipitation by iron oxidizing microbes (Fe(II)-oxidizing phototrophs) at 20–25 °C and lower Fe oxide precipitation and abiotic silica precipitation at higher or lower temperatures (Posth & others, 2008); and 3) formation and deposition of silt-size iron-rich silicate microgranules accompanied by alternating seafloor silicification during nondeposition and burial compaction of non-silicified lamina sets (Rasmussen & others, 2013). Based on the first two hypotheses, it seems that temperature could have been an important factor controlling BIF formation in the Archean and Proterozoic oceans. However, because temperature estimates for the Archean and Proterozoic are still a matter of considerable debate, this require further studies.

PALEOOCEANIC REDOX STRUCTURE AND THE FORMATION OF BIFS

Secular variations of cerium (Ce) and europium (Eu) anomalies in banded iron formations (BIFs) have been used to understand the redox state and hydrothermal versus riverine input to the Precambrian oceans and the bio-geochemical evolution of Earth (Klein, 2005; Kato, Yamaguchi, & Ohmoto, 2006; Bekker & others, 2010; Planavsky & others, 2010). In general, the concentration of REEs and the size of the positive Eu anomaly in BIFs seem to decrease with decreasing BIF age (Klein, 2005; Kato, Yamaguchi, & Ohmoto, 2006; Planavsky & others, 2010). Pre-2.7 Ga, Algoma-type BIFs (Isua BIF) have very strong positive Eu anomalies. Middle Archean BIFs (Cleaverville, Australia, and Sargur, India BIFs) have distinct positive Eu anomalies but they are smaller than those in the early Archean BIFs (Rao & Naqvi, 1995; Huston & Logan, 2004; Kato, Yamaguchi, & Ohmoto, 2006). Late Paleoproterozoic BIFs have smaller Eu anomalies. Neoproterozoic BIFs have REE patterns with no or slightly positive Eu anomalies (Fryer, 1976; Klein & Beukes, 1993; Klein & Ladeira, 2004). This trend in Eu anomalies suggests a declining hydrothermal input into the deep ocean from the Eoarchean to the Early Proterozoic, likely linked to falling temperatures of the hydrothermal solutions as a result of lowering upper-mantle temperatures (Bau & Möller, 1993). In addition, no or slightly positive Eu anomalies in Neoproterozoic BIFs indicate

the dilution of local hydrothermal fluids by mixing with mildly oxidized seawater in semi-isolated basins (e.g., Maynard, 2003).

New studies show that bulk Archean and early Paleoproterozoic BIFs lack significant shale-normalized negative Ce anomalies, and that strong positive Ce anomalies are only present in BIFs younger than 1.9 Ga (Planavsky & others, 2010). Some earlier studies of smaller samples have suggested that Ce anomalies were also present in Archean and early Paleoproterozoic BIFs (e.g., Kato, Yamaguchi, & Ohmoto, 2006; Ohmoto & others, 2006). However, bulk-rock studies reflect the overall chemistry of the water mass and the latest findings have been used to propose that late Paleoproterozoic BIFs record the shuttle of metal and Ce oxides from oxic shallow seawater to deeper anoxic waters, similar to the process taking place in modern redox-stratified basins (e.g., Planavsky & others, 2010). In this scenario, as the Ce-bearing oxides (mainly Mn) are transported to the deeper part of the water column, they dissolve under anoxic conditions and release Ce to the water, which is later incorporated in Fe oxides that precipitate at the redoxcline or in the shallow oxygenated water, thus resulting in a positive Ce anomaly (Planavsky & others, 2010; Bekker & others, 2010). In contrast, Archean BIFs do not show the effects of an oxide shuttle, implying the absence of a redoxcline before the rise of atmospheric oxygen (Planavsky & others, 2010; Bekker & others, 2010). This model supports the idea that Archean BIFs formed by metabolic oxidation of iron and not by oxidation of iron by free oxygen in shallow ocean environments (Planavsky & others, 2010; Czaja & others, 2013).

INORGANIC HYPOTHESES FOR BIF FORMATION

UV Photo Oxidation of Fe(II) by Radiation of a Young Sun

An inorganic mechanism to explain Fe(II) oxidation in the Archean is photo oxidation by UV radiation (Cairns-Smith, 1978; Braterman, Cairns-Smith, & Sloper, 1983). This process could have been possible due to the high levels of ultraviolet radiation that reached Earth prior to the formation of the protective ozone layer (Cairns-Smith, 1978). UV photolysis would not have required free oxygen to oxidize dissolved ferrous Fe but instead requires absorption of radiation (wavelengths in the ~200–400 nm range) to form dissolved ferric iron:

$$2Fe^{2+}_{(aq)} + 2H^{+} + h\upsilon = 2Fe^{3+}_{(aq)} + H_{2(g)}$$

Dissolved ferric iron is subsequently hydrolyzed to form solid ferric hydroxide at circumneutral pH (Cairns-Smith, 1978; Braterman, Cairns-Smith, & Sloper, 1983). This mechanism has been demonstrated in laboratory experiments (Braterman, Cairns-Smith, & Sloper, 1983), although only for simple aqueous solutions in which other ions were not available for reactions with original dissolved ferrous iron. Experiments with silica- and calcite-saturated solutions that mimic deep water conditions suggested that the process of photo oxidation would have been slower than and inhibited by the formation of ferrous silicate minerals (such as greenalite) and carbonates (siderite) in the silica-saturated Precambrian ocean waters from which BIF minerals precipitated (Konhauser & others, 2007). In addition, the calculated precipitation rates of ferric iron oxides through photo-oxidation obtained from the earlier experiments yield an annual amount of Fe(II) oxidized from 2.3×10^{13} to 1.8×10^{14} mol/yr (Braterman & Cairns-Smith, 1986; François, 1986). These precipitation rates, however, are faster than sedimentation rates calculated for the Kuruman and Brockman BIFs (compacted sedimentation rates = 22–33 m/myr) (Pickard, 2002, 2003). The consensus seems to be that UV photo oxidation was not likely a dominant process in the formation of ferric oxide minerals in BIFs older than 2.5 Ga (e.g., Koehler, Konhauser, & Kappler, 2010). However, more detailed experiments would help understand the role of this process in the generation of BIFs prior to the rise of atmospheric oxygen.

Abiotic Fe(II) Oxidation by O_2 Produced by Cyanobacteria

A traditional view of Fe(II) oxidation considers inorganic oxidation of dissolved Fe(II) with oxygen produced by photosynthetic cyanobacteria (Cloud, 1965). Prokaryotic microbes, such as oxygenic photosynthesizing cyanobacteria, were likely abundant in the nutrient- and Fe(II)-rich photic zones of nearshore Archean oceans, where Fe(II) and nutrients originated by a combination of continental weathering and upwelling of deep hydrothermal waters (Cloud, 1973). This model envisions an anoxic atmosphere where Fe could have been oxidized by a reaction with O_2 in so-called oxygen oases via oxygenic photosynthesis:

$$CO_2 + H_2O \rightarrow [CH_2O] + O_2$$

followed by:

$$2Fe^{2+}_{aq} + 0.5O_2 + 5H_2O \rightarrow 2Fe(OH)_3 + 4H^+$$

Other studies considered a stratified ocean with a thin upper oxic zone and a lower anoxic ferruginous layer (e.g., James, 1954; Klein & Beukes, 1989). In this model, earlier views considered that Fe^{2+} was provided by continental weathering under an anoxic atmosphere and transported to chemically stratified oceans by rivers (James, 1954), whereas in most modern hypotheses, the Fe^{2+} is derived from hydrothermal alteration of oceanic crust in the deep ocean (e.g., Isley, 1995). Both of these models require the existence of oxygenic photosynthesizers, and several studies have suggested their existence by the Neoarchean (see also *Clues from Molecular Biomarkers,* p. 118). A new model of BIF genesis was recently proposed to explain the formation of BIFs in the ~1.8 Chiall Formation, North America, by inorganic precipitation of Fe oxyhydroxides in riverine systems from Fe derived from terrestrial weathering and coastal upwelling (Pufahl, Pirajno, & Hiatt, 2013).

Low $\delta^{13}C$ values (-57 to -28‰) in preserved organic carbon in ~2.7 to 2.57 Ga shales and carbonates from the Hamersley Province in Western Australia were interpreted as evidence of oxygenated microbial ecosystems comprised of cyanobacteria and aerobic methanotrophs (Eigenbrode & Freeman, 2006; Eigenbrode, Freeman, & Summons, 2008). Additionally, 2.7 Ga stromatolites from the Tumbiana Formation in the same stratigraphic sequence were considered to be evidence of a microbial mat community of cyanobacteria (Buick, 1992). However, this does not explain the formation of earlier BIFs. Further, no single type of bacteria can be assigned unequivocally to the construction of the mats and stromatolites.

In situ observations and quantitative geochemical modeling of oxidation of Fe(II) by cyanobacterial oxygenic photosynthesis in high-Fe(II) anoxic waters buffered by bicarbonate and silica at Chocolate Pots hot springs, Yellowstone National Park, USA, also supported the Cloud (1965, 1973) hypothesis (Parenteau & Cady, 2010). In the Parenteau and Cady study, the contributions to *in situ* Fe(II) oxidation by oxygenic photosynthesis (by cyanobacteria), anoxygenic photosynthesis (by *Chloroflexus* Pierson & Castenholz, 1974, purple bacteria, plus any other bacteriochlorophyll-containing phototrophs), and chemolithotrophy (by e.g., *Gallionella* Ehrenberg, 1838) were assessed, and the results suggest that oxygenic photosynthesis was the sole mechanism of Fe(II) oxidation in the anoxic vent waters. Light intensity was the primary variable affecting the rate of oxygen production and subsequent Fe(II) oxidation in the benthic cyanobacterial mats that are surrounded by anoxic water (Parenteau & Cady, 2010). However, a large body of evidence suggests that molecular oxygen was very scarce before ~2.4 Ga (Farquhar & Johnston, 2008) and this would have made abiotic Fe(II) oxidation extremely slow (Konhauser, Newman, & Kappler, 2005). Biological oxidation of Fe(II) at low oxygen partial pressure is much faster (Søgaard, Medenwaldt, & Abraham-Peskir, 2000), and Fe(II) chemoautotrophic metabolic oxidation is known to occur in modern microaerophilic environments (e.g., Crowe

& others, 2008a, 2008b). However, this mechanism also requires the supply of O_2 (see *Bacterial Metabolic Iron Oxidation,* below, for elaboration).

Direct Precipitation from Seawater

It is possible that some siderite (e.g., spheroidal siderite) formed directly by precipitation from anoxic water by mixing of ferrous iron and bicarbonate originating from a combination of hydrothermal fluids and microbial respiration of sedimented organic carbon (Beukes & others, 1990; Tice & Lowe, 2004; Klein, 2005) via:

$$4Fe^{2+} + 8HCO_3^- \rightarrow 4FeCO_3 + 4H_2O + 4CO_2$$

By this mechanism, siderite precipitates along the chemocline where there is supply of some organic carbon. Magnetite and hematite can precipitate in deeper areas where the organic supply is low and some oxygen is available (Beukes & others, 1990). However, it is difficult to envision enough oxygen to form magnetite and hematite in the deeper parts (below the redoxcline) of the Archean–Paleoproterozoic oceans where BIFs precipitated.

A later petrographic study of the Dales Gorge Member of the Brockman Iron Formation found silt-sized microgranules comprised of stilpnomelane and proposed the inorganic origin of 2.5 Ga BIFs as Fe-rich, Al-poor silicates that formed in the water column or ocean floor (Rasmussen & others, 2013).

BIOLOGICAL HYPOTHESES FOR BIF FORMATION

The hypothesis that biological processes could have an important role in the deposition of iron-rich sediments was first proposed by Ehrenberg (1836). Winogradsky (1888) later showed that a bacterium (*Leptothrix* Kützing, 1843) was able to live and grow only in the presence of ferrous iron in solution. Cloud (1965, 1973), while studying the microfossils of the Paleoproterozoic banded iron formations of the Lake Superior area, suggested that cyanobacteria could have participated in the oxidation and precipitation of Fe. Others proposed that BIF formation was related to carbon-cycling processes in which oxidation of Fe(II) driven by photosynthesis (oxygenic or anoxygenic) led to the contemporaneous deposition of Fe(III) oxides and organic matter. In this model, the formation of BIFs was ultimately the result of coupled organic carbon oxidation and iron reduction by anaerobic bacteria, such as iron-reducing bacteria (Walker, 1984; Konhauser, Newman, & Kappler, 2005; Kappler & others, 2005). Based on new observations of microbes and biofilms living in extreme conditions, such as near hydrothermal vents or deep in boreholes, the realization has occurred that prokaryotes probably also thrived in similar hostile environments in shallow Archean ocean waters and that they also likely utilized iron.

Mechanisms of BIF formation: Fe(II)-oxidizing and Fe(III)-reducing bacteria

Bacterial metabolic iron oxidation. Bacterial microaerophilic (chemolithotrophy) Fe(II) oxidation was likely an important process for the generation of banded iron formations (e.g., Holm, 1989; Konhauser & others, 2002). Iron-metabolic (chemolithotrophy) proteobacteria, such as *Leptothrix* and *Gallionella* are common in iron-rich freshwater streams and groundwater seeps (e.g., Harder, 1919). In addition, microaerophilic Fe(II) oxidizers are widespread in marine environments, including iron-rich hydrothermal vents (Emerson & Moyer, 2002) and at the chemocline of ferruginous lakes, such as Pavin Lake (France), where Fe-rich sediments are being deposited (e.g., Lehours & others, 2007). These bacteria use oxygen, carbon dioxide, and water to form ferric iron hydroxides, possibly by reactions such as:

$$6Fe^{2+} + 0.5O_2 + CO_2 + 16H_2O \rightarrow CH_2O + 6Fe(OH)_3 + 12H^+$$

This microbial Fe(II) oxidation reaction by microaerophilic bacteria could have dominated the redox Fe cycle in the low-oxygen conditions of the Precambrian oceans because its rate can be 60 times

faster than abiotic oxidation reactions (e.g., Søgaard, Medenwaldt, & Abraham-Peskir, 2000). The limitation, however, is that sulfur isotope studies have demonstrated that the oxygen levels of the atmosphere ($<10^{-5}$ present levels) and the surface ocean water layer (<0.003 μmol/liter at 25° C) in the Archean were too low to sustain abiotic oxidation (Farquhar, Bao, & Thiemens, 2000; Pavlov & Kasting, 2002). These low O_2 levels could also have restricted the availability of O_2 for biologic oxidation (Farquhar, Bao, Thiemens, 2000; Pavlov & Kasting, 2002).

Another metabolic Fe(II) oxidation mechanism that has been proposed to explain the origin of Fe(III) deposition in BIFs is anoxygenic photosynthetic oxidation, or photoferrotrophy, in which Fe(II) is used instead of H_2O as an electron donor to produce Fe(III) and biomass (Garrels & Perry, 1974; Ehrenreich & Widdel, 1994; Kappler & others, 2005) via:

$$4Fe^{2+} + 11H_2O + CO_2 \rightarrow CH_2O + 4Fe(OH)_3 + 8H^+$$

The presence of enormous amounts of Fe(II) in Archean seawater suggests that these bacteria could have existed and oxidized ferrous iron to ferric iron within the photic zone of the oceans through photosynthesis involving CO_2 fixation fueled by light energy (Konhauser & others, 2002). Until recently, all Fe(II)-oxidizing anoxygenic phototrophs had been cultured in the laboratory from iron-rich springs, ditches, and other shallow, ephemeral environments (Widdel & others, 1993; Ehrenreich & Widdel, 1994; Heising & Schink, 1998; Heising & others, 1999; Straub, Rainey, & Widdel, 1999). In particular, laboratory cultures of green *Chlorobium ferrooxidans* (Heising & others, 1999) (a green sulfur bacterium) and purple bacteria (α and γ *Proteobacteria*) have shown that they can phototrophically oxidize dissolved Fe(II) for carbon dioxide fixation by using Fe(II) as a reductant (Widdel & others, 1993; Heising & others, 1999; Straub, Rainey, & Widdel, 1999). Later, phototrophic Fe(II)-oxidizing bacteria were found in the photic zone of the water column in two Fe(II)-rich lakes (Lake Matano, Indonesia, and Lake La Cruz, Spain) (Crowe & others, 2008a, 2008b; Walter & others, 2009). Finally, although physical and chemical evidence for the existence of phototrophic Fe(II)-oxidizing bacteria in the Archean is yet to be found, phylogenetic studies of the enzymes that are involved in the biosynthesis of bacteriochlorophyll showed that anoxygenic photosynthetic lineages are more deeply rooted than oxygenic cyanobacterial lineages (Xiong, 2006; Posth, Konhauser, & Kappler, 2011). The main takeaway from these studies is that the anoxygenic photoferrotrophy mechanism of Fe(II) oxidation could have been dominant in the Precambrian oceans when molecular oxygen was absent and could have aided in the formation of BIFs.

Bacterial dissimilatory iron reduction (DIR). Based on evidence from natural observations, a role for DIR in the formation of banded iron formations, such as the Brockman and Kuruman BIFs, has been proposed by several researchers (Walker, 1984; Nealson & Myers, 1990; Lovley, 1991; Coleman & others, 1993; Beard & others, 1999; Johnson & others, 2003; Johnson & others 2008; Johnson, Beard, & Roden, 2008; Konhauser & others, 2002; Konhauser, Newman, & Kappler, 2005). It is known that magnetite and siderite, two abundant Fe minerals present in Archean and Proterozoic BIFs, are common products of DIR (Lovley & others 1987). Under complete reduction of iron oxides, the reaction to form siderite proceeds via:

$$4Fe(OH)_3 + CH_2O + 3HCO_3^- \rightarrow 4FeCO_3 + 3OH^- + 7H_2O$$

This reaction requires two sources of carbon, organic carbon and seawater carbon, to form siderite. If bicarbonate is not present in excess, Fe reduction is incomplete and Fe^{2+}_{aq} is also formed as a product via:

$$4Fe(OH)_3 + CH_2O + 2HCO_3^- \rightarrow 3FeCO_3 + Fe^{2+}_{aq} + 4OH^- + 6H_2O$$

Similar reactions can be written for different organic carbon vs. inorganic carbon ratios. Mass balance considerations using the values of $\delta^{13}C$ for organic matter and carbonate carbon in the ~2.5 Ga Kuruman BIF, estimated Archean–early Paleoproterozoic seawater $\delta^{13}C$ and $\delta^{56}Fe$ values, and the stoichiometric coefficients of these equations show that the predicted C (~-8‰) and Fe (+1‰ to -1‰) isotope compositions for siderite actually match those measured in siderite BIFs (Heimann & others, 2010) (see *Clues from Iron Isotope Investigations,* p. 114–116, for elaboration). By this mechanism, DIR produces aqueous Fe(II), which was likely present in relatively high concentrations in the Fe(III)-reducing precursor sediments to BIFs (e.g., Johnson & others 2008; Johnson, Beard, & Roden, 2008). High concentrations of Fe(III) present in the sedimentary pile along with organic matter would have suppressed DSR and allowed DIR to dominate and generate the Fe(II) present in BIFs (Walker, 1984).

Magnetite present in BIFs could have also formed by the reaction of Fe^{2+}_{aq} generated by DIR with original ferric oxyhydroxides in an anaerobic setting (Lovley & others, 1987; Lovley, 1991; Brown, Gross, & Sawicki, 1995; Johnson & others, 2003, Johnson & others 2008; Johnson, Beard, & Roden, 2008) via:

$$8Fe^{2+} + 16Fe(OH)_3 + 16OH^- \rightarrow 8Fe_3O_4 + 32H_2O$$

In addition, magnetite could have originated during diagenesis (or metamorphism) through oxidation of Fe(II) in siderite by O_2 via:

$$3FeCO_3 + \tfrac{1}{2}O_2 \rightarrow Fe_3O_4 + 3CO_2$$

or by reaction of siderite with hematite via:

$$Fe_2O_3 + FeCO_3 \rightarrow Fe_3O_4 + CO_2$$

The very low organic carbon content of most BIFs, in particular oxide facies, has been used in support of an inorganic origin for BIFs (e.g., Klein, 2005), or to explain the metamorphic origin of magnetite or siderite by a reaction between organic carbon and iron oxides (e.g., Perry, Tan, & Morey, 1973; Trendall, 2002) such as:

$$6Fe_2O_3 + C \rightarrow 4Fe_3O_4 + CO_2$$

Other mechanisms proposed to explain the loss of organic carbon from the sediment pile include transformation by hydrolysis and fermentation and utilization of some of the organic matter by methanogens (Hayes, 1983; Konhauser, Newman, & Kappler, 2005).

Bacterial DIR provides an alternative and consistent explanation for the formation of the large amount of Fe(II) present in BIFs, the formation of mixed-valence minerals, such as magnetite, as well as the negative $\delta^{13}C$ values measured in BIF carbonates (Johnson & others, 2003, 2008; Heimann & others, 2010; Cradock & Dauphas, 2011; Li & others, 2013). This mechanism also explains the low amount of organic carbon present in BIFs if organic carbon was the limiting factor in the reactions (Walker, 1984; Heimann & others, 2010). Moreover, the finding of a variety of deeply branching, presumably very ancient, hyperthermophilic bacteria and archaea that can reduce Fe(III) to Fe(II) reinforces the idea that DIR is a deeply rooted metabolism (Vargas & others, 1998; Lovley, 2004) that was likely active and played a role during the formation of Archean and Paleoproterozoic BIFs.

Clues from Biological Experiments and Cell Calculations

Two studies investigated the size of the bacterial communities and oxidation rates necessary to oxidize Fe(II) to Fe(III) in ancient marine settings and form the vast amounts of Fe oxides in Precambrian BIFs (Konhauser & others, 2002; Kappler & others, 2005). These studies showed that these settings would have had enough nutrients and light to sustain a community large enough to generate the necessary iron. It was also shown, by ecophysiological experiments and quantitatively by modeling, that direct chemolithotrophic or photoferrotrophic Fe(II) oxidation by phototrophic bacteria would have been capable of generating most, if not all, of the original ferric iron hosted in BIFs (Konhauser & others, 2002).

Konhauser and others (2002) calculated the number of metabolizing cells required to form an annual BIF deposit (layer) based on: 1) the Fe content of iron-rich mesobands in the 2.5 Ga Dales Gorge Member of the Brockman Iron Formation; 2) the density of the layers; 3) estimated maximum annual Fe depositional rates for the Hamersley Basin of ~1 m/700 yr (Morris, 1993), or 1 mm of hematite per year; 4) the area of the basin; and 5) cell production from iron oxidation by *Gallionella* and *Chromatium* Perty, 1852. Konhauser and others (2002) showed that bacterial oxidation could account for most, if not all, of the ferric iron present in BIFs. Kappler and others (2005) also demonstrated experimentally using radiation at wavelengths that penetrate to 100 meters depth in the water column at only 1% surface radiance, that photoferrotrophs could have oxidized Fe(II) down to a few hundred meters of water depth and generate enough Fe(III) to account for all the ferric iron in BIFs. This means that photoferrotrophs could have potentially oxidized all the Fe(II) during upwelling before they reached shallow levels and possibly shallow oxygenated waters (Kappler & others, 2005). These studies also calculated the amount of reduced Fe necessary to produce during diagenesis all the magnetite present in BIFs. Finally, they proposed that a complex bacterial community likely existed on the Archean seafloor, including Fe(III) reducers and possibly methanotrophs that could link Fe(III) reduction to methane oxidation (Konhauser, Newman, & Kappler, 2005).

Clues from Carbon Isotope Studies

Numerous studies have investigated the carbon isotope composition of BIFs (expressed as $\delta^{13}C$, in per mil, ‰, relative to Pee Dee Belemnite (PDB)—a standard for carbon) as a way of understanding their genesis. In particular, abundant data exist for the carbonates and organic matter from the low metamorphic grade ~2.5 Ga Kuruman BIF (Klein & Beukes, 1989; Beukes & Klein, 1990; Kaufman, Hayes, & Klein, 1990; Johnson & others, 2003; Heimann & others, 2010), the ~2.5 Ga Brockman BIF (Becker & Clayton, 1972; Baur & others, 1985; Craddock & Dauphas, 2011), and the ~1.88 Ga Gunflint and Biwabik BIFs (Fig. 48.1) (Perty, 1852; Perry, Tan, & Morey, 1973; Winter & Knauth, 1992). Iron formation carbonates have very negative carbon isotope compositions as low as -12‰, and organic carbon isotope values are extremely negative with values as low as -40‰ (Becker & Clayton, 1972; Walker, 1984; Baur & others, 1985; Kaufman, Hayes, & Klein, 1990; Johnson & others, 2003; 2008; Beukes & Gutzmer, 2008; Fischer & others, 2009; Heimann & others, 2010; Craddock & Dauphas, 2011). In contrast, most Ca-Mg-rich carbonates have near-zero $\delta^{13}C$ values (Beukes & others, 1990; Shields & Veizer, 2002; Fischer & others, 2009; Heimann & others, 2010; Craddock & Dauphas, 2011).

The negative carbonate C isotope values in BIF carbonates have been interpreted in various ways as a result of: 1) direct precipitation of siderite from an iron-rich water column that was stratified with respect to the carbon isotope composition of inorganic carbon (e.g., Beukes & Klein, 1990); 2) a fermentative mechanism and anaerobic respiration in the water column (Perry, Tan, & Morey, 1973; Walker, 1984; Fischer & others, 2009; Johnson & others, 2003; Heimann & others, 2010); 3) a hydrothermal flux dominated by mantle-derived carbon (e.g., Beukes & Klein, 1990); and 4) methane oxidation linked to ferric iron reduction (Konhauser, Newman, & Kappler, 2005). Inorganic mechanisms, such as Fischer-Tropsch processes, can also produce large carbon isotope fractionations (between -50 and -100‰), which make it difficult to be certain that the negative $\delta^{13}C$ values measured in BIF carbonates reflect biologic processes. Most researchers, however, interpret the negative $\delta^{13}C$ values of carbonates as reflecting diagenetic siderite precipitation by microbial oxidation of organic matter derived from photosynthesis coupled to reduction of ferric

oxides via DIR (Walker, 1984; Johnson & others, 2003; Heimann & others, 2010; Craddock & Dauphas, 2011).

Clues from Iron Isotope Investigations

Investigations of the iron isotope composition (expressed as δ^{56}Fe in units of per mil, ‰, relative to igneous rocks) of ancient marine sedimentary rocks have been undertaken in the last 20 years to understand the formation of BIFs and the biogeochemical cycling of iron in the early oceans (Beard & others, 1999, 2003; Johnson & others, 2003; Johnson & others, 2008; Johnson, Beard, & Roden, 2008; Dauphas & others, 2004, 2007; Rouxel, Bekker, & Edwards, 2005; Whitehouse & Fedo, 2007; Planavsky & others, 2009, 2012; Heimann & others, 2010; Tsikos & others, 2010; Steinhoefel, Horn, & von Blanckenburg, 2009; Craddock & Dauphas, 2011; Fabre & others, 2011; Halverson & others, 2011; Czaja & others, 2013; Li & others, 2013). This is possible because iron isotopes fractionate during redox changes when iron species are separated, and iron cycling was extensive in the Archean–Proterozoic Earth. In modern marine environments, DSR is the dominant pathway for the oxidation of sediment organic carbon (Thamdrup, 2000). The sulfide produced by this process reacts with sediment or hydrothermal iron with near-zero δ^{56}Fe values to form iron sulfides that have near zero or slightly positive δ^{56}Fe values (e.g., Severmann & others, 2006). In contrast, in the Archean and early Proterozoic oceans, high rates of reactive iron flux and low sulfate and sulfide concentrations, as evidenced by the compositions of BIFs (Klein, 2005), would have favored bacterial DIR over bacterial DSR (e.g., Johnson & others, 2008; Johnson, Beard, & Roden, 2008). This, in turn, would have favored extensive bacterial redox iron cycling and phase separation that resulted in iron isotope fractionation.

Iron isotope studies of millimeter scale samples reveal processes that took place in the sediment pile during the formation of BIFs prior to lithification (Johnson & others, 2003; Heimann & others, 2010). Bulk-rock analyses (e.g., Planavsky & others, 2009, 2012), however, give an average of different processes that possibly operated in various places and at different scales, and provide an estimate of the bulk or average iron isotope composition of BIFs. The record through time of iron isotope compositions of marine sedimentary rocks, including pyrite in shales, bulk BIFs, and BIF minerals, shows a large, slightly positive to highly negative (~ -3‰) excursion at ~2.7–2.5 Ga (Rouxel, Bekker, & Edwards, 2005; Johnson & others, 2008; Johnson, Beard, & Roden, 2008; Planavsky & others, 2012; Li & others, 2013). In contrast, δ^{56}Fe values are mostly near zero to positive in the Eoarchean 3.8 Ga BIFs from Isua in Greenland, the Nuvvuagittuq greenstone belt in northern Quebec, Canada (Dauphas & others, 2004, 2007; Whitehouse & Fedo, 2007; Johnson & others, 2008; Johnson, Beard, & Roden, 2008; Czaja & others, 2013), and the ~1.88 Ga late Paleoproterozoic Gunflint and Biwabik BIFs from the Animikie basin of North America (Planavsky & others, 2009). The majority of younger rocks have near-zero δ^{56}Fe values. These variations in iron isotope compositions have been interpreted as reflecting inorganic processes and direct precipitation of iron-rich minerals from seawater or the dominance of bacterial DIR in the Precambrian oceans and their role during BIF formation. Specifically, the iron isotope variations in Precambrian marine sedimentary rocks have been interpreted by some authors to reflect inorganic oxidation of Fe(II) and precipitation of iron oxides and to record changes in the δ^{56}Fe values of ancient seawater (Rouxel, Bekker, & Edwards, 2005) and not the interplay of biologic and geologic processes in the sedimentary pile prior to lithification (e.g., Yamaguchi & others, 2005). The negative δ^{56}Fe values of minerals (siderite, magnetite, and pyrite) could result from partial abiotic oxidation of near-zero δ^{56}Fe iron in the water column (Rouxel, Bekker,

& Edwards, 2005) or partial Fe(II) utilization during abiotic pyrite precipitation (Guilbaud, Butler, & Ellam, 2011), which would leave behind low-δ^{56}Fe Fe^{2+} to form these minerals. A counter argument to the abiotic partial oxidation hypothesis is that the wide range in δ^{56}Fe values of marine precipitates at small scales cannot directly record the iron isotope composition of seawater due to the large size of the iron pool and its expected long residence time in Archean and early Paleoproterozoic seawater (Johnson & others, 2008). Finally, although abiotic pyrite formation may explain some iron isotope variations, the idea has been questioned for most low-δ^{56}Fe samples on the grounds of detailed studies of the depositional setting, mineralogy, and geologic history of Precambrian sedimentary rocks (Czaja & others, 2012).

The positive δ^{56}Fe values of Eoarchean BIFs from Greenland have been interpreted to reflect incomplete oxidation of near-zero δ^{56}Fe hydrothermal Fe(II), possibly via anaerobic photosynthetic oxidation by bacteria (Dauphas & others, 2004; Johnson, Beard, & Roden, 2008; Czaja & others, 2013), although the Fe isotope fractionations alone could not be taken as a biosignature (Bullen & others, 2001; Dauphas & others, 2004). Similarly, the positive δ^{56}Fe values in the late Paleoproterozoic Gunflint and Biwabik BIFs seem to reflect the cycling of Fe by iron-oxidizing microbial ecosystems in redox-stratified oceans (Planavsky & others, 2009). The excursion in Fe isotope compositions toward negative values at ~2.7–2.5 Ga, as measured in the giant ~2.5 Ga Kuruman and Brockman BIFs, has been interpreted to represent the expansion of DIR bacteria in the Precambrian oceans starting as early as 2.9 Ga (Johnson & others, 2003; Johnson & others, 2008; Johnson, Beard, & Roden, 2008), which points to the antiquity of this anaerobic respiratory pathway. The decrease in iron isotope variations in BIFs after the GOE at ~2.4 Ga (Rouxel, Bekker, & Edwards, 2005) has been interpreted as indicating a change from the peak of DIR activity at 2.7–2.5 Ga to an increase in seawater sulfate and the expansion of DSR bacteria in the oceans with the consequent removal of Fe(II) by pyrite after that (Johnson & others, 2008; Johnson, Beard, & Roden, 2008). This interpretation is also consistent with the change in sulfur isotope composition of sulfides in marine sedimentary rocks toward negative values and disappearance of strong sulfur mass-independent fractionation effects at ~2.4 Ga, which are evident at > ~2.5 Ga (e.g., Canfield, 2001; Ono & others, 2003; Farquhar & Wing, 2003; 2005; Johnson, Beard, & Roden, 2008). Furthermore, this change in isotope compositions also coincides with a shift from extremely negative carbon isotope compositions of kerogens (δ^{13}C down to -60‰) toward less negative values, which all together suggest some major changes in geobiological processes and isotope pathways at this time (Johnson, Beard, & Roden, 2008).

Experimental work on iron isotope fractionation during iron oxidation and reduction with and without bacteria and observations of natural environments provide the needed basis for the interpretation of the large iron isotope excursion toward negative δ^{56}Fe values at 2-7–2.5 Ga. Based on laboratory experiments and evidence from natural environments, the majority of highly negative δ^{56}Fe Fe^{2+}_{aq} is derived from biogenic reduction of Fe(III) by DIR (Beard & others, 1999, 2003; Crosby & others, 2005, 2007; Croal & others, 2004; Johnson & others, 2005; Tangalos & others, 2010; Wu & others, 2012). Experiments show that the iron isotope fractionation factor between Fe^{2+}_{aq} in a simulated Archean seawater analog and Fe(III) in iron-silica co-precipitates (analogous to the ones assumed to have formed BIFs) is up to -4‰ (Wu & others, 2012). These experiments indicate that the highly negative δ^{56}Fe values (~ -2.0 ‰) measured in BIF minerals (magnetite, siderite) and pyrite in black shales could have resulted from a multi-stage process involving the generation of low-δ^{56}Fe Fe^{2+}_{aq} by bacterial DIR

[Reaction: $4Fe(OH)_3 + CH_2O + 2HCO_3^- \rightarrow 3FeCO_3 + Fe^{2+}_{aq} + 4OH^- + 6H_2O$ (see p. 111)] and its mobilization (e.g., Johnson & others, 2003; Johnson & others, 2008; Johnson, Beard, & Roden, 2008; Heimann & others, 2010). In a second stage, the $Fe(II)_{aq}$ produced by DIR would have reacted with bicarbonate to form siderite, or could have been mobilized in the sediment pile and reacted with near-zero $\delta^{56}Fe$ ferric oxides to form magnetite [Reaction: $8Fe^{2+} + 16Fe(OH)_3 + 16OH^- \rightarrow 8Fe_3O_4 + 32H_2O$ (see p. 112)] or reacted with sulfur to form pyrite. These minerals would have retained the negative $\delta^{56}Fe$ value of the $Fe(II)_{aq}$ generated by DIR (Johnson & others, 2003; Johnson & others, 2008; Johnson, Beard, & Roden, 2008; Heimann & others, 2010). In this view, the original Fe(III) oxyhydroxides had near-zero $\delta^{56}Fe$ values that resulted from complete or near-complete oxidation, either biologic or abiologic, of hydrothermal Fe(II) with $\delta^{56}Fe$ values similar to modern-day hydrothermal Fe(II) at ~ 0‰ (Beard & others, 2003; Johnson, Beard, & Roden, 2008).

Near-complete reduction of ~0‰ $\delta^{56}Fe$ Fe(III) oxides by DIR would result in Fe(II) with negative $\delta^{56}Fe$ values, as noted above, and would leave behind ferric oxides enriched in the heavy iron isotopes. A study of coupled iron, carbon, and oxygen isotope compositions of millimeter scale samples of carbonates from the ~2.5 Ga Kuruman BIF found that in laminations where the carbonates (siderite) did not have negative but positive $\delta^{56}Fe$ values, they had micrometric inclusions of hematite, which were interpreted as remains of the original iron oxides (Heimann & others, 2010). All carbonates had negative $\delta^{13}C$ values (> -8‰) indicative of incorporation of oxidized organic matter. The iron and carbon isotope values of these carbonates do not reflect precipitation in equilibrium with ancient seawater but are exactly what is expected from near-complete reduction of Fe(III) in original ferric hydroxides by bacterial DIR coupled to organic matter oxidation (Heimann & others, 2010) (see *Bacterial Dissimilatory Iron Reduction*, p. 111). Furthermore, Sr isotope studies of the same siderite BIF samples also indicate that the carbonates did not precipitate in equilibrium with seawater (Johnson & others, 2013). Therefore, these data point to the likely participation of bacterial DIR in the formation of at least these BIF carbonates.

Clues from Microfossils

Microfossils have been found in chert layers of Precambrian banded iron formations (e.g., Tyler & Barghoorn, 1954), as well as in other older cherts not associated with BIFs (e.g., Schopf, 2006b). This section deals only with the former. The first assemblage of structurally preserved microorganisms was discovered in dense black cherts of the 1.88 Ga Gunflint Iron Formation of southern Ontario, Canada (Fig. 48.1–48.2)(Tyler & Barghoorn, 1954; Barghoorn & Tyler, 1965; Cloud, 1965; Awramik & Barghoorn, 1977). The Gunflint BIF also contains siliceous and calcitic stromatolites of various morphologies (Fig. 48.2) (Hoffman, 1969; Fralick, 1989; Sommers, Awramik, & Woo, 2000; Planavsky & others, 2009). The microorganisms were described in detail in the black cherts that owe their color to the presence of fine-grained pyrite and organic matter (Barghoorn & Tyler, 1965). Spherical structures, filaments, spore-like bodies, and other organic structures are preserved (Barghoorn & Tyler, 1965).

The most abundant microfossils in the Gunflint chert are filaments ranging from 0.5 to 6.0 μm in diameter. The best-preserved filaments appear to be both septate and nonseptate. The grossly septate filaments were placed in a new genus, *Gunflintia* Barghoorn & Tyler, 1965 and divided by the authors into two species (*G. grandis* and *G. minuta*). These are the most abundant microfossils, are characterized by randomly oriented filaments, and occur preferentially in stromatolites (Planavsky & others, 2009).

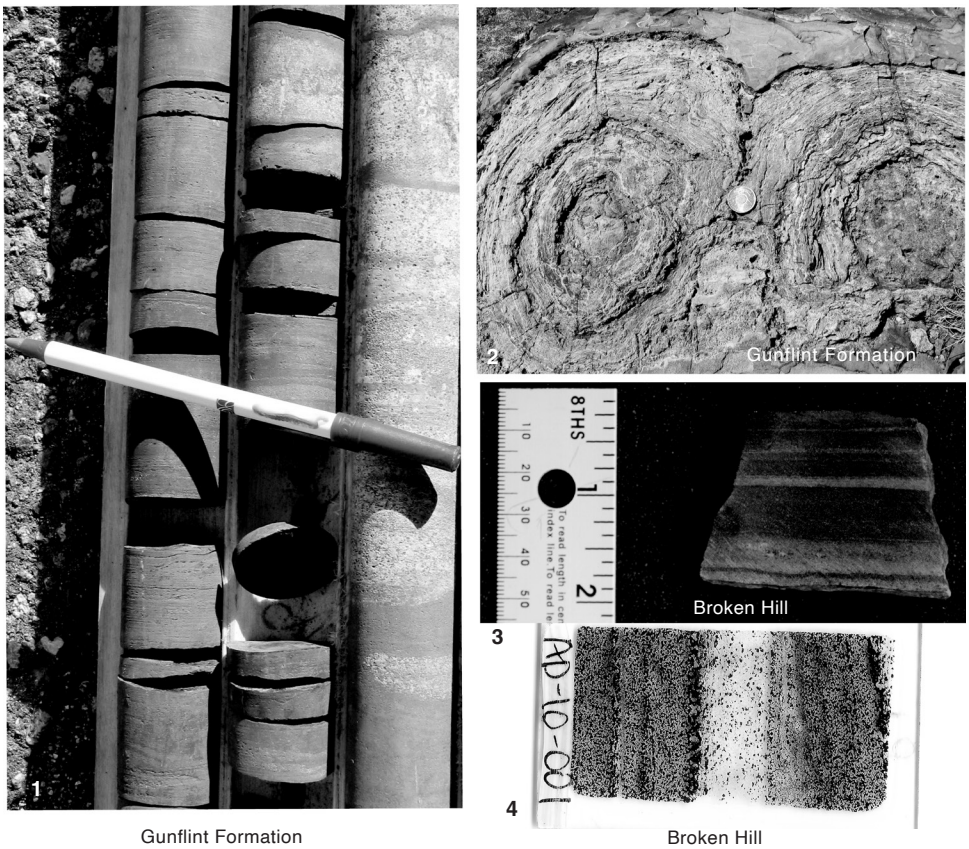

FIG. 48. *1,* Drill core of the Gunflint Formation, Ontario, Canada, showing red, magnetite-rich laminated chemical sediments of the late Paleoproterozoic (1,878 Ma) Gunflint Iron Formation (red/brown) overlaying light color, coarse grained sandstone with magnetite-rich laminations (reddish), drill core 89-mc-1 at ~160 m, Ministry of Northern Development and Mines Core Library (new; photo, Adriana Heimann). *2,* Stromatolites of the Gunflint Formation, coin for scale (new; photo, Adriana Heimann). *3,* Core slab sample of metamorphosed banded iron formation spatially associated with massive sulfide mineralization near the giant late Paleoproterozoic (1.69 Ga) Broken Hill Pb-Zn-Ag deposit, Curnamona Province, Australia, metamorphosed to granulite facies; brown is garnet in quartz, black is magnetite and minor quartz and/or garnet, sample AD-10-010, sample provided by Paul G. Spry (new; photo, Erica Serna). *4,* Scanned polished thin section of BIF near the Broken Hill deposit showing the delicate nature of the magnetite-rich laminations; black is magnetite, clear is quartz, brownish is garnet, sample AD-10-001 (new; image, Erica Serna). Color version available in *Treatise Online* 147 (paleo.ku.edu/treatiseonline).

Some of the finely septate types of filaments exhibit a basic morphology comparable to that present in extant filamentous blue-green algae (cyanobacteria), such as *Oscillatoria* GOMONT, 1892b and *Lyngbya* GOMONT, 1892 and were grouped into a new taxon, *Animikiea septata* by BARGHOORN and TYLER, 1965. Some of the non-septate filaments include very uncommon forms that contain spores and endogonidia and were grouped by the authors into a new taxon, *Entosphaeroides amplus*. These structures have a morphology comparable to a few extant genera of cyanobacteria and the iron bacteria *Crenothrix* COHN, 1870. The spheroidal spore-like organisms that are ubiquitous in the chert exhibit a variety of sizes (1–16 μm), structures, and shapes and were grouped into a new genus, *Huroniospora* BARGHOORN & TYLER, 1965, and subdivided by the authors into three species based on the wall-sculpturing pattern.

Other organisms were also found and assigned to a genus, but these were more rare

and of unclear relationship to any known living group. In particular, some types of organisms are characterized by segmented or septated filaments radiating from a central structure of poorly defined morphology, and are grouped into the new genus *Eoastrion,* defined by Barghoorn and Tyler, 1965. Rare spiral threads (<1 μm in diameter, <35 μm length), either single corkscrew-like filaments or interwoven pairs, have a gross morphology that resembles spiral threads secreted by the living iron bacterium *Gallionella* (see Cloud, 1965). Although some of the biota appear to be planktonic (coccoidal forms), other forms, such as dense intertwined filaments of *Gunflintia,* appear to be benthic (Planavsky & others, 2009).

Earlier studies considered that the microfossils reflected the dominance of oxygenic photosynthesis in the early Precambrian (Barghoorn & Tyler, 1965; Cloud, 1965; Awramik & Barghoorn, 1977). However, a later study concluded that many of the Gunflint-type microfossils that were interpreted as oxygenic photosynthesizers were more likely to be metabolic iron oxidizers (Golubic & Seong-Joo, 1999). A more recent study that combined iron isotope compositions and REEs in microfossil-rich stromatolites from the Gunflint BIF also suggested that the late Paleoproterozoic environment likely hosted an iron-oxidizing microbial ecosystem and not cyanobacteria (Planavsky & others, 2009). It is more likely that the ecosystem present during the formation of the Gunflint BIF was actually quite complex.

Clues from Molecular Biomarkers

Biomarkers are fossil remains of chemically stable organic molecules derived from the carbon skeletons of precursor lipids preserved in the rock record (Waldbauer & others, 2009). They have been found in sedimentary rocks associated with BIFs and in BIFs themselves, and have been used to infer the presence and role of bacteria during their formation (Brocks & others, 1999, 2003a, 2003b; Summons & others, 1999; Waldbauer & others, 2009). For example, fossil hopanes and steranes (biomarkers typically present in eukaryotes) were found in the 2.6 Ga sedimentary rocks of the Transvaal Supergroup, South Africa (Waldbauer & others, 2009). The biosynthesis of steranes requires free oxygen, implying that oxygen was readily available at 2.6 Ga, or about 0.1 Ga before the formation of the Kuruman BIF, one of the largest BIF deposits that occurs in the same Transvaal Supergroup, and 0.2 Ga before the full oxygenation of the atmosphere took place (Noffke, 2009). In another study, 2a-methylhopanes, organic molecules present in membranes of modern cyanobacteria, were extracted from bitumen in the ~2.6 Ga very low metamorphic grade shales of the Marra Mamba Iron Formation and underlying 2.7 Ga rocks of the Hamersley Group, Western Australia (Brocks & others, 1999; Summons & others, 1999). This finding was interpreted as indicative of the existence of cyanobacteria, or oxygen-producing bacteria, 300–200 million years before the rise of atmospheric oxygen. This may also indicate that the BIFs of the Hamersley Group formed as the result of bacterial production of oxygen (Brocks & others, 1999). However, the hopane molecules found in the Marra Mamba shales were also identified in anoxygenic phototrophic Fe(II)-oxidizing bacteria (Rashby & others, 2007) and, therefore, are not an unequivocal fingerprint for the presence of cyanobacteria at the time the rocks formed. Furthermore, it was later found that the carbon isotope composition of pyrobitumen and kerogen extracted from the same rocks is 10–20‰ lighter than the extracted hydrocarbons, providing a strong argument against the indigenous origin of the biomarkers (Rasmussen & others, 2008). Thus, there is much work to be done on molecular biomarkers to determine unequivocally the first appearance of oxygenic photosynthesis and the role of this bacterial metabolism in the formation of BIFs.

The Possible Role of Iron-enriched Biofilms

Iron-enriched biofilms or mats can be considered as possible precursors to the

formation of finely laminated banded iron formation deposits. For example, recent studies of ~2.75 Ga BIFs in the Carajás mining district, Carajás Formation, Grão Pará Group, Brazil, presented evidence (morphology, carbon content, and very negative C isotope compositions) for the biogenicity of stromatolitic structures present in these Neoarchean BIFs that strongly suggests that the BIFs could have originated as biomats (Ribeiro da Luz & Crowley, 2012). The hypothesis is that Fe(III) precipitation would have taken place through Fe oxidation by contact of Fe(II) with bacterial slime and chemical reactions with organic compounds (Ribeiro da Luz & Crowley, 2012). The Fe(III) is considered to have been available later for dissimilatory Fe(III) reduction.

Bacterial processes related to iron oxide deposition in some modern bacterial mats give us clues about similar processes in the Archean–Proterozoic oceans where BIFs formed. In nutrient-limited environments, bacteria form biofilms that preferentially grow as slime-encased microbes on the surface of rocks instead of as free-swimming (planktonic) organisms (ZoBell, 1943). For example, in modern environments, photosynthetic bacteria and filamentous bacteria form laminated mats next to hydrothermal vents and hot springs, where they can be several millimeters thick (Walter, Bauld, & Brock, 1972; Walter & others, 1992; Doemel & Brock, 1977; Brown, Gross, & Sawicki, 1995; Little, Glynn, & Mills, 2004). Bacteria act as substrate or polyionic trap for the precipitation of minerals, promote mineral crystallization by metabolically generating products (e.g., OH^-, CO_2, H^+) that combine with dissolved metallic ions, or mediate enzymatic oxidation of others (e.g., Fe^{2+} to Fe^{3+}) (Konhauser, 1997, 1998; Thompson & Ferris, 1990; Ghiorse & Ehrlich, 1992; Brown, Gross, & Sawicki, 1995).

Modern microbial mats are commonly associated with the formation of iron hydroxides where bacterial biomineralization takes place (Pierson, Parenteau, & Griffin, 1999; Konhauser, 2000; Little, Glynn, & Mills, 2004; Parenteau & Cady, 2010). Studies of hot springs, active black smokers, and deep hydrothermal areas indicate: 1) that the iron-rich mats are mainly comprised of living cells and remains of bacteria (for example, *Gallionella ferruginea* Ehrenberg, 1836) (Boström & Widenfalk, 1984; Holm, 1987); 2) that microbial mats are the favored sites of deposition of iron hydroxides; and 3) that iron oxides form biogenically in areas of low O_2 and slightly acidic pH (Baross & Deming, 1985; Tunnicliffe & Fontaine, 1987; Karl, Brittain, & Tibrook, 1989; Pierson, Parenteau, & Griffin, 1999; Little, Glynn, & Mills, 2004; Parenteau & Cady, 2010).

Earth's possibly oldest fossil cyanobacterial mats found in sandy deposits of a tidal environment in the 2.9 Ga Nhlazatse Section, Pongola Supergroup, South Africa, suggest the existence and diversification of cyanobacteria as early as the Mesoarchean (Noffke, 2010). Therefore, modern microbial mats and biofilms, including relatively young (Pleistocene) fossilized mat-forming prokaryote examples, are possibly one of the keys to understanding ancient benthic microbial communities and their habitats (Brown, Gross, & Sawicki, 1995; Noffke, 2010). Particular examples are described below. The question still remains, however, as to exactly what kind of microbial communities formed these mats, because the mechanism of formation of the mats is not unique to oxygenic photosynthetic bacteria (Tice, 2008).

POSSIBLE PHANEROZOIC AND MODERN ENVIRONMENT ANALOGS

There is no perfect analog for Archean–Proterozoic banded iron formations (BIFs) in chemical composition, environment of formation (physicochemical conditions), and genesis. Paleozoic siliceous iron oxyhydroxide deposits, Phanerozoic hematite-quartz ironstones, and iron-oxide chemical precipitates that form in the modern oceans and deep

lakes from hydrothermal fluids and brines are the closest analogs and are described below. In addition, continental sites where iron oxyhydroxides currently form under somewhat similar environmental conditions (low sulfate, low oxygen) as those in Archean–Proterozoic oceans and where biogenic Fe(III) reduction takes place are also included because even though they are terrestrial environments, they have been considered modern environmental analogs to those in Archean–Proterozoic times where BIFs formed.

MODERN SILICEOUS IRON OXYHYDROXIDE MARINE DEPOSITS

Iron Deposits of Marine Hydrothermal Vents

In modern marine environments, siliceous iron oxyhydroxide deposits commonly form spatially and genetically related to hydrothermal activity; examples occur at the Juan de Fuca Ridge (northeast Pacific Ocean), the Lilliput hydrothermal field on the Mid Atlantic Ridge, Trans-Atlantic Geotraverse (TAG), Loihi seamount hydrothermal vents (Hawaii), Coriolis Troughs (southwest Pacific), Red Sea Mount, and the Jan-Mayen vent fields in the Arctic-Ocean Ridge System (Rona & others, 1986; Alt, 1988; Emerson & Moyer, 2002; Little, Glynn, & Mills, 2004; Toner & others, 2009; Dekov & others, 2010; Moeller & others, 2013). In some of these settings, for example at the Jan-Mayen vent field, iron oxyhydroxides precipitate at depths greater than 1,000 m from diffuse, low-temperature hydrothermal fluids that emanate at the seafloor through fissures and faults distal to high-temperature hydrothermal vents (e.g., Moeller & others, 2013). The siliceous iron oxyhydroxide layers in all these locations consist of iron-rich amorphous phases or ferrihydrite and minor amounts of crystalline iron oxides, such as goethite, with up to 50 wt% Fe_2O_3 in bulk analysis and are intimately associated with filamentous structures of biogenic origin (e.g., Little, Glynn, & Mills, 2004; Moeller & others, 2013). All of the vents, for example at Loihi, are surrounded by microbial mats with a gelatinous texture and are encrusted with iron oxides (Emerson & Moyer, 2002; Little, Glynn, & Mills, 2004).

It has been shown that iron-oxidizing bacteria—for example species similar to *Mariprofundus ferrooxidans* Emerson & others, 2007—play a key role in mediating the oxidation of Fe(II) derived from the low temperature hydrothermal fluids (Emerson & Moyer, 2002; Toner & others, 2009; Moeller & others, 2013). At TAG, the filaments have been described as identical to the iron oxide encrusted stalks of *Gallionella* spp and *Leptothrix ochracea* Kützing 1843 (e.g., Little, Glynn, & Mills, 2004). What is more, studies at Loihi showed that up to 60% of the iron oxyhydroxides occur as filaments or sheaths interpreted to be direct deposition by bacteria (Emerson & Moyer, 2002).

Because of their similarities, modern deep-sea hydrothermal vent iron deposits are considered analogs of Ordovician to late Eocene jaspers, which points to a record of bacteriogenic iron oxide precipitation at marine hydrothermal vent sites of at least 490 million years (Little, Glynn, & Mills, 2004). Even though there are environmental differences between the origin of ancient BIFs and modern siliceous Fe oxyhydroxides, their Si-Fe enrichment and chemical precipitation from hydrothermal fluids makes them the closest modern analogs to ancient BIFs. If we consider the setting near hydrothermal vents, then these Si-Fe precipitates can be considered closer analogs to Algoma-type BIFs, which formed in tectonically active areas and probably close to hydrothermal vents, than to Superior-type BIFs, which formed in stable platforms away from hydrothermal vent sites. The fact that biologic oxidation mediates the precipitation of these iron oxyhydroxides in modern settings also supports the idea of a link between iron precipitation and organic mediation during the formation of BIFs in the ancient oceans.

Iron Deposits of the Red Sea

The Red Sea rift system is characterized by active tectonics and igneous and hydrothermal activities and by a stratified body of water comprised of denser, saline anoxic bottom water overlain by lighter, less saline, cooler, oxic surface water. The deep water that penetrates the sediments achieves a high salinity by leaching of Miocene evaporates and a high temperature by a geothermal gradient and interaction with hot basaltic rocks (e.g., Cocherie, Calvez, & Oudin-Dunlop, 1994). The hot brine that discharges into the basin creates a stratified system with a lower hot (56–67 °C) layer enriched in Fe and Mn (81 mg/kg for each) and with a pH between ~5.5 and 6.4 depending on the location, and an upper, cooler (44°–56 °C) water layer (Taitel-Goldman, Ezrsky, & Mogilyanski, 2009). The Discovery Deep and the Atlantis II Deep are 5 km apart and separated by a sill at a depth of ~1990 m below sea level (Taitel-Goldman, Ezrsky, & Mogilyanski, 2009, and references therein). The lower layer brine flows into various deeps through a fracture and fissure system. The Fe oxyhydroxide minerals crystallize as authigenic minerals and occur at water depths between 2000 and 2216 m.

The mineralogy of the Atlantis II Deep includes Mn-Fe carbonates and rounded particles of Si-associated Fe oxyhydroxides, including well crystallized hematite (α-Fe_2O_3), goethite (α-FeO(OH)), and clusters of ferrihydrite ($Fe_5^{3+}OH_8.4H_2O$), as well as feroxyhyte (δFeO(OH)), lepidocrocite (γ-$Fe^{3+}O(OH)$), and Mn oxyhydroxides (Taitel-Goldman, Ezrsky, & Mogilyanski, 2009). Pure hematite is thought to result from the recrystallization of a former phase, whereas the other oxides are original Si-associated Fe and Mn oxyhydroxides (Taitel-Goldman, Ezrsky, & Mogilyanski, 2009). A lepidocrocite-goethite association crystallizes out of the hot hydrothermal brine with no Mn impurities, whereas the presence of Mn components reflects precipitation from the upper layer or the transition zone. In addition, silicon also discharges from the brine system and precipitates in association with Fe and Mn authigenic phases (Taitel-Goldman, Ezrsky, & Mogilyanski, 2009).

The clusters of hematite, or hematite microspheroids, and the Si-associated rounded particles of Fe oxyhydroxides that form in the Red Sea are similar to fine-grained hematite microspheroids, some containing pore-filling inclusions of early diagenetic silica, present in banded iron formations (Trendall & Blockley, 1970). This similarity suggests that the formation of the Red Sea Fe oxyhydroxides can be considered a close analog to that of BIFs. Because the Fe oxides also coexist with Mn oxides, these modern deposits can be compared with the BIFs and Mn deposits of the 2.4–2.2 Ga Hotazel Formation of South Africa that formed after the Kuruman Iron Formation and close to the timing of the GOE (e.g., Tsikos & others, 2010).

LAKE MATANO, INDONESIA

Lake Matano is located on Sulawesi Island, Indonesia (Crowe & others, 2008a), and is the eighth deepest (>590 m) lake in the world. The steep margins, great depth, and the geographic location, characterized by the lack of strong seasonal temperature changes, allow the existence of a persistent pycnocline at ~100 m depth that separates an oxic surface layer from anoxic bottom waters. Sulfate concentrations are low (<20 μmol/liter) in the surface mixed layer and the rates of sulfate reduction within the anoxic waters of the chemocline are slow (<0.015 μmol/liter/day) (Crowe & others, 2008a). The slow sulfate reduction rates within the chemocline are fast enough to reduce all the sulfate and remove it from the surface waters, which results in deep waters with sulfate concentrations below detection limits. This also results in very low but detectable sulfide concentrations (including free sulfide, sulfide-bearing colloids, and larger particles of NiS and FeS). The low

sulfur results in the accumulation of high concentrations of dissolved ferrous iron (~150 µmol/l). A low, suspended load of inorganic particulate matter, scavenging of phosphate by allogenic and authigenic iron (hydr)oxides, and low primary productivity in the surface mixed layer allows light to penetrate well into the anoxic bottom waters (Crowe & others, 2008a, 2008b).

The presence and abundance peaks with depth of the dominant photosynthetic pigment bacteriochlorophyll *e* (BChl *e*), a light-harvesting pigment used by brown-colored phototrophic green sulfur bacteria (GSB) of the family Chlorobiaceae, which are specially well adapted to low light conditions, indicate that GSB are an important component of the phototrophic bacterial community in Lake Matano (Crowe & others, 2008a). Molecular fingerprinting by Crowe and others (2008a) indicated the existence of an abundant and mixed bacterial community between 110 and 120 m depth, including several phyllogenetically distinct members of Chlorobiaceae. Lake Matano clones have up to 95% sequence similarity to a known photoferrotroph, *Chlorobium ferrooxidans* Heising & others, 1999 (Crowe & others, 2008a). In contrast to most known Chlorobiaceae (obligate photolithoautotrophs that fix carbon using sulfide as an electron donor), *C. ferrooxidans* is an exception that uses ferrous iron as electron donor (Heising & others, 1999).

Unlike other water bodies, such as anoxic sulfidic lakes and euxinic marine basins like the Black Sea, the extremely low dissolved sulfide concentrations in Lake Matano suggest that the community of GSB is sustained by using the abundant concentration of Fe(II) as electron donor (Crowe & others, 2008a). The concentration of free sulfide is considered too low to sustain sulfide-fueled anoxygenic phototrophy by GSB. What is more, calculations of the irradiance in the lake at ~110 m show that the light flux is sufficient to phototrophically oxidize the entire Fe(II) flux through the chemocline (Crowe & others, 2008a). The rates of Fe(II) oxidation are also consistent with the rates of oxidation of known photoferrotrophs. Therefore, the population of GSB is largely sustained by photoferrotrophy, and this mechanism could explain BIF deposition in Archean and Proterozoic oceans. This hypothesis remains to be fully proven, however, because Fe(II) oxidizing GSB have yet to be isolated and cultured in the laboratory (Crowe & others, 2008a). Studies also concluded that iron oxides currently precipitate from the water column in Lake Matano, including the mixed ferrous-ferric mineral green rust, at the oxycline, and that authigenic magnetite formation takes place in the water column and during diagenesis (Poulton, 2011). This has been used to argue that similar processes of formation under anoxic, ferruginous conditions could have formed BIFs in ancient oceans (Poulton, 2011). Further investigations of the paths of formation of these minerals will also help improve our understanding of the cycling of iron in the Archean–Proterozoic oceans and the formations of BIFs.

Because of its high ferrous iron concentration, low sulfate content, deep light penetration, and presence of a mixed upper layer and bottom anoxic layer, as well as other physical and chemical characteristics, Lake Matano is a good modern analog for the chemistry and biology of Archean and early Proterozoic oceans (Crowe & others, 2008a). This setting at Lake Matano can be compared to that of the Archean–Proterozoic oceans where Superior-type BIFs formed in stable basins from a stratified water column. It is important to note, however, that the size of the system is small and the salinity is much lower compared to Archean–Proterozoic marine environments where BIFs formed.

PHANEROZOIC IRONSTONES

Phanerozoic iron-rich sedimentary rocks, called ironstones, are rocks with relatively high iron contents (>15% Fe) and some of them can be considered younger analogs to banded iron formations. Ironstones are rare,

temporally related to marine anoxic events and mainly restricted to the Ordovician–Devonian and Jurassic–Paleogene and to modern local areas of closed to semi-closed basins (Van Houten, 1985; Van Houten & Arthur, 1989; Bekker & others, 2010; Ciobotă & others, 2011; Salama, Aref, & Gaupp, 2012, 2013). Many are temporally associated with peaks in abundance of volcanogenic massive sulfide deposits (MSDs), sea level rise, major anoxic events, and volcanic episodes (Van Houten & Arthur, 1989; Maynard & Van Houten, 1992; Burkhalter, 1995; Taylor & others, 2002; Peter, 2003; Franklin & others, 2005; Garzani, 1993; Bekker & others, 2010; Ciobotă & others, 2011; Salama, Aref, & Gaupp, 2012, 2013). The temporal association between ironstones and volcanogenic MSDs has been used to suggest a hydrothermal origin for the iron and that the deposition of ironstones was linked to global ocean anoxic periods and superplume events (see Bekker & others, 2010 and references therein).

Ironstones are commonly small (most <2 m thick, some 20 m thick) but large examples (>1,000 km) occur along ancient continental margins in Fennoscandia (covers present-day Finland, Norway, Sweden, and the Kola Peninsula in Russia) and the Himalayas (Garzani, 1993; Sturesson, Dronov, & Saadre, 1999; Sturesson, 2003). Large examples of Phanerozoic oolitic ironstones include the Jurassic Minnette deposits of central and western Europe, and the Silurian Clinton ores of North America. Phanerozoic ironstones are comprised of oolites of Fe oxyhydroxides (goethite and limonite), Fe silicates (chamosite and berthierite), and minor amounts of amorphous silica (less chert than BIFs) and are typically enriched in phosphorous. Some ironstones are non-cherty, sandy, fine-grained siliciclastic or siliciclastic-carbonate rocks (e.g., Petránek & Van Houten, 1997).

Even though the genesis of some ironstones is likely different than that of BIFs, others, for example the Phanerozoic deposits from the Løkken ophiolite and the Eocene ironstones of Egypt, have similarities to older jaspers and modern Fe-Si deposits with origins closely linked to Fe(II) oxidation by bacterial processes (Salama, Aref, & Gaupp, 2012; Moeller & others, 2013). This suggests that they can be considered younger equivalents of BIFs. The Phanerozoic Ordovician hematite-quartz deposits from the Løkken ophiolite complex in Norway, which have been metamorphosed to lower greenschist facies, are related to volcanogenic MSDs and associated hydrothermal feeders (e.g., Grenne & Slack, 2005). The rocks consist of fine-grained hematite microspheroids comprised of cryptocrystalline hematite and quartz in a quartz matrix (e.g., Grenne & Slack, 2005). The jasper deposits have soft-sediment deformation structures that along with the presence of the cryptocrystalline hematite reflect their formation as gel-like amorphous iron oxyhydroxides, such as ferrihydrite (Grenne & Slack, 2003). They are interpreted as siliceous ferrihydrite fallout deposits formed from a hydrothermal plume during times of oxic or suboxic conditions in a preponderantly widespread anoxic period (Grenne & Slack, 2005). Therefore, this kind of Phanerozoic ironstone may be somewhat similar to BIFs in its formation. If we take into account the association with volcanogenic MSDs and the occurrence in the ophiolite, the genesis of these ironstones would resemble that of Algoma-type BIFs rather than that of Superior-type BIFs.

Some recent studies also suggest that at least some Phanerozoic ferruginous and stromatolitic ironstones, such as those in the Eocene ironstones of the Western Desert in Egypt, formed by similar processes as those described for hot springs and other hydrothermal venting areas (e.g., Ciobotă & others, 2011; Salama, Aref, & Gaupp, 2013). The Egypt ironstones are interpreted to be genetically linked to iron-oxidizing bacteria and their biofilms, where oxidation of Fe^{2+} in solution by these bacteria in shallow water with near acidic pH and low fO_2 precipitated a hydrous ferric gel that was also colonized by bacteria (Salama,

Aref, & Gaupp, 2013). Ferruginous ooids and oncoids, now comprised of goethite, which coexist with ferruginous stromatolitic microbialites, seem to have been formed *in situ* and later reworked from shallow marine areas during storms to form the ironstones (Salama, Aref, & Gaupp, 2013). Based on the association with stromatolitic rocks, the genesis of these ironstones can be compared with that of Superior-type BIFs, such as the ~2.75 Ga Carajás (Brazil) BIF (Ribeiro da Luz & Crowley, 2012).

IRON MOUNTAIN MINE DRAINAGE SITE, NORTHERN CALIFORNIA

Iron Mountain Mine is a group of mines on Iron Mountain, Shasta County, northern California, USA (Alpers, Nordstrom, & Spitzley, 2003). The acid drainage effluent from Iron Mountain Mine has extremely low pH (-3.6) within the Richmond mine portal, ranging to pH values of +1 to +4 in drainage tributaries, such as Spring Creek (Nordstrom & Alpers, 1999; Edwards, Gihring, & Banfield, 1999; Norstrom & others 2000; Alpers, Nordstrom, & Spitzley, 2003). Concentrations of total dissolved solids in the effluent can exceed 900 g/L, and the waters are iron rich (Nordstrom, 2000). Mixing of neutral pH waters from an upstream reservoir with the iron-rich water of the acid mine drainage from Spring Creek has formed three large surface accumulation piles (>260,000 m^3 total volume) comprised of fine-grained Fe(III) oxide-rich sediment. Minerals present in the piles include ferrihydrite [$Fe(OH)_3$], goethite [α-FeO(OH)], and minerals with structures similar to synthetic schwertmannite [$Fe(III)_8O_8(OH)_6(SO_4)$] (Nordstrom & Alpers, 1999). The concentration of iron in the wet sediments ranges from 4% to 47% and the pore waters have extremely high concentrations of aqueous Fe(II) up to 36 mM (Nordstrom & Alpers, 1999). The pore waters have pH values of 5.5–6.5 and sulfate concentrations of 10 mM (Nordstrom & Alpers, 1999).

Iron Mountain iron-rich sediments represent a potential modern analog to early diagenetic BIF minerals formed in Archean and Proterozoic marine environments (Tangalos & others, 2010). Although the setting where the sediments form is an aerobic continental environment, it is characterized by high concentrations of reactive Fe(III) oxide that result in the dominance of dissimilatory iron reduction (DIR) over dissimilatory sulfate reduction (DSR) in early sediment diagenesis and large quantities of mobile Fe(II) in the pore waters. Additionally, the sediments contain significant concentrations of sulfate (4–23 mM), but there is an absence of acid volatile sulfides and a very low content of Cr(II)-extracted reduced inorganic sulfur (pyrite and/or elemental sulfur) compared with dilute HCl-extractable Fe(II). The sediments also have a relatively high ratio of nonsulfide-associated reactive iron to reduced inorganic sulfur, which are significantly higher than those in most modern marine sediments but similar to oxide and siderite BIFs from the Kuruman BIF and the Dales Gorge Member of the Brockman BIF (Tangalos & others, 2010). These characteristics and the chemical composition of the Iron Mountain sediments make the environment a good analog to study the processes that operated in the sedimentary pile prior to diagenesis and authigenic formation of magnetite and siderite in Archean BIFs (Tangalos & others, 2010). In particular, this site is a natural example of the diagenetic process of bacterial DIR that likely took place in the sedimentary pile during the formation of siderite and magnetite in Superior-type BIFs, such as the Kuruman Iron Formation (Heimann & others, 2010).

Tangalos and others (2010) considered that the high amounts of $Fe(II)_{aq}$ in the Iron Mountain sediment pore water were generated by bacterial DIR of Fe(III) minerals (goethite and ferrihydrite) in the sediments. This is based on the assumption that DIR predominates over DSR due to the high concentration of reactive Fe(III) oxides, which allows dissimilatory iron-reducing microorganisms to outcompete dissimilatory sulfate-reducing bacteria for organic electron

donors (Lovley & Phillips, 1987; Tangalos & others, 2010). The sediments also contain 1.5%–4% (dry weight) particulate organic carbon, derived from primary production in the overlying water or inputs of organic matter from the surrounding terrestrial environment, which is thought to serve as electron donors for DIR. The dominance of DIR was confirmed by gene sequencing of cultures of the material in the sediments and pore waters that showed that the sediments contained gene sequences closely related (97% similarity) to known dissimilatory iron-reducing microorganisms (*Geobacter* Lovley & others 1993 and *Geothrix* Coates & others, 1999). Four different culture isolates of *Geothrix fermentans* Coates & others, 1999 were also obtained, which also confirm that dissimilatory iron-reducing microorganisms are active in the Iron Mountain materials (Tangalos & others, 2010).

Iron isotope analysis indicates that $Fe(II)_{aq}$ from the sediments pore water at Iron Mountain has negative $\delta^{56}Fe$ values (-0.8% to -1.2‰), in contrast to the near-zero $\delta^{56}Fe$ values for the bulk Fe sediments that are isotopically similar to the average crust (Tangalos & others, 2010). The near-zero $\delta^{56}Fe$ values of the bulk sediments indicate that complete oxidation of Fe(II) took place in the near-neutral ~6.5 pH environment prior to the deposition of the Fe(III) oxide sediment. Isotopic fractionations between Fe(II)aq and Fe(III) extractable are similar to those measured in pure culture DIR experiments with Fe(III) oxides that showed the generation of low-$\delta^{56}Fe$ Fe(II) generated by DIR (Crosby & others, 2005, 2007). These *in situ* results were also reproduced in the laboratory with cultured iron oxides (Crosby & others, 2005, 2007). The less negative isotopic composition of $Fe(II)_{aq}$, compared to those measured in modern marine sediments (-1.3‰ to -3‰) (e.g., Severmann & others, 2006; Bergquist & Boyle, 2006) or stratified water bodies (Teutsch & others, 2009), are likely due to differences in the iron redox cycle and redistribution, which are more limited in the Iron Mountain sedimentary piles than they were in Archean and Proterozoic marine environments. At Iron Mountain, therefore, DIR is linked directly to the generation of large quantities of isotopically light, mobile $Fe(II)_{aq}$, which suggests that DIR could have led to the formation of low-$\delta^{56}Fe$ iron-bearing minerals (siderite, magnetite) during early diagenesis of Precambrian BIFs (Tangalos & others, 2010).

CHOCOLATE POTS HOT SPRINGS, YELLOWSTONE NATIONAL PARK

Iron-rich sediments are actively being deposited at Chocolate Pots hot springs, Yellowstone National Park, USA (Pierson, Parenteau, & Griffin, 1999). Colorful, iron-rich phototrophic microbial mats form a boundary layer at the interface between the iron-rich sediment surface and flowing spring water that contains high concentrations (~100 μM) of ferrous iron at the source (Pierson, Parenteau, & Griffin, 1999; Klatt & others, 2013; Wu & others, 2013). The source waters have a near-neutral pH and lack sulfide. Beneath the surface of the microbial mat-water interface the environment is anoxic and rich in Fe(II). Although in a terrestrial surficial location, this site serves as an analog for the extensive anoxic environments of and processes operating in the Precambrian oceans where iron oxides formed (e.g., Pierson, Parenteau, & Griffin, 1999; Wu & others, 2013).

The microbial mats are comprised mainly of filamentous gliding phototrophs that stabilize oxidized iron and enhance the accumulation of sediments that are later compacted to form the iron deposits (Pierson, Parenteau, & Griffin, 1999). The intimate association between the filamentous phototrophs and the iron minerals, as well as the observation that the motility and orientation of the filaments may be important in trapping and stabilizing the sediments to produce the iron formation, is most evident in an olive green-color mat consisting of a narrow (cyanobacteria)

Oscillatoria sp. (Pierson, Parenteau, & Griffin, 1999).

Measurements in the olive mat indicate that both under light and in the dark, ferrous iron stimulates bicarbonate uptake (photosynthesis), with the highest stimulation taking place at Fe contents of 1.0 mM, whereas Fe(II) concentrations of 5 mM inhibited photosynthesis (Pierson, Parenteau, & Griffin, 1999). What is not known with certainty is whether Fe(II)-stimulated photosynthesis in anoxygenic phototrophs (*Chloroflexus* filaments) occurs in the cyanobacterial mat suspensions or only in the cyanobacteria themselves (Pierson, Parenteau, & Griffin, 1999). Isolation of Chocolate Pots mat phototrophs and experiments performed with pure cultures may help resolve which bacteria are stimulated by Fe(II) (Pierson, Parenteau, & Griffin, 1999). Newer studies indicate that the Fe isotope compositions measured at Chocolate Pots could be important to predict those on a limited-oxygen early Earth or on Mars (Wu & others, 2013). This is because the range of Fe isotopic compositions (-1.57‰ to +0.88‰) measured in the iron oxides and hot springs at Chocolate Pots do not reflect simple equilibrium oxidation or Rayleigh oxidation of Fe(II) but rather reflect different extents and rates of Fe(II) oxidation as well as the possible reduction of iron by dissimilatory Fe(III)-reducing bacteria (Wu & others, 2013). Because of the link between iron oxide precipitation, microbial mats, and bacterial iron oxidation, the processes operating at Chocolate Pots hot springs can be considered analogs to those taking place during BIF formation.

FUTURE DIRECTIONS

The following are a few lines of research that will help improve our understanding of the genesis of banded iron formations (BIFs) and the role of various biological processes directly and indirectly involved in their formation. The search for new physical biosignatures in low-metamorphic grade oxide-facies BIFs older than the Gunflint BIF in North America—for example, permineralized cells similar to those present in iron-rich modern microbial mats (e.g., Klein, 2005; Parenteau & Cady, 2010)—will help elucidate the role of bacterial processes in the generation of BIFs (Walter & Hoffman, 1983). Further search for stromatolitic structures and organic matter in BIFs, similar to the ones described from the ~2.75 Carajás BIFs from Brazil (Ribeiro da Luz & Crowley, 2012), will help determine if biomats and BIFs could have a strong genetic link. A common aspect to most, if not all, modern water environments where iron oxide precipitation takes place is their intrinsic association with bacterial mats and biofilms. Further studies of modern environments and BIFs will help to understand the likely role of these bacterial structures in the formation of BIFs, especially the striking extremely fine-scale laminations of iron oxides and chert.

The search in Archean BIFs for chemical fingerprints unique to Fe(II)-oxidizing phototrophs will provide the physical evidence for the existence of these organisms in Archean oceans. For example, the discovery of biomarkers of pigments involved in photosynthesis and radical scavenging (radicals that form during Fe-Fenton reactions), which are two processes important in systems where photosynthetic Fe(II) oxidizers exist, would provide definite clues about their presence during the Archean (Koehler, Konhauser, & Kappler, 2010). Similarly, isolation and culture in the laboratory of Fe(II) oxidizing green sulfur bacteria (GSB) that occur in modern analogs to Archean marine environments, such as the deep Lake Matano, are needed (Crowe & others, 2008a). Culturing of Fe(II)-oxidizing GSB will improve our understanding of the physiology and metabolism of the GSB, help prove that photoferrotrophy is the responsible bacterial process oxidizing iron in the lake (Crowe & others, 2008a), and provide clues as to what bacterial metabolism likely existed and played a role during the formation of BIFs.

Geochemical investigations of iron isotopes to fill the gaps in the iron isotope record through time as well as in modern natural environments will help prove that large variations in iron isotope compositions, observed particularly at ~2.7–2.5 Ga, indicate the expansion of bacterial dissimilatory iron reduction (DIR) in the Precambrian oceans and its likely role during BIF formation. More detailed iron isotope studies similar to the ones conducted at Chocolate Pots, Yellowstone National Park (Wu & others, 2013) will help to understand the processes responsible for the fractionation of iron isotopes in oxygenated and oxygen-limited environments and the implications for the formation of iron deposits on early Earth and Mars. In addition, studies of iron, carbon, and sulfur isotopes on the same rocks in Archean–Proterozoic sequences, including multiple sulfur isotopes to detect mass-independent sulfur isotope effects, will help test the hypothesis that these isotopic records are coupled and reflect photosynthesis and heterotrophic respiration (e.g., Johnson, Beard, & Roden, 2008). Furthermore, basin-wide scale iron isotope studies of BIFs, similar to those undertaken in other sedimentary rocks (mostly shale and carbonate) from Western Australia (e.g., Czaja & others, 2010), will help improve our understanding of the biogeochemical cycling of iron in ancient oceans. Finally, new rare earth element studies of BIFs, coupled with iron and carbon isotopes, as well as isotopes of other redox metals, may also help elucidate the presence or absence of a redoxcline in Archean oceans and the role of bacterial iron oxidation and reduction in the formation of different BIFs in the Archean–Paleoproterozoic and in the late Paleoproterozoic (Planavsky & others, 2010).

ACKNOWLEDGEMENTS

I wish to thank Steve Culver, Terri Woods, Jens Gutzmer, Christopher Fedo, and Nora Noffke for their comments, suggestions, and revisions, which greatly improved this manuscript. I also thank Clark Johnson for kindly providing an image of BIFs.